YEAR-END TECHNICAL REPORT

May 7, 2010 to May 17, 2011

Rapid Deployment of Engineered Solutions for Environmental Problems at Hanford

Principal Investigators:
Dave Roelant, Ph.D.
Leonel E. Lagos, Ph.D., PMP®

Florida International University Collaborators:
Leonel E. Lagos, Ph.D., PMP® (Project Manager)

Yelena Katsenovich, Ph.D.

Prabhakar Pant, Ph.D.

Ravi Gudavalli, M.S.

Denny Alejandro Carvajal, M.S, DOE Fellow

Rakesh Guduru, M.S.

Amaury Betancourt, M.S., DOE Fellow

Yulian Ariaz, B.S., DOE Fellow

Maite Barroso, Research Assistant, DOE Fellow

Sheidyn Ng, B.S., DOE Fellow

Alex Henao, B.S., DOE Fellow

PNNL Collaborators:
Dawn Wellman, Ph.D.

Prepared for:
U.S. Department of Energy
Office of Environmental Management
Office of Science and Technology
Under Grant No. DE-EM0000598

Table of Contents

List of Tables

List of Figures

EXECUTIVE SUMMARY

The Applied Research Center (ARC) at Florida International University (FIU) is assisting the U.S. Department of Energy's (DOE) Hanford Site in developing solutions to uranium contamination, including the incorporation of emerging technologies for the efficient management of the uranium-contaminated subsurface in the deep vadose zone. The investigation under task 1.1 targets uranium (U) contamination in the vadose zone (VZ) of the central plateau (200 Area) that may affect groundwater migrating to the Columbia River. The Hanford Site 200 Area is subdivided into two regions, the 200 West Area and the 200 East Area. These two areas contain four designated plumes: (1) 200-ZP-1, (2) 200-UP-1, (3) 200-BP-5 and (4) 200-PO-1, consisting mainly of uranium, technetium, and chromium. This study focuses on the plumes contaminated with uranium, which include 200-UP-1 and 200-BP-5. The study involves a series of batch experiments to evaluate the mechanisms and effectiveness of NH_3 gas injection, which has significant uncertainties under Hanford VZ site-specific conditions. The injection of a NH_3 gaseous mixture causes the formation of NH_4OH and a subsequent increase in pH. This manipulation will significantly alter the pore water chemistry and promote the formation of various aluminosilicates during recrystallization of minerals followed by co-precipitation of U(VI) [as uranyl (UO_2^{2+})] and Al at higher pH conditions. These chemical reactions can potentially control the mobility of uranyl cations in soil systems since co-precipitated contaminants are less available for migration. This study evaluates the role of major pore water constituents such as Al, Si, and bicarbonate on the formation of uranium – bearing precipitates created after NH_3 gas injection.

Research under task 1.2 investigated the effect of bicarbonate on the autunite mineral microbial leaching and U(VI) biouptake by *Arthrobacter* sp., soil bacteria previously isolated from Hanford Site soil. The obtained data suggests that bacteria is responsible for autunite dissolution and is able to influence U(VI) leaching while are even not in direct contact with the mineral. The G975 strain U(VI) biouptake, found in the 83-90% range for the aqueous solutions at equilibrium with CO_2 atmospheric pressure, was shown to exponentially reduce as the bicarbonate concentration was increased.

The studies carried out under task 1.2 included bioleaching experiments using autunite-bearing glass reactor bottles inoculated with the *Arthrobacter* sp. G975 strain and sterile cultureware. These experiments were conducted in a non-contact mode between the autunite mineral and bacterial cells. In addition, task 1.2 presents results evaluating the effect of bicarbonate on the bio-sorption of uranium by G975 cells and atomic force microscopy data used to monitor changes at the nanoscale level in cell surface topography, roughness and adhesion before and after the cells were exposed to various concentrations of uranium. The research under task 1.2 increases our understanding of the bacteria-uranium interactions in the presence of bicarbonate and assist in the remediation of groundwater and soil in the vadoze zone contaminated with U(VI).

The purpose of task 1.3 was to examine the effect of the carbonate complexation on the dissolution of the synthetic autunite mineral that was created as a result of the uranium stabilization through polyphosphate injection in contaminated groundwater. FY10 work was focused on finalizing the experimental work in order to obtain the rate of uranium released from the autunite mineral and to examine the effect of factors such as concentration of carbonate, pH

and temperature on the autunite weathering process. Chemical analysis on samples collected during the leaching experiments with synthetic autunite are still ongoing and these analytical results as well as a comparison with the rate of uranium release from natural autunite will be reflected in subsequent quarterly reports.

The study under Task 2 focused on adsorption of uranium by Hanford sediments and investigated calcite influence on the adsorption process. The information provided in this task will be helpful in understanding uranium mobility in the Hanford sediments in the presence and absence of calcite minerals and may help in the development of a remediation plan utilizing calcite-based technology.

ACRONYMS

AFM- atomic force microscope

atm- atmosphere

bgs- below ground surface

C- Celsius

CF-SGW- carbonate-free synthetic groundwater

CFU- colony forming units

DIW- deionized water

DOE- U.S. Department of Energy

EDS- energy-dispersive spectroscopy

FD- force distance

FS- force spectroscopy

HEPES-Na-2-(2-hydroxyethyl)-1-piperazine ethanesulfonic acid sodium salt hydrate

HMDS- hexamethyldisilazane

ICP-OES- inductively coupled plasma optical emission spectroscopy

KPA- Kinetic Phosphorescence Analyzer

mg/L- parts per million (ppm)

µg/L- parts per billion (ppb)

Na_2EDTA- ethylenediaminetetra-acetic acid disodium salt

PSD- position sensitive diode

SEM- scanning electron microscopy

SGW- synthetic groundwater

SMCC- Subsurface Microbial Culture Collection

SPW- synthetic pore water

TEM- transmission electron microscope

XRD- x-ray diffraction

INTRODUCTION

The Hanford Site is a facility located on the Columbia River in the state of Washington, built in 1943 as part of the Manhattan Project for the production of plutonium for the first atomic weapons. From 1944 to1980, the facilities of the Hanford Site were involved in the production of nuclear fuel (Young and Fruchter 1991). The fabrication of natural and slightly enriched uranium into fuel elements for nuclear reactors in Hanford's 300 Area, and the reprocessing of irradiated fuel in Hanford's 200 Area to obtain plutonium and other useful radioisotopes, has resulted in a wide variety of hazardous waste streams that contained chemical and radiological constituents (DeFord et al. 1994). Uranium (VI) is a key contaminant of concern at the Hanford Site, where the variety of hazardous waste streams were disposed onto the ground surface have directly impacted the vadose zone by creating a potential future source for groundwater contamination and risk to receptors through water uptake from contaminated wells or discharge to surface water. Despite extensive remediation efforts initiated in the early 1990s, uranium groundwater plumes identified in multiple locations around the site have persisted for many years.

Uranium (VI) is the most stable valence of uranium under oxidizing conditions, and due to complicated chemical behavior, it readily forms complexes with a variety of ligands (e.g., Grenthe, et al. 1992 and references therein). These complexation reactions often result in the formation of mobile aqueous species or precipitation of U-bearing minerals. The migration of U(VI) in the Hanford subsurface is retarded by both complexation to mineral surfaces and precipitation as uranium-bearing silicate and phosphate phases (Zachara et al. 2005). Environmental factors, such as pH, temperature, the presence of bicarbonate ions, and microbial activities have tremendous effects on both uranium and its minerals. Additional research is necessary to understand the effect of these factors on the behavior of U(VI) in groundwater and sediments.

During the fiscal year 2010, FIU ARC conducted three subtasks under Task 1 of this project: Task 1.1 - Sequestering Uranium at the Hanford 200 Area by In-Situ Subsurface pH Manipulation Using Ammonia (NH_3) Gas Injection, Task 1.2 - Investigation on Microbial-Meta-Autunite Interaction: Effect of Bicarbonate, and Task 1.3 - Effect of Bicarbonate on the Dissolution of Meta-Autunite. Task 2- Uranium (VI) Stabilization in the Hanford Site Vadose Zone (200 Area) Sediment Utilizing In Situ Calcite Mineral.

TASK 1.1 SEQUESTERING URANIUM AT THE 200 AREA BY IN SITU SUBSURFACE PH MANIPULATION USING NH_3 GAS

TASK 1.1 BACKGROUND

The study under task 1.1 involved a series of batch experiments outlined in the experimental matrix (Table 6) to evaluate the mechanisms and effectiveness of NH_3 gas injection, which has significant uncertainties under vadose zone specific conditions. The injection of a NH_3 gaseous mixture causes the formation of NH_4OH and a subsequent increase in pH; this manipulation will significantly alter the pore water chemistry due to dissolution of aluminosilicates and then upon the system pH returning to natural conditions various phases precipitate out and include uranium in those reactions. These chemical reactions can potentially control the mobility of uranyl cations in soil systems since co-precipitated contaminants have lower solubility of uranium-bearing phases and therefore are less available for migration (Szecsody et al. 2010).

A range of candidate technologies have been identified in the treatability of the main contaminants of concern and the technology that is being evaluated under task 1.1 is a new remediation approach for a vadose zone contaminated with radionuclides.

Silicate Chemistry: Interaction with Aluminum and Uranium

Silicone is the most common element found in the Earth's crust. About 95% of the rocks of the Earth's crust contain Si (Rayner-Canham and Overton, 2002). Given the abundance of Si-bearing minerals in the lithosphere, it is not surprising that silicate ion is found in most of the natural water bodies. Siever (1972) has reported a silicate concentration range of 3×10^{-5} to 1.3×10^{-3} M for rivers and 1×10^{-5} to 1.6×10^{-3} M for groundwater. Simple silicate mineral has a tetrahedral structure and is commonly referred to as silicate tetrahedron (Figure 1). The dissolution process of silicates and silica in aqueous solutions is mainly due to hydrolysis of Si-O-Si bonds, which results in the liberation of silicic acid and silicate into the aqueous phase (Sjoberg 1996).

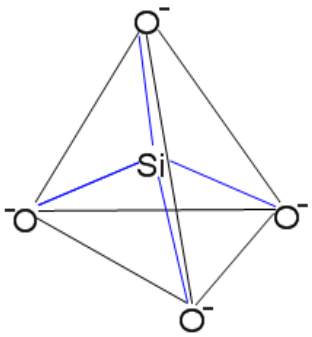

Figure 1. Silica-tetrahedron structure showing four oxygen atoms bonded (single) to an atom of silica.

While most of the silicates are not readily water soluble, sodium silicate (Na_4SiO_4) is soluble in water. When Na_4SiO_4 is dissolved in water, it has a tendency to increase the pH of the resulting solution, which is mainly due to its dissociation into SiO_4^{4-} containing four negatively charged oxygen atoms that are capable of scavenging H^+ ions (protonation) from the solution. Figure 2 (adapted from Yang et al. 2008) shows the speciation of silicate at different pH conditions,

which illustrates the role of protonation on the formation of different silicate/silica species. Yang et al. (2008) noted that with an increase in the concentration of silicate in solution, other complex forms like dimers, trimers, and oligomers were observed and tetramers and polymers reported at a concentration of 10 mmol L^{-1} for the pH values ranging between 9 and 13. In addition, at pH 9.5, Yang et al. (2008) discussed that 37% of the total Si is expected to be polymeric; the authors attributed this polymerization to the process of condensation of monomers at high concentration.

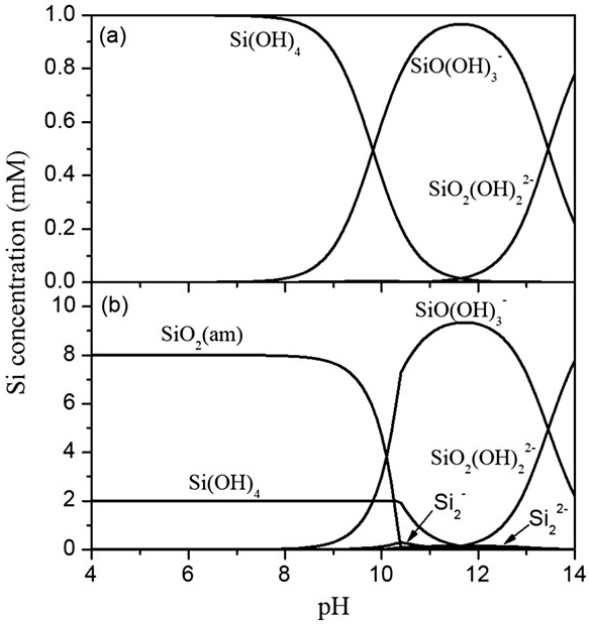

Figure 2. Equilibrium distribution diagram of silicate anions as a function of pH in (a) 1 mmolL^{-1} and (b) 10 mmol L^{-1} aqueous sodium metasilicate solution (Adapted from Yang et al. 2008).

Aluminum is the most abundant metal (8.3% by weight) in the earth's crust, and is found largely in igneous rocks and, to some extent, in other minerals like cryolite (Na_3AlF_6), spinel ($MgAl_2O_4$), garnet [$Ca_3Al_2(SiO_4)_3$], and beryl ($Be_3Al_2Si_6O_{18}$) to mention a few (Downs 1993). In natural waters and also in laboratory settings, aluminum reacts with silicate to form aluminosilicate mineral, which is insoluble in water and thus precipitates.

Al(III) has a tendency to expand its coordination number, thus giving possibilities for various other complexes, such as $Al(H_2O)_6^{3+}$ and $Al(H_2O)_5OH^{2+}$, with a coordination number of 6, and $Al(OH)_4^-$, with a coordination number of 4. Both the coordination number and the speciation depend on pH. It has been reported by Swaddle et al. (2005) that at low pH (pH< 3), Al (III) exists as the octahedral $Al(H_2O)_6^{3+}$ ion, while at basic pH (pH >7), tetrahedral $Al(OH)_4^-$ ions are dominant. Various other ions, including $Al(H_2O)_4(OH)_2^+$, $Al(OH)_3(aq)$, and $Al(OH)_4^-$, have been found to co-exist at pH values between 5 and 7. Since the pH of a solution has a significant influence on speciation of Al(III) in aqueous phase, the pH may also control aluminosilicate precipitation, as mentioned earlier. Based on the work of Pokrovsky et al. (1996), Farmer and Lumsdon (1994), Gout et al. (1999), and Swaddle (2001), it has been estimated that about 90% of Al(III) in water at pH 7 would be available as a complex $(H_2O)_5AlOSi(OH)_3^{2+}$. It is described in the following equation:

$$Al(H_2O)_6^{3+} + Si(OH)_4 \rightarrow (H_2O)_5AlOSi(OH)_3^{2+} + H^+ + H_2O \quad (1)$$

Hingston and Raupach (1967) investigated the reaction between aqueous silica and the crystalline aluminum hydroxide [$Al(OH)_3$] surface. The reaction between monosilicic acid and crystalline aluminum hydroxide resulted in multiple layers of silicic acid that eventually sorbed onto the aluminum hydroxide surface, with maximum sorption at pH 9.2. Aqueous sodium silicate solutions, at increasingly higher concentrations, were able to form very complex mixtures of polymers and charged species, which may slow the interaction with the aluminate anion and thereby affect the resulting kinetics and final product. Photomicrographs of solids obtained at high Si:Al molar ratio such as 25:1 and 40:1 that were utilized in the research for controlling the deposition of aluminosilicates on stainless steel surfaces, revealed that aluminosilicates are attached to the surfaces of large silica-rich, amorphous siliceous spheres, which produce some open porosity (Mattus et al. 2002). Although no trend in porosity was observed from lower to higher Si:Al ratios, this finding might have important implications for a co-precipitation process with U(VI).

In oxidized systems, uranium exists as the highly soluble uranyl [$U(VI)O_2^{2+}$] species. Sorption experiments for U(VI), conducted at basic pH ranging between 9 and 9.5 under atmospheric partial CO_2 pressure (pCO_2) conditions, demonstrated low affinity for silicate mineral mixtures (Prikryl 2001). At high pH (between 9 and 11) and in the presence of bicarbonate, most actinides reside as negatively charged hydroxide or carbonate (CO_3^{2-}) species, such as $(UO_2)_2(OH)_5^-$ and $UO_2(CO_3)_3^{4-}$. The surfaces of most solids are negatively charged at these pH values and are unlikely to adsorb ionic species, which can explain why the formation of negatively-charged, highly soluble U(VI)-carbonate species typically suppress U(VI) sorption in alkaline conditions. Co-precipitation is most likely the favored mechanism that can retard movement of U(VI) for the condition when these U(VI) complexes dominate the solution speciation.

Co-precipitation

An increase in pH following the injection of ammonia gas in a vadose zone has been proposed to affect mineral phases, which can potentially induce the dissolution of silica and aluminum from soil minerals (Szecsody et al. 2010). The subsequent decrease in pH to natural conditions would lead to precipitation of aluminosilicates that could possibly coat adsorbed U(VI) species in a process called co-precipitation.

Co-precipitation is defined as a process in which a solid is precipitated from a solution containing other ions (Curti 1997). These ions are incorporated into the solid by adsorption on the surface of the growing particles, physical entrapment in the pore spaces, or substitution in the crystal lattice. A co-precipitate may form either through precipitation of a new phase from a supersaturated solution or through recrystallization of a pre-existing phase at saturation (Curti 1997). This process will reduce the mobility and toxicity of the toxic trace elements that are incorporated into the mineral. Adsorption is one of the principle mechanisms of co-precipitation. It is a process responsible for the reversible uptake of ions, atoms, and molecules on a mineral surface. In this case, the adsorbates are bound to the solid's surface by physical or chemical interactions between an adsorbate and the adsorbent. Co-precipitation and adsorption are thus related by the time during which an adsorbate is present in a suspension (mixture of solid and liquid).

Several solid and solution variables must be considered when dealing with co-precipitation as a treatment option. These include the equilibrium concentration of the species in solution, the suspension pH, and the presence of other interacting ions. Also, the properties of the solid

adsorbent are important. These comprise of the type of solid formed, surface area available, and surface charge. In short, co-precipitation is controlled by a number of important variables, which are specific to a given system. The classification of various co-precipitation mechanisms has been presented by Curti (1997):

- Isomorphous replacement when the trace ions are fixed at lattice sites occupied by regular ions. This mechanism is favored in case of chemical affinity between the trace ion and the substituted ion.
- Incorporation in crystal defects when the co-precipitation trace ions are incorporated on sites of crystal dislocations or defects.
- Non-uniform incorporation when trace components may be incorporated into a solid through physical isolation of discrete particles from the solution.

Two different approaches are commonly used to quantify co-precipitation processes: solid solution models and distribution models based on phenomelogical partition coefficients. The first approach is based on the laws of chemical thermodynamics. A common problem with this model is the lack of parameter values needed to evaluate the activities of chemical components in the solid. Moreover, current thermodynamic models are limited to isomorphous solid solutions and are inherently unable to account for kinetic effects (the rate of mineral precipitation has a profound effect on co-precipitation reactions).

Distribution laws are not affected by the problems mentioned previously for thermodynamic models, and distribution laws can be also applied to non-isomorphous mixtures. However, a strong limitation of distribution models is that partition coefficients used in these models are conditional constants, which depend on a number of physicochemical parameters. To be able to use distribution laws, knowledge of the dependence of partition coefficients is fundamentally important. The definition of a partition coefficient is given in the classic paper of Doerner and Hoskins (1925):

$$\lambda = \frac{\{T\}_{surface}}{\{C\}_{Surface}} \frac{[C]}{[T]} \quad (2)$$

In the above equation, λ is a proportionality factor, and λ is called a heterogeneous partition coefficient, T is the trace element, and C is the carrier element; [T] and $\{T\}_{surface}$ are the total concentration of the co-precipitated trace element in solution (in units of molarity, M) and the mole fraction of the trace element at the surface layer of the precipitating solid, respectively; [C] and $\{C\}_{Surface}$ are the total concentration of the co-precipitated carrier ion in solution (in units of molarity, M) and the mole fraction of the carrier ion at the surface layer of the precipitating solid, respectively. The Doerner-Hoskins relation for heterogeneous co-precipitation of trace elements with major (carrier) elements was used to analyze coprecipitation process of various trace metals (Gordon and Rowley, 1956; Curti, 1997; Curti , 1999; Roden et al, 2002). It is important to note that the composition of a crystal precipitating from a solution is not uniform.

TASK 1.1 OBJECTIVES

The objective of this task was to evaluate the roles of major pore water constituents and time on the formation of precipitates after NH_3 injection to the vadose zone in the Hanford Site 200 Area. This task examined the effect of concentration ratio of silicon and aluminum, in the presence of various bicarbonate concentrations, on the co-precipitation process of U(VI) under conditions mimicking the pore water of the vadose zone in the Hanford Site 200 Area. Further studies will

focus on the detailed characterization of precipitates with uranium and evaluation of their solubility. Solubility studies will be conducted over the pH range of 6 to 11 in the presence of bicarbonate, calcium, and major pore water ions and cations. Studies will analyze mineralogical and morphological characteristics by means of X-ray diffraction (XRD), Scanning Electron Microscope Energy-Dispersive Spectroscopy (SEM-EDS), to confirm the identity of the solid phase before and after solubility experiments.

TASK 1.1 MATERIALS AND METHODS

Hanford Site Synthetic Porewater Composition

The synthetic pore water (SPW) composition was created to mimic conditions found in the vadose zone at the Hanford Site 200 Area. The composition of borehole 299-E33-45 pore water that has been previously characterized in terms of concentrations of major cations (Al, Ba, Ca, Fe, K, Mg, Na, Si, Sr), anions (NO_3, F, NO_2, Cl, SO_4, PO_4, HCO_3), and pH (Serne et al. 2002) was used to prepare the SPW formulation. The concentrations of ions and uranium for different sediment layers were averaged and the summary is presented in Table 1, Table 2, and Table 3. The average pH in all sediment layers was observed as 7.5 (Serne et al. 2002).

Table 1. Major Anions in Hanford Site Pore Water Near Borehole 299-E33-45

Depths, ft	NO_3, mg/L	F, mg/L	NO_2, mg/L	Cl, mg/L	SO_4, mg/L	PO_4, mg/L	HCO_3, mg/L
111.14-119.04	661.00	16.45	2.85	20.50	389.50	167.50	5466.50
120.1-120.9	1163.50	6.33	1.98	33.25	775.25	1080.50	4754.75
121.24-141.25	1020.60	18.62	1.55	34.00	899.40	681.80	7716.60
150.55-165.55	2327.13	12.70	8.00	85.88	21714.13	10.87	1843.67
168.65-169.55	1740.50	3.48	4.65	129.00	2013.75	7.27	665.00
C_{Ave}	1637.30	11.60	4.52	67.26	8267.17	355.74	3945.57

Table 2. Major Cations in Hanford Site Pore Water Near Borehole 299-E33-45

Depths, ft	Al, mg/L	Ba, mg/L	Ca, mg/L	Fe, mg/L	K, mg/L	Mg, mg/L	Na, mg/L	Si, mg/L	Sr, mg/L
111.14-119.04	42.80	0.48	44.85	48.15	55.70	13.55	3320.00	435.50	0.19
120.1-120-9	17.67	0.20	47.03	16.66	43.33	12.19	3235.00	214.95	0.17
121.4-141.25	16.92	0.22	36.80	15.40	54.10	7.66	4254.00	301.62	0.16
151.55-165.55	9.91	0.43	1306.00	0.61	325.38	387.31	8036.13	195.13	5.59
168.65-169.55	2.27	0.16	383.75	0.07	68.23	117.80	1077.25	65.68	1.70
Average concentrations in the layers with highest U concentrations	14.32	0.30	541.08	10.66	149.18	160.17	4758.61	220.11	2.32

Table 3. Uranium in Hanford Site Pore Water Near Borehole 299-E33-45

Depths, ft	U_{238}, mg/L
111.14-119.04	138.20
120.1-120-9	559.50
121.4-141.25	492.60
151.55-165.55	142.26
168.65-169.55	117.09
Average concentrations in the layers with max U concentrations	286.26

For the series of experiments conducted in the present study, two relatively low concentrations of U(VI) were tested: 0.5 ppm and 2.0 ppm. These U(VI) concentrations were considered as preliminary concentrations to test the potential remediation technique of NH_3 gas injection into contaminated solutions. These U(VI) concentrations are also relatively higher than those found at the depths just below the ground surface. In future experiments, higher concentrations of U(VI) will be tested.

The SPW, which mimics the background pore water composition, was formulated by combining three distinct solutions (described in Table 4) and then injecting U(VI) at a concentration of either 2.0 parts per million (ppm) or 0.5 ppm.

Table 4. Stock Solutions A, B, and C

Stock Solution	Salts	Salt amount (g) in 50ml
A	$KHCO_3$	0.1
	$NaHCO_3$	9.2
B	Na_2SO_4	3.4
	$MgSO_4$	0.3
C	$Ca(NO_3)_2{\cdot}4H_2O$	1.0
	$CaCl_2{\cdot}2H_2O$	0.1
	Al(NO3)3	0.5
D	$Na_2SiO_3{\cdot}9H_20$	0.07

Sample Preparation

In the initial experiments, only four components were used in the test solutions: uranium, silica, aluminum and bicarbonate. Past observations showed that the concentration of Al released during the dissolution from soil by 1 mol L^{-1} NaOH is relatively small, resulting in 5.1 mM of Al in the soil solution (Qafoku et al. 2003). On the other hand, as a result of increasing soil pH, the concentration of Si in pore water was observed to be as high as 10 g L^{-1} (Szecsody 2010). For

these reasons, the tests were performed with varied Si concentrations to study different Si:Al molar ratios, including 1.8:1, 17.6:1, 35.2:1, 52.8:1, 70.4:1, and 88:1. The concentration of Al in all tests remained unchanged at 2.8 mM. This concentration of Al (2.8 mM Al) represents a value that is between the highest observed Al concentration in the pore water of the Hanford Site 200 Area, which is about 0.8 mM Al, and the concentration of Al released during the dissolution from soil by 1 mol L^{-1} NaOH reported by Qafoku et al. (2003), which was 5.1 mM Al.

Stock solutions of Al (28.4 mM), Si (350 and 420 mM), and HCO_3^- (29 and 100 mM) were first prepared in deionized water (DIW) from the salts $Al(NO_3)_3 \cdot 9H_2O$, $Na_2SiO_3 \cdot 9H_20$, and $KHCO_3$, respectively (Table 5). The stock solution of uranyl nitrate dissolved in DIW was prepared from uranyl nitrate hexahydrate 1000 ppm stock (Fisher Scientific).

Table 5. Stock Solutions Used to Prepare Various Si/Al Molar Ratios

Stock solutions	
Solutions	**Concentration**
Aluminum	28.4 mM
Silicate	350-420 mM
Bicarbonate	29 mM
	100 mM
Uranium	100 ppm

As discussed, two different U(VI) concentrations (0.5 ppm and 2 ppm) and three different bicarbonate concentrations (0 mM, 2.9 mM, and 25 mM) were tested. For each bicarbonate concentration, six different test solutions were prepared. Each of these test solutions had a different molar ratio of Si:Al, which was prepared by mixing a measured volume of the silicate stock solution with a measured volume of the aluminum stock solution. This mixture was then added to the test solution with a measured volume of the appropriate bicarbonate stock solution (unless no bicarbonate was used). The pH of the resulting solution was adjusted to 7.5 by titration with concentrated nitric acid and deionized water (DIW) was added to each test solutions so that each test solution had a total final volume of 50 mL. The pH value of 7.5 was previously observed in pore water composition in the Hanford Site 200 Area vadose zone (Serne et al. 2002). After that, NH_3 gas (5% NH_3 in 95% N_2) was injected into each solution through 20 µm pores of a metal gas sparger (Mott Corporation) until the pH of the solution reached a value of approximately 11. Then, six test samples, each with a volume of 5 mL, were extracted from each test solution and added to individual polyethylene 15mL tubes: three of the samples were each amended with a U(VI) concentration of 0.5 ppm, and the other three samples were each amended with a U(VI) concentration of 2 ppm. Control samples were prepared in DIW amended with U(VI) at concentrations of 0.5 ppm and 2 ppm U(VI) to test for U(VI) losses from the solutions due to sorption to tube walls and caps. All control and experimental tubes were kept in an incubator/shaker at 100 rpm and at a temperature of 25 °C. After two days, the solutions were centrifuged for 15 minutes at 4000 rpm and analyzed for U(VI), Si, and Al.

There were a total of six experimental sets, each with a different combination of U(VI) concentration and bicarbonate concentration. Each set had six different test solutions (each test

solution with a different Si:Al molar ratio), for a total of thirty-six test solutions. A description of the experimental matrix is shown in Table 6 (batches 1, 2, and 3).

Table 6. Experimental Matrix

Batch number	HCO_3, mM	Si:Al molar ratio (Al=2.8mM)					
1	0	1.8	17.6	35.2	52.8	70.4	88.0
2	2.9	1.8	17.6	35.2	52.8	70.4	88.0
3	25	1.8	17.6	35.2	52.8	70.4	88.0
4	50	1.8	17.6	35.2	52.8	70.4	88.0
5	75	1.8	17.6	35.2	52.8	70.4	88.0
6	100	1.8	17.6	35.2	52.8	70.4	88.0

The sodium metasilicate used to prepare the silicate stock solution has a high solubility in water, up to 61 wt % (percent by weight) at 30^{o}C. However, the experiments were run by limiting the Si:Al molar ratio to a maximum of 88:1, which corresponds to a Si concentration of about 7.0 g L^{-1}. Experiments to evaluate the effect of higher bicarbonate concentration, up to a concentration of 100 mM bicarbonate found in the pore water composition (Table 1) on the U(VI) sequestration process (batches 4 through 6, Table 6) are ongoing and results will be available in the next report.

Analysis Procedures

After completing the initial experiments described above, samples of the supernatant from each vial were analyzed to determine the remaining U(VI) concentration in each solution using a Kinetic Phosphorescence Analyzer KPA-11 (Chemcheck Instruments, Richland, WA) instrument, and to determine the remaining Al and Si concentrations in each solution, using inductively coupled plasma-optical emission spectroscopy (ICP-OES) (PerkinElmer). In addition, the accuracy of the initial Al and Si stock solutions, prepared by weight, were tested with ICP-OES.

For analysis with the KPA machine, an aliquot was extracted from the supernatant of each test sample and diluted with 1% nitric acid between 5 to 100 times, and then each aliquot was analyzed using the KPA machine. Samples with higher Si:Al ratios and bicarbonate concentrations were generally diluted more to avoid interferences with the KPA readings. For analysis with the ICP-OES machine, an aliquot was extracted from the supernatant of each test sample and diluted between 100 to 200 times with DIW in conical polypropylene tubes, and then each aliquot was analyzed with the IPC-OES machine.

TASK 1.1 RESULTS AND DISCUSSION

As discussed above and as outlined in the experimental matrix in Table 6, six sets of experiments with two different uranium concentrations and three different bicarbonate concentrations were performed. Presented results are based on the percentage removal of the elements of interest: U(VI), Al and Si. Since the present work employed high silicate concentrations, a few of the data points appear to be out of line with the remaining data points, which may have been due to

additional reactions with silicate in solution, or possibly due to the high dilution factors used for analyzing the test samples. The results of the analysis are summarized in the following plots.

Figure 3 represents the percent reduction of Si in solutions that had U(VI) concentrations of 0.5 ppm and 2 ppm.

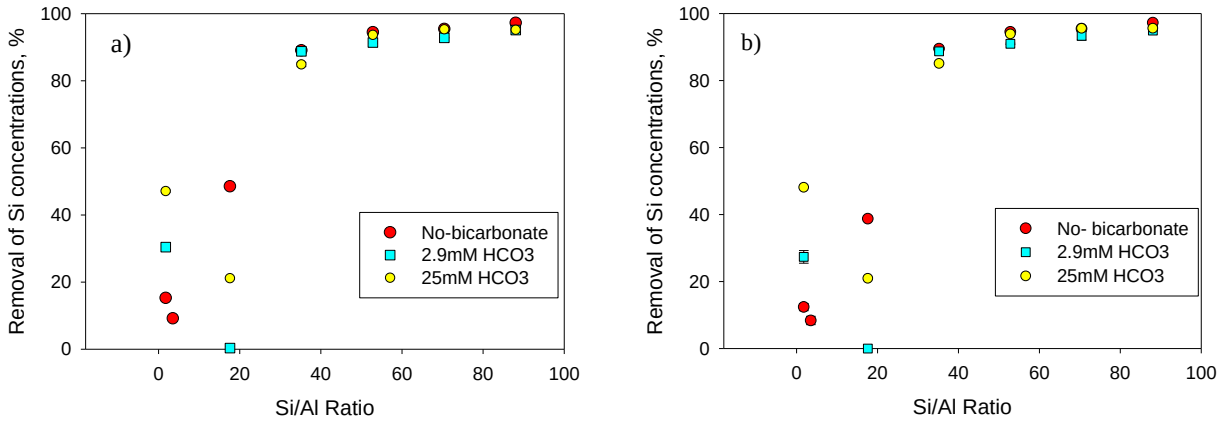

Figure 3. Reduction of Si concentration in solution for U(VI) of a) 0.5ppm b) 2ppm.

From

Figure **3**, a reduction in Si concentration can be observed for most of the molar ratios of Si:Al. The experimental runs with Si:Al molar ratios below 35.2:1 had relatively low values in the range of 0-50% for the removal efficiency of Si concentration. On the other hand, the experimental runs with higher Si:Al molar ratios had relatively high removal efficiencies reaching up to 97% removal of Si concentration. Concentrations of bicarbonate (HCO_3^-) up to 25 mM did not appear to alter the efficiency of removal of Si concentration at higher molar ratios of Si:Al. These results suggest that the percent removal of Si increases with an increase in Si concentration in solution until it's stabilized to a constant value. Nevertheless, future experiments with higher HCO_3^- concentrations will be performed to provide further results for Si removal efficiency.

Figure 4 corresponds to the percent reduction of Al in test solutions with U(VI) concentrations of 0.5 ppm and 2.0 ppm. For solutions that had no bicarbonate. The results for Al removal (Figure 4) were found to be more consistent than the results for Si removal (Figure 3) over the various molar ratios of Si:Al.

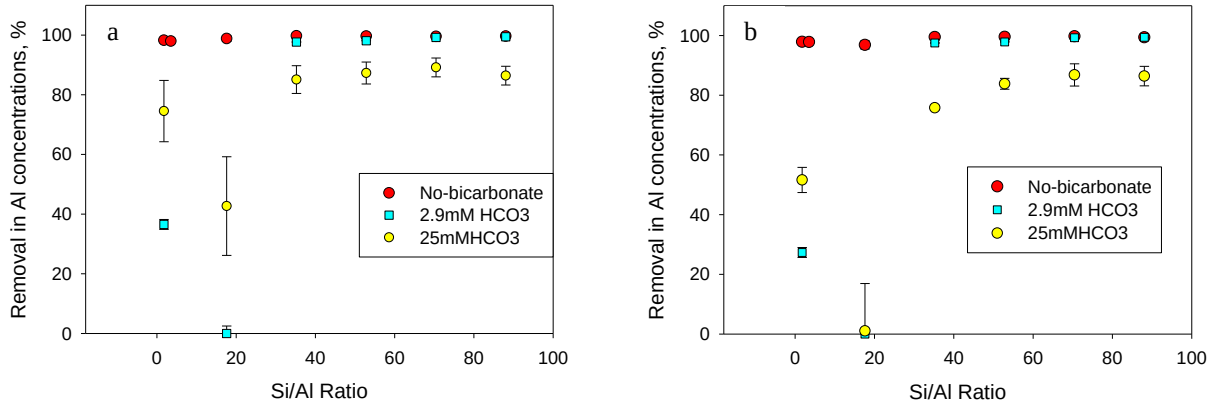

Figure 3Figure 4. Reduction of Al concentration in solution for U(VI) of a) 0.5ppm b) 2ppm.

From Figure 4, it can be observed that different HCO_3^- (bicarbonate) concentrations in the test solutions affected the removal efficiency of Al. In solutions that did not contain HCO_3^-, the overall removal efficiency of Al was close to 98%-99% for all the molar ratios of Si:Al. However, when HCO_3^- was present in the solutions, percent removal of Al deviated. This was first noted for the solutions that contained 25 mM HCO_3^-, where the maximum percentage removal of Al was close to 89%, almost 10% less compared to that of the solutions that did not contain HCO_3^-; however, as discussed above, future experiments with HCO_3^- concentrations of 50 mM will provide more results and further conclusions. For the molar ratio of Si:Al at 17.6:1, the removal efficiencies for Si and Al exhibited a decline. Solutions with higher concentrations of bicarbonate tended to have a sharper decline in removal efficiencies for Si and Al, and solutions with no bicarbonate had little or no observable change in removal efficiencies for these elements. As discussed above, future experiments with HCO_3^- concentrations of 50 mM, 75 mM, and 100 mM will provide more results and further conclusions.

Figure 3 and Figure 4 both suggest that the addition of NH_3 to test solutions resulted in the removal of Si and Al from the supernatant solutions. Figure **5** presents the analyses for the percent removal of U(VI) from the test samples at the two different concentrations of U(VI) of 0.5 ppm and 2 ppm over the range of HCO_3^- concentrations tested. Results obtained for both of the tested U(VI) concentrations showed similar trends, indicating that the chosen range of initial U(VI) concentration did not appear to affect the efficiency of U(VI) removal.

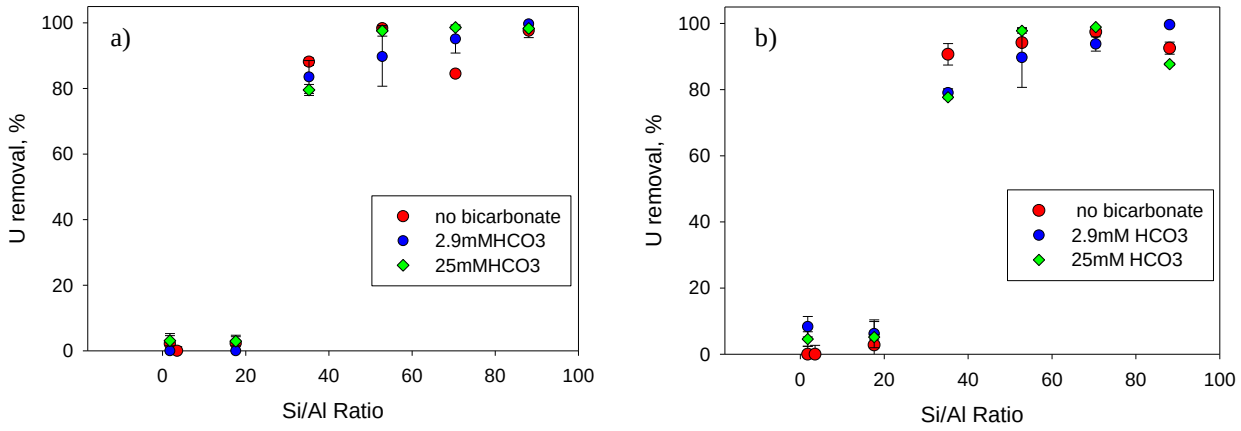

Figure 5. Reduction of U(VI) concentrations a) 0.5ppm & b) 2ppm.

Data analysis of U(VI) reduction in the supernatant solutions, presented in Figure 5, shows that the maximum percent removal of U(VI) was close to 98% for molar ratios of Si:Al over 52.8:1. At Si:Al molar ratios of 1.8:1 and 17.6:1, there was no observed reduction in the U(VI) concentration in the supernatant solutions; therefore, the process of U(VI) removal does not appear to be efficient when the concentration of Si is up to 10 times higher than the concentration of Al in solution. Samples containing HCO_3^- did not reveal any significant changes in the percent removal of U(VI) compared to samples that did not contain HCO_3^-; at least for concentrations of HCO_3^- of 25 mM or less, the reduction in the U(VI) concentrations in the supernatant solutions were not affected by the different HCO_3^- concentrations tested. Experimental runs for both concentrations of U(VI) that were tested followed the same trend: no

observed reduction of U(VI) concentrations at Si:Al molar ratios of 1.8:1 and 17.6:1, then a percent removal of U(VI) between 75% -85% at a Si:Al molar ratio of 35.2:1, and then the highest percent removal of U(VI) at Si:Al molar ratios of 52.8:1, 70.4:1 and 88:1.

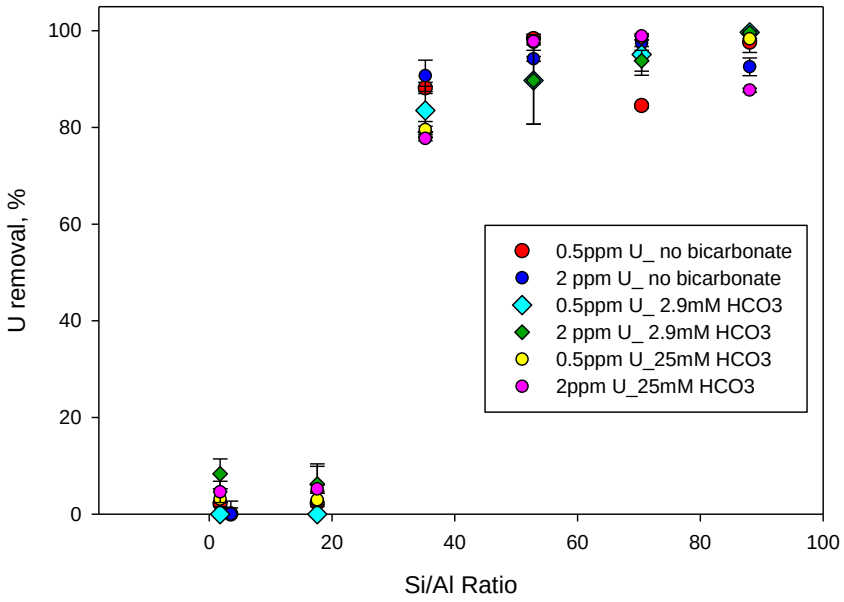

Figure 6 illustrates the comparison between the six sets of the experiments in the present study that have been performed thus far. It is evident that results of the six sets of experiments follow a similar path with relatively small deviations between triplicate samples.

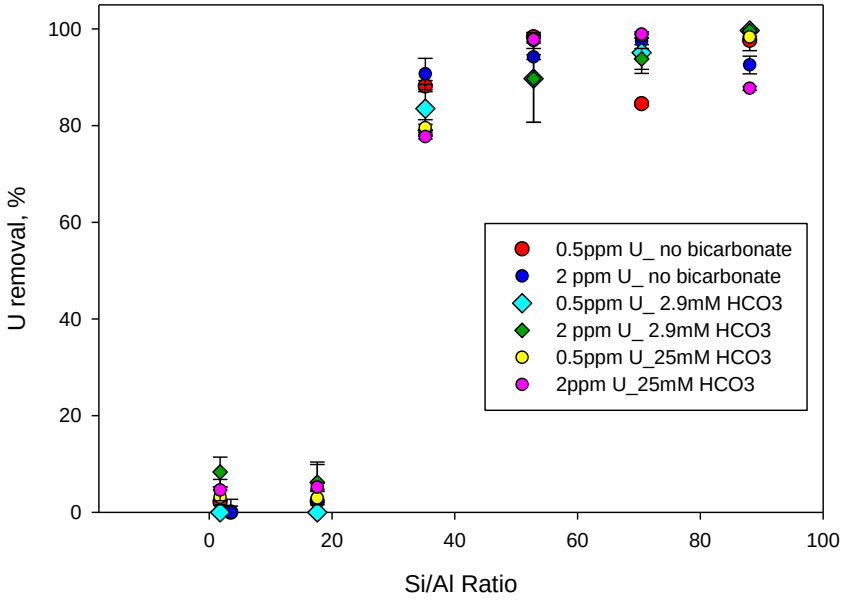

Figure 6. Reduction of U concentration for initial U concentrations of 0.5 ppm & 2 ppm.

Future experiments, the details of which are discussed below, will explore the effect of higher concentrations of bicarbonate (up to 100 mM) on the U(VI) co-precipitation process with Al and Si, and examine the mineralogy and microstructure of the formed precipitate.

TASK 1.1 CONCLUSION

From the data presented above, the removal efficiency of uranium (Figure 5) was not significantly affected by the different bicarbonate concentrations tested thus far, which were 0 mM, 2.9 mM, and 25 mM bicarbonate. Moreover, the removal efficiency of uranium was not significantly affected by the different U(VI) concentrations tested: 0.5 ppm and 2.0 ppm. For the lower Si:Al molar ratios of 1.8:1 and 17.6:1, the removal efficiency of uranium was relatively low (≤ 8% or less). For the following Si:Al molar ratio of 35.2:1, the removal efficiency of uranium increased to average ~82% for all three bicarbonate concentrations. For the higher Si:Al molar ratios of 52.8:1, 70.4:1, and 88:1, the removal efficiency of uranium increased to between ~85% and ~97%. For the test solutions with 2.9 mM and 25 mM bicarbonate, there was a decrease and then a sharp increase in Si removal efficiency over the first three tested molar ratios of Si:Al, followed by slightly increasing Si removal efficiency over the higher Si:Al molar ratios. In addition, the removal efficiency of Si appeared to fluctuate slightly with changing bicarbonate concentration. At the lower Si:Al molar ratio of 1.8:1, the removal efficiency of Si was higher for higher bicarbonate concentrations. However, for the Si:Al molar ratios above 1.8:1, this trend appeared to reverse, with higher removal efficiencies of Si observed for the solutions without bicarbonate.

For the test solutions without bicarbonate, the removal efficiency of Al was relatively high, around 98%, for all the Si:Al molar ratios that had been tested. For the test solutions with 2.9 mM and 25 mM bicarbonate, a decrease and then a sharp increase in removal efficiency of Al was observed over the first three tested Si:Al molar ratios, followed by constant or slightly increasing Al removal efficiency over the higher Si:Al molar ratios. In addition, the removal efficiency of Al was significantly lower for the solutions with the higher bicarbonate concentration of 25 mM. The removal efficiency of Al appeared to increase with decreasing bicarbonate concentration.

From the above results, it appears that U(VI) removal efficiency is affected more by the Si:Al molar ratio in solution than by the bicarbonate concentration in solution. At the higher Si:Al molar ratios (35.2:1 and above), a relatively high removal efficiency of U(VI) (approximately 93% and higher) was observed. These results are promising for the potential implementation of NH_3 gas injection in the VZ for removal of U(VI) from pore water. The following section discusses the future work in this task to further explore this potential remediation technology and to give more support to the results presented so far.

Task 1.1 Future Work

For the next series of experiments to be conducted in Task 1.1, the potential of using NH_3 gas injection into a vadose zone to remove uranium from pore water will be further investigated. Test solutions will be prepared at three different bicarbonate concentrations to test how higher bicarbonate concentrations affect the removal efficiency of uranium and other constituents from solution. The additional bicarbonate concentrations that will be tested include 50 mM, 75 mM, and 100 mM. In addition, a higher aluminum concentration of 5 mM Al will also be tested. The experimental matrix for the next set of experiments is presented in Table 7.

Table 7. Experimental Matrix for the Next Experiments to be Conducted in Task 1.1

Batch number	HCO_3^-, mM	U(VI), ppm	Si:Al molar ratio (Al = 5mM)					
1	0	0.5	1	10	20	30	40	50
1	0	2.0	1	10	20	30	40	50
2	2.9	0.5	1	10	20	30	40	50
2	2.9	2.0	1	10	20	30	40	50
3	25	0.5	1	10	20	30	40	50
3	25	2.0	1	10	20	30	40	50
4	50	0.5	1	10	20	30	40	50
4	50	2.0	1	10	20	30	40	50
5	75	0.5	1	10	20	30	40	50
5	75	2.0	1	10	20	30	40	50
6	100	0.5	1	10	20	30	40	50
6	100	2.0	1	10	20	30	40	50

In addition, samples will be taken over time to determine the kinetics of the removal of uranium from test samples. For the initial experiments, samples were taken two days after the addition of U(VI) to the test samples.

The first series of experiments for Task 1.1 show promising results for the potential remediation technique of NH_3 gas injection into a vadose zone, which presumably would cause the precipitation of aluminum and silicon minerals and the co-precipitation of U(VI). Further experiments with NH_3 gas injection into solutions, discussed above, are required to properly evaluate the potential of using the proposed remediation technique of NH_3 gas injection into a vadose zone contaminated with U(VI).

TASK 1.1 REFERENCES

Curti, E, 1997. Coprecipitation of radionuclides: basic concepts, literature review and first applications. PSI-Bericht Nr. 97-10

Curti, E., 1998. Coprecipitation of Radionuclides During Cement Degradation: A Preliminary Modelling Study for the Swiss L/ILW Repository. CH-5332. Switzerland.

Curti, E, 1999. Coprecipitation of radionuclides with calcite: estimation of partition coefficients based on a review of laboratory investigations and geochemical data. Applied Geochemistry 14, pp.433-445.

Farmer, V.C., and Lumsdon, D.G. (1994). An assessment of complex formation between aluminum and silicic acid in acid solutions. Geochim. Cosmochim. Acta 58 (1994), pp. 3331–3334

Gordon, L and K.Rowley, 1956. Coprecipitation of Radium with Barium Sulfate. Anal. Chem., 1957, 29 (1), pp 34–37

Gout, R., Pokrovski, G.S., Schott, J., Zwick, A.,2000. Raman Spectroscopic Study of Aluminum Silicate. Complexes at 20C in Basic Solutions. Journal of Solution Chemistry, Vol. 29, 12, pp.1173-1186

Hingston FJ and M Raupach. 1967. The reaction between monosilicic acid and aluminium hydroxide. I. Kinetics of adsorption of silicic acid by aluminium hydroxide. Australian Journal of Soil Research 5, 2, pp. 295 – 309.

Roden, EE., Leonardo, MR. and F. Grant Ferris, 2002. Immobilization of strontium during iron biomineralization coupled to dissimilatory hydrous ferric oxide reduction. Geochimica et Cosmochimica Acta, Vol. 66, No. 16, pp. 2823–2839.

Mattus A. J., Mattus, C. H., Hunt, R. D., 2002. Investigation into the control and kinetics of aluminosilicate formation on stainless steel surfaces at 100^{o}C. Report ORNL/TM-2002/47 prepared for the U.S. DOE under contract DE-AC05-00OR22725.

Pokrovsky, G.S., Schott, J., Harrichoury, J.-C., Sergeyev, A.S. (1996). The stability of aluminum silicate complexes in acidic solutions from 25 to 150^{o}C. Geochim. Cosmochim. Acta, 60, 14, pp. 2495-2501.

Prikryl, J., Jain, A., Turner, D. R. and R. T. Pabalan, 2001. Uranium(VI) sorption behavior on silicate mineral mixtures, J. Contam. Hydrol. 47, pp.241-253.

Qafoku NP, Ainsworth CC, Szecsody JE, Qafoku OS, 2003. Aluminum Effect on Dissolution and Precipitation under Hyperalkaline Conditions: I. Liquid Phase Transformations. J Environ Qual. 32, 6, pp.2354-63.

Serne RJ, MJ Lindberg, SR Baum, GV Last, RE Clayton, KN Geiszler, GW Gee, VL LeGore, CF Brown, HT Schaef, RD Orr, MM Valenta, DC Lanigan, IV Kutnyakov, TS Vickerman, CW Lindenmeie, 2008. Characterization of Vadose Zone Sediment: Borehole 299-E33-45 Near BX-102 in the B-BX-BY Waste Management Area. 2002. PNNL-14083. Contract DE-AC06-76RL01830.

Siever R. (1972) Silicon-abundance in natural waters. In Handbook of Chemistry, vol. II-2 (ed. K. H. Wedepohl). Springer, Berlin, II-2, 14-I.

Sjoberg, S, 1996. Silica in aqueous environment. Journal of non-crystalline solids, 196, pp.51-57.

Swaddle, T.W., Rosenqvist, J. Yu, P., Bylaska, E., Phillips, B.L., Casey, W.H. (2005). Kinetic evidence for five-coordination in $AlOH(aq)^{2+}$ ion. Science, vol. 308, 5727 pp. 1450-1453.

Szecsody, JE, MJ Truex, L Zhong, MD Williams, CT Resch, JP McKinley, 2010. Remediation of Uranium in the Hanford Vadose Zone Using Gas-Transported Reactants: Laboratory-Scale Experiments. PNNL-18879. Contract DE-AC05-76RL01830.

Yang , X., Roonasi, P., Holmgren, A. 2008 A study of sodium silicate in aqueous solution and sorbed by synthetic magnetite using in situ ATR-FTIR spectroscopy Journal of Colloid and Interface Science 328 (2008) 41–47

TASK 1.2. INVESTIGATION ON MICROBIAL-META-AUTUNITE INTERACTIONS: EFFECT OF BICARBONATE

TASK 1.2 BACKGROUND

Uranium contamination is primarily found in oxic circumneutral-to-mildly-basic geochemical conditions, where U(VI) dominates as the highly soluble and stable uranyl ion, UO_2^{2+} (Langmuir1997, Murphy and Shock 1999). Its behavior in natural systems depends on aqueous speciation and concentration of ligands (e.g. carbonate, phosphate) forming uranyl complexes (Langmuir 1997). These complexation reactions often result in the formation of mobile aqueous species or precipitation of insoluble U-bearing minerals (Finch and Murakami 1999).

The presence of phosphate in soil and groundwater systems can control the actinide behavior in geological settings due to the formation of uranyl-phosphate complexes that feature extremely low solubilities under circumneutral pH conditions (Devivo et al. 1984). Autunite and meta-autunite minerals $\{X^{n+}_{3-n}[(UO_2)(PO_4)]_2\ xH_2O\}$ largely limit the mobility of dissolved U(VI) in soils contaminated by actinides and are an extremely important group of uranyl minerals when considering U sequestration. Autunite minerals precipitation as a result of polyphosphate injection was identified as a feasible remediation strategy for sequestering uranium in contaminated groundwater and soil in situ at the Hanford Site (Vermeul et al. 2009). Autunite stability under vadose and saturated zone environmental conditions can help to determine the long-term effectiveness of this remediation strategy (Wellman et al. 2007).

The autunite mineral features a basal sheet-like structure due to the ability of uranyl ion to polymerize and bond with ligands along its equatorial plane (Burns et al. 1996). Autunite sheet structure, normally characterized by tetragonal morphology, is formed by the sharing of vertices between uranyl square bipyramids and phosphate tetrahedra, with composition of $[(UO_2)(PO_4)]^-$. The solubility constant of the calcium form of autunite, log K_{sp}, has been measured as -44.7 (Grenthe et al. 1992, Langmuir 1997). Associated solubility products are presented in eq. 3.

$$Ca(UO_2)_2(PO_4)_2 \bullet xH_2O_{(s)} = xH_2O_{(l)} + Ca^{2+} + 2PO_4^{3-} + 2UO_2^{2+} \quad (3)$$

The release of U and P during dissolution, as previously investigated by Wellman et al. (2006), was found non-stoichiometric over the pH 7-10 range conditions. The aqueous phosphate concentrations were basically unchanged during the equilibrations, indicating that the solid phase dissolution reactions did not significantly affect the phosphate concentrations (Rai et al. 2005).

Aqueous carbonate at a common groundwater CO_2 pressure of 10^{-2} to$10^{-3.5}$ atm are predominant species affecting the dissolution of actinides and facilitating uranium desorption reactions from soil and sediments, thus increasing uranium mobility in natural waters (Langmuir 1978). The mobility of U(VI) in aquifers with circumneutral pH conditions is explained by the formation of highly soluble and stable uranyl-carbonato complexes, $UO_2(CO_3)_2^{2-}$ and $UO_2(CO_3)_3^{4-}$. In a calcium-rich environment, the large formation constants of soluble calcium uranyl carbonate complexes, $[Ca_2UO_2(CO_3)_3^0(aq);\ CaUO_2(CO_3)_3^{2-}]$, influences the speciation of uranium (Langmuir 1978, Bernhard et al. 2001). The stability constants for these reactions are presented in Table 8 (Guillaumont et al. 2003). Simulations conducted by varying Ca concentrations at a constant pH 8.0 showed that $CaUO_2(CO_3)_3^{2-}$ dominates in the Ca concentration range of 0.3-2.2

mmol/L and $Ca_2UO_2(CO_3)_3^0$ becomes the major species at Ca>2.2 mmol/L (Dong and Brooks 2006).

Table 8. Stability Constants for Some Reactions Involving Uranyl-Carbonate Aqueous Species

Reactions	$Log_{10}K$
$UO_2^{2+} + CO_3^{2-} = UO_2CO_3^0$	9.94
$UO_2^{2+} + 2CO_3^{2-} = UO_2(CO_3)_2^{2-}$	16.61
$UO_2^{2+} + 3CO_3^{2-} = UO_2(CO_3)_3^{4-}$	21.84
$2Ca^{2+} + UO_2^{2+} + 3CO_3^{2-} = Ca_2UO_2(CO_3)_3(aq)$	29.80[a]
$UO_2^{2+} + Ca^{2+} + 3CO_3^{2-} = CaUO_2(CO_3)_3^{-2}$	25.4

[a] Kalmykov and Choppin, 2000.

Microbial activities in many environmental systems are additional layers of complexity that affect U(VI) mobility. In nature, a variety of bacteria may enhance the mobility of heavy metals or radionuclides by dissolution and desorption due to the secretion of protons and various ligands. The bacterial cell wall contains functional groups such as the carboxyl and phosphate that help in the adsorption of the uranyl species at environmentally relevant pH values (Beazley et al. 2007, Merroun et al. 2005). Previous research (Suzuki and Banfield 2004, Martinez et al. 2007, Nedelkova et al. 2007) identified surface bacterial uranium precipitation as autunite/meta-autunite mineral phases at pH ranging from 4.5 to 7. Macaskie et al. (1992, 1994) observed precipitation around the cells of *Citrobacter* sp. composed of HUO_2PO_4 and $NaUO_2PO_4$ at pH 6.9.

The most recent results on the effects of temperature, pH, and aqueous organic material on the abiotic dissolution of synthetic Na meta-autunite and natural Ca meta-autunite minerals have been reported by Wellman et al. (2006, 2007). The results indicated that meta-autunite dissolution kinetics is strongly dependent on pH and the concentration of dissolved organic material. The presence of aqueous organic material does not alter the dissolution mechanism, but rather enhances the dissolution rate.

There has been only one study on the microbial dissolution of autunite examining anaerobic effects of a dissimilatory metal-reducing bacteria (*Shewanella putrefaciens 200R*) on solid synthetic metaautunite $\{Ca[(UO_2)(PO_4)]_2(H_2O)_6\}$(Smeaton et al. 2008). To the best of our knowledge, there is no research that investigated microbial dissolution of autunite in the aerobic conditions.

In this study, we attempted to demonstrate the significance of bacteria–uranium interactions by focusing on three bacterial strains of *Arthrobacter* sp. These bacteria are one of the most common groups in soils and are found in fairly large numbers in Hanford soil as well as other subsurface environments contaminated with heavy metals and radioactive materials (Boylen 1973, Balkwill et al. 1997, Van Waasbergen et al. 2000, Crocker et al. 2000). Balkwill et al. (1997) reported the predominance of the genus *Arthrobacter* among the culturable aerobic heterotrophic bacteria from the Hanford Site sediments with this group accounting for roughly up to 25% of the subsurface isolates. In addition, *Arthrobacter*-like bacteria were the most prevalent in the highly radioactive sediment samples collected underneath the leaking high-level

waste storage tanks and accounted for about of one-third of the total soil isolatable bacterial population (Fredrickson et al. 2004). This research provides a more comprehensive understanding on the stability of autunite mineral in the oxidized conditions pertaining to the Hanford Site and the environmental fate and transport of uranium in subsurface.

TASK 1.2 OBJECTIVES

The present study aimed to (i) investigate bacterial interactions under oxidizing conditions with uranium (VI), which is a predominant contaminant at the Hanford Site; (ii) report results from uranium adsorption experiments with *Arthrobacter* strain G975; (iii) study the potential role of bicarbonate, which is an important complexing ligand for U(VI) and a major ion in groundwater and porewater compositions; (iv) present initial data from autunite leaching experiments; and (v) report high-resolution atomic-force microscopy (AFM) results on the formation of microbial uranyl-phosphate precipitates on the bacterial surface. These observations can provide insight into important microbiological processes affecting the fate and transport of uranium within subsurface bicarbonate-bearing environments.

TASK 1.2 MATERIALS AND METHODS

Arthrobacter Strains and Growth Culture Conditions

Three *Arthrobacter* strains, previously isolated from the Hanford subsurface as a part of the geomicrobiological investigation conducted for the DOE Deep-Subsurface Science Program, were obtained from the Subsurface Microbial Culture Collection (SMCC) (Florida State University, Tallahassee). Detailed descriptions of site geology, sample collections procedures, and methods of bacteria isolation are available from Van Waasbergen et al. (2000). The strains identification, previously confirmed by 16S rDNA phylogeny, was *Arthrobacter globiformis* (G954) and *Arthrobacter oxydans* (G968, G975) (Balkwill et al. 1997, Van Waasbergen et al. 2000). The strains were cultured in PYTG medium consisting of 5 g/L peptone, 5 g/L tryptone, 10 g/L yeast extract, 10 g/L glucose, 0.6 g/L $MgSO_4.7H_2O$, 0.07 g/L $CaCl_2.2H_2O$ and 15 g/L agar. Media was prepared in deionized water (DIW) (Barnstead NANOpure Diamond Life Science (UV/UF), Thermo Scientific), autoclaved at 121^{o}C and 15 psi for 15 minutes, then allowed to cool down to about 50^{o}C before being poured into sterile petri dishes. These studies were carried out in 5% liquid culture media and agar plates. The *Arthrobacter* strains were aerobically grown to reach confluence in 15 ml polypropylene sterile centrifuge tubes with a foam stopper amended with 3 ml of PYTG media at 29˚C in the shaker/incubator.

The uranyl nitrate stock solution was prepared from uranyl nitrate hexahydrate in DIW water and subsequently diluted to varying U(VI) concentrations from 1 to 80 ppm. The U(VI) in the stock solution was analyzed using a Kinetic Phosphorescence Analyzer KPA-11 (Chemcheck Instruments, Richland, WA) in the amount close to the theoretical value of 47.4%.

To account for viable bacteria, a well-mixed homogeneous aliquot (0.01 mL - 0.1 mL) of the suspension from each test vial was uniformly spread on the sterile petri dishes containing a 5% PTYG growth media mixed with 15 g/L of agar. Inoculated plates were kept inverted in an incubator at 29^{o}C. Viable microorganisms were calculated from the number of colony-forming units (CFU) found on a specific dilution. In addition, the agar plating was used to provide a

quick visual check for contamination and to maintain colonies from each stage of the enrichment for the duration of the experiment.

The morphological details, such as cell size and the presence of a rod-coccus growth cycle were continually monitored using an optical microscope. The morphological features recorded for colonies included the presence of pigmentation, shape, type of edge, type of surface, and elevation. The cell density (cells/mL) was calculated with the help of a glass hemocytometer (Fisher Scientific, Pittsburg, PA). Cell counts in the samples containing uranium employed INCYTO C-Chip disposable hemocytometers. The hemocytometer is a microscope slide with a rectangular indentation, creating a chamber that is engraved with a grid of perpendicular lines (Figure 7).

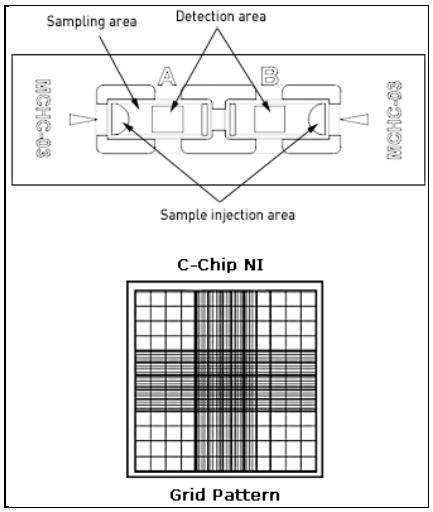

Figure 7. INCYTO C-Chip disposable hemocytometer and counting grid.

Having known the area bounded by the lines as well as the depth of the chamber, the cell density in a specific volume of fluid and in a bacterial broth solution was calculated from a sample, homogenously distributed inside the chamber. Once the average cells count was obtained, it was multiplied by the dilution factor and the volume factor, 10^4, in order to obtain the final concentration of cells per mL. In addition, cell density was determined by measuring the absorbance at 660 nm by means of spectrophotometer (UV-1601, Shimadzu) and relating them to known cell numbers counted via the use of the hemocytometer.

Bioleaching of U(VI) from Autunite

Two types of bioreactors were used in the initial bioleaching experiments: (1) sterile 100 mL glass mixed reactors with autunite where cells were injected after autunite equilibrated with media solution and (2) sterile cultureware with inserts where bacteria and autunite solids were separated.

Bicarbonate Media Solution Preparation

Autunite leaching solutions were made from 5% minimal PTG media consisting of 5 g/L peptone, 5 g/L tryptone, 10 g/L glucose, 0.6 g/L $MgSO_4.7H_2O$, and 0.07 g/L $CaCl_2.2H_2O$. Yeast extract due to the high phosphorus content was not included in the media. Media was prepared in deionized water (DIW) (Barnstead NANOpure Diamond Life Science (UV/UF), Thermo Scientific), autoclaved at 121^{o}C, 15 psi for 15 minutes, and allowed to cool down to about 30^{o}C.

Then media solution was equally distributed between five 250 ml bottles and separately amended to contain 0, 1 mM, 3 mM, 5 mM and 10 mM of $KHCO_3$. Media pH in each bottle was adjusted to pH 7.5 with 0.1 mol/L HCl or NaOH and buffered with 20 mM 2-(2-hydroxyethyl)-1-piperazine ethanesulfonic acid sodium salt hydrate (HEPES-Na). Each bicarbonate media solution was filter-sterilized (0.2 μm) and kept refrigerated until the time of the experiment.

Autunite bioleaching in mixed reactors

Natural Ca meta-autunite, $Ca[(UO_2)(PO_4)]_2 \cdot 3H_2O$ obtained from Pacific North National Laboratory (PNNL), was characterized prior to experiments using ICP-OES, ICP-MS analyses, X-ray diffraction and SEM/EDS to confirm the mineral composition, structure, and morphology as 98-99% pure autunite. The autunite sample was powdered to have a size fraction of 75 to 150 μm or -100 to +200 mesh with a surface area of 0.88 m^2/g (Wellman et al. 2006). The surface area of the samples used in the dissolution experiments was determined by Kr-adsorption BET analysis (Wellman et al. 2006). Autunite microbial leaching experiments were conducted using stoppered 100 mL glass serum bottles filled with 91 mg of autunite powder and 50 mL of sterile media followed by 0, 1, 3, 5, and 10 mM added $KHCO_3$ to provide a final U(VI) concentration of 4.4 mmol/L. The suspensions were shaken with 60 rpm in an incubator/shaker at 25^{o}C. G975 cells in the amount of log 10^6 cells/ml were injected into the reactors at day 13 when autunite dissolved was close to a steady state. Following bacteria inoculation, the reactors were covered with sterile foam stoppers to sustain inside aerobic conditions. Abiotic non-carbonate controls were kept without bacteria inoculation to compare results with their biotic counterparts.

The aqueous speciation of U(VI) and saturation indexes were computed using visual MINTEQ software [v.3.0, maintained by J.Gustafsson at KTH, Sweden, available at http://www.lwr.kth.se/English/OurSoftware/vminteq/ updated with the Nuclear Energy Agency's thermodynamic database for uranium (Guillaumont et al. 2003)]. The modeling was performed in the aqueous yeast-free 5% PTG media system amended with 20 mM Na-Hepes and 0 mM, 1 mM, 3 mM, 5 mM, and 10 mM $KHCO_3$ concentrations. The pH of the solutions was measured after the completion of experiment, and U(VI), Ca, P data were collected following inoculation of bacteria when U(VI) leaching reached its maximum. In bicarbonate-free solutions, a CO_2 partial pressure (p_{CO2}) was assumed $10^{-3.5}$atm. Growth media components, pepton, trypton, and glucose, could not be added to the list of initial concentrations due to a lack of thermodynamic equilibrium constants in the MINTEQ database.

Autunite bioleaching in cultureware with inserts

Sterile 6-well cell culture plates with inserts (Figure 8) were used in the non-contact bioleaching experiments where natural Ca meta-autunite and bacteria cells were kept separately. The maximum recommended volume for the cultureware was used to increase the sampling number. A 3.2 ml aliquot of sterile media prepared as previously described for the mixed reactors was dispensed in the appropriate well and 2.5 ml inside the insert receptacle. The total volume inside each well added up to 5.7 ml. The cultureware inserts have 0.4 μm cylindrical pores that transverse the membrane and only allow the diffusion of soluble uranium. Ten mg (10 mg) of sterilized autunite powder was added to the bottom of the well to reach a U(VI) concentration of 4.4 mmol/L with the insert in place; the same U(VI)-autunite concentration was used for bioleaching experiments employing mixed reactors. Abiotic controls were prepared to compare results with bacteria- bearing wells. Uranium leaching from autunite was determined by taking a 10 μL sample from the inserts, at the same time intervals as the mixed reactors, and processed on

the KPA instrument after following the wet/dry ashing steps described in detail in the subsequent analytical procedure section.

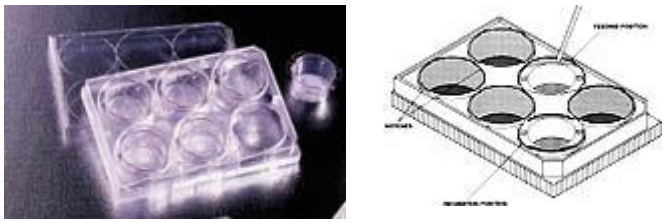

Figure 8. Cell Culture Inserts (BD Falcon).

Analytical procedures

At certain times, 0.3 mL of solution was aseptically withdrawn from each bottle, filtered (0.2 µm), and then analyzed for dissolved U(VI) by means of KPA. The dilution factors for sample analysis ranged between 100 and 400. Prior to KPA analysis, sample aliquots were ashed on a hot plate in the presence of concentrated plasma grade nitric acid and hydrogen peroxide solutions. Wet digestion in 20 ml scintillation glass vials was continued until a dry white precipitate was obtained, then vials were dry ashed in a furnace at 450^{o}C for 15 min. Samples were allowed to cool down at room temperature followed by the dissolution of the precipitate by the addition of 1 M nitric acid (HNO_3). Aqueous concentrations of calcium and phosphorus were determined from the digested samples by means of Optima 7300 ICP-OES (Perkin Elmer). Uranium calibration standards (SPEX certiPrep), blanks and check standards (95-105% recovery) were analyzed for quality control. At the end of the leaching experiments, suspension pH was measured and samples of the solid phase were transferred to a centrifuge tube, washed three times with DIW to clean from uranium residuals, re-centrifuged again and then fixed to characterize the solid phase by means of a field emission scanning electron microscope (Fe-SEM) and energy dispersive spectroscopy (EDS) analysis. Samples were treated with 2% glutaraldehyde in 0.1M HEPES-Na buffer at pH 7.2 for 2 h at 4^{o}C, subsequently dehydrated in ethanol/water solutions and dried. The microstructure of the gold-coated samples (Pelco SC-7, Auto sputter coater) was characterized using a JOEL, JSM-6330F SEM at 15 kV. Changes of the chemical composition of the mineral and cell surface were analyzed using a SEM-EDSNoran System Six Model 200. Details on the solutions used for the SEM/EDS analysis are in the "Cell surface composition analysis" section.

Biosorption experiments

Synthetic Groundwater and changes in bicarbonate concentrations

The sorption experiments were conducted with carbonate-free (CF-SGW) and carbonate amended synthetic groundwater (SGW) under conditions relevant to the 300 Area Hanford Site subsurface. The CF-SGW formulation that mimics the natural groundwater composition at an excavation site above the former South Process Pond in the 300 Area was made up from available salts. The formulation was based on the April 19, 2003 analysis (Zachara 2004). The CF-SGW consists of 88.21 mg/L of $CaCl_2.2H_2O$, 19.99 mg/L of $MgCl_2$, 5.22 mg/L of KCl, 520.58 mg/L of HEPES, dissolved in DIW. The SGW amended with various bicarbonate

concentrations was created using $KHCO_3$ with pH adjusted to 7.3 by 0.5 M HCL or 0.5M NaOH, as required. SGW solutions with ambient levels of bicarbonate concentrations and those amended with 0, 0.5, 2.5, and 5 mM of $KHCO_3$ were tested in the sorption experiments.

Biosorption kinetics

A preliminary experiment was conducted to determine the appropriate sampling rate for future experiments. A CF-SGW solution amended with 917.2 ±120.6 ppb of U(VI) and inoculated with 4E+10 cells of G975 strain bacteria was randomly sampled for 5.25 hours. Based on the preliminary results discussed in the Results & Discussion section, the experiment was modified with the changes outlined below.

The U(VI) biouptake rate was studied by conducting a 2^2 factorial design approach using as the two independent variables uranium and bicarbonate concentrations at two different levels or concentrations, and the bacterial uranium uptake as the dependent variable. SGW solutions at equilibrium with atmospheric CO_2 were referred to as the low-bicarbonate media and SGW modified with 2.5 mM $KHCO_3$ was referred to as the high bicarbonate concentration. The low and high concentrations of U(VI) in SGW media, 0.3 ppm/0.005 µM and 14.7 ppm/0.247 µM respectively, was made by the addition of the appropriate volumes from an 100 ppm uranyl nitrate $[UO_2(NO_3)_2 \cdot 6H_2O]$ stock solution prepared in DIW. The chosen experimental design scheme allowed us to investigate the influence of bicarbonate on the uranium biosorption kinetics and statistically model the relationships between two major variables, U(VI) and bicarbonate at equilibrium. The design provided four possible treatments (Figure 9) sampled at different time intervals. The time–based experiment was conducted in triplicate and all treatments were sampled and measured at the same time: 0.25, 0.75, 2, 4, 6, 24, 48 hours to avoid statistical blocks with their respective controls. Experiments were conducted in triplicate using 4 ml of SGW inoculated with 4E+10 cells of G975 strain in 15 ml polypropylene sterile tubes. The tubes were kept in the incubator shaker at 60 rpm and 25°C for 24 hours. Tubes were centrifuged for 5 min at 3000 rpm and cell-free supernatants from all treatments were sampled and processed for U(VI) by means of KPA. In addition, bacterial samples after 24 hours of U(VI) exposure were tested for cell viability, by plating subsequently diluted homogeneous aliquots on the sterile agar-containing petri dishes. The metal uptake q (mg ion metal / g bacteria) was determined by solving the mass balance equation presented in eq. 4.

$$q = \frac{(C_0 - C_t) * V}{m} \quad (4)$$

Where C_0 and C_t are the initial and final metal ion concentrations (mg/L), respectively, V is the volume of solution (mL), and m is the bacteria dry weight (g).

		Factor C Time, hours 0.25, 0.75, 2, 4, 6, 24, 48	
		Factor B Atmospheric CO_2 with additional [KHCO3] Low 0 mM	Factor B Atmospheric CO_2 with additional [KHCO3] High 2.5 mM
Factor A	[U(VI)] Low 299.1 ppb	--	-+
	[U(VI)] High 14,721.4 ppb	+-	++

Figure 9. Outline of 2^2 factorial design to study biosorption kinetics.

Adsorption isotherm

The equilibrium U(VI) adsorption was carried at different initial concentrations of U(VI) ranging from 0.5 to 20 ppm while maintaining the dry weight of *Arthrobacter* sp. G975 at 0.24 ± 0.05 mg in each treatment. The dry weight of bacteria was indirectly estimated by relating the direct cell count obtained by a hemocytometer and the bacterial mass acquired by following the modified EPA method 340.2 for the same number of cells. The role of bicarbonate ions and their impact on U(VI) adsorption by bacteria was investigated using bicarbonate-bearing SGW at concentrations up to 5 mM.

The bacteria-inoculated uranium solutions were prepared in triplicate having equal volumes of 4 ml in 15 ml polypropylene sterile tubes that were kept in the incubator shaker at 60 rpm and 25°C allowing 24 hours for equilibration time. This time was determined from the results of the preliminary adsorption kinetics experiments previously described. In addition, the abiotic control tubes were prepared to quantify U(VI) losses due to adsorption on tube walls and caps. The pH for each solution remained unchanged for 24 hours, adjusted to 7.3 using 0.5 M of NaOH or HCL. Tubes were centrifuged for 5 min at 3000 rpm and then supernatant samples were assayed with the KPA instrument. The uranium uptake by the bacteria was calculated with eq. (4). Sorption isotherms were created by plotting the amount of metal uptake (q) against the equilibrium concentration of metal ions detected in the solution. The slope of this correlation is known as the partition coefficient, K_d, that corresponds to the distribution of metal ions between the aqueous and solid phases.

The linear, Freundlich, and the Langmuir sorption isotherms were used to simulate the adsorption capacity of uranium by *Arthrobacter* sp. G975 at equilibrium (Chang and Wang 2002, Schluter 1997, Xie et al. 2008, Aksu 2001, Benguella and Benaissa 2002). The Linear isotherm is presented in eq. (5) by the measured uranium concentration at equilibrium Ce, and the partition coefficient, K_d , eq. (6).

$$q = K_d C_{equilibrium} \tag{5}$$

$$K_d = \frac{q}{Ce} = \frac{mol\ g^{-1}}{mol\ mL^{-1}} = (\frac{mL}{g}) \tag{6}$$

The Freundlich isotherm is an empirical generalization of the linear isotherm, with K_f and 1/n as empirical constants (eq. 7).

$$q = K_f C_e^{1/n} \text{ or } \log(q) = \log(K_f) + \frac{1}{n}\log(C_e) \tag{7}$$

The Langmuir isotherm equation, eq. (8), describes the adsorption of gases onto clean solids and implies uniform adsorption on the saturated monolayer surface (Stumm et al. 1996).

$$\frac{1}{q} = \frac{1}{S_{max}} + \frac{1}{C_e K_L S_{max}} \tag{8}$$

A basic assumption of the Langmuir theory is that adsorption occurs at specific homogenous sites of the sorbent, and once a metal ion resides on a site, no further adsorption can take place (Ho et al. 2008). The characteristic constants of the Langmuir equation are S_{max}, the maximum adsorption for a complete monolayer (mg/g), and $K_{L,}$ the adsorption equilibrium constant (mg/mL).

Desorption experiments

After biosorption experiments, the U(VI)- loaded G975 cells were harvested from the solutions to measure the amount of U(VI) adsorbed onto the bacterial surface versus U(VI) accumulated inside the cell. Cells were rinsed in DIW and re-suspended in 10 ml of a strong uranium chelating agent, 10 mM Ethylenediaminetetra-acetic acid disodium salt (Na_2EDTA) with the pH adjusted to 7.2 (Acharya 2009). After 10 min of gentle agitation, the samples were centrifuged and the U(VI) concentrations in the supernatant were determined with the KPA instrument. This process allowed to desorp U(VI) bound to the cell membrane back into solution. The mass of desorbed U(VI) was counted using eq. 9.

$$\mathbf{U(VI)\ adsorbed},\ \mu\mathbf{g} = \mathbf{C_{desorbed}}\ \frac{\mu\mathbf{g}}{\mathbf{L}} * \mathbf{EDTA\ volume}\ (\mathbf{L}) \tag{9}$$

The mass of uranium in solution at equilibrium and the total uranium mass was calculated in the same fashion, using initial (C_0) and equilibrium (C_e) U(VI) concentrations along with the 4 ml of starting solution volume. Thus, the mass of internal accumulated U(VI) was estimated by solving the mass balance equation (10).

$$[U]_{Internal\ Accumulation} = [U]_{total} - [U]_{in\ solution} - [U]_{\ adsorbed} \tag{10}$$

Cell Viability

After the biosoption experiment, each biotic treatment was tested for the cells ability to reproduce its numbers after 24 hours exposure to U(VI). Cell viability was assayed by inoculating a 5 µL volume of cells in several agar plates containing 5% PTGY medium in serial dilutions, and then counting grown colonies on the plate. A serial dilution helped to obtain a

colonies number on each plate ranging between 30-300. The colony-forming units were then calculated as eq. (11).

$$\frac{CFU}{ml} = \frac{CFU * Dilution\ Factor}{Sample\ volume\ (ml)} \quad (11)$$

Statistical analysis

All experiments were conducted in duplicate or triplicate to obtain descriptive statistics such as mean, standard deviation, and confidence interval of the mean. Where applicable, such as the experimental data for sorption isotherm, relationships were modeled and evaluated with least squares regression analyses. Uranium calibration standards (SPEX certiPrep), blanks, and check standards (95-105% recovery) were analyzed for quality control before each experiment utilizing the KPA to check on variability of the machine. Comparison between specific experimental K_d values against soil of the study area was investigated using a one sample t-test. Results with multiple experimental groups and independent factors, such as the study on the effects of U(VI) uptake due to different bicarbonate and uranium concentrations, were examined with ANOVA statistics. The Holm-Sidak multiple comparison test was performed when significant differences were found between samples. All statistical tests were carried out by Sigma plot 11.2 (Systat Software Inc). Significant levels were set $\alpha = 0.05$.

SEM/EDS microscopy analysis

Growth Conditions

The *Arthrobacter* strains were aerobically grown to reach confluence in 15 ml polypropylene sterile foam-stoppered centrifuge tubes amended with 3 mL of 5% PYTG media at 29˚C. Experimental tubes were inoculated with approximately 3.E+08 cells of the corresponding strain to bring the concentration of bacterial cells close to 1.E+08 (Log 8) cells/mL. Prior to inoculation, cells stock suspension was counted using an INCYTO C-Chip disposable hemocytometer to determine the amount of cells in the media needed to obtain the desired concentration in the tubes. Uranium was injected as a uranyl nitrate from a stock solution of 0.005M of U(VI) to achieve the required concentration ranging between 0.5 ppm-27 ppm. Each set was prepared in triplicate and tubes were independently sampled at 24 hrs to (i) obtain cell counts, (ii) prepare samples for the microscopy assays via atomic force microscope (AFM) and energy dispersive X-ray spectroscopy (EDS), and (iii) determine aqueous uranium concentrations. Aliquots of solution were collected for analysis of dissolved U(VI) followed by tubes centrifugation for 10 min at 2000 rpm. Analyses were conducted by means of a KPA using a dilution factor of 1:200. Bioaccumulation of uranium was calculated against bacteria-free controls. They were prepared with the same media solution amended with corresponding uranium concentrations and sampled at the same time intervals as experimental vials.

Cell Surface Composition Analysis

The confirmation of precipitated uranium on the bacterial surface was obtained via SEM/EDS analysis. Sample preparation procedures included cells harvesting by centrifugation at 4000 rpm for 5 min from PTYG media amended with certain concentration of U(VI) and washing twice with a 50 mM of HEPES-Na prepared in deionized water (DIW). The pH of HEPES-Na solution was adjusted to 7.2 with concentrated Fisher Scientific nitric acid. The cells were fixed in the 5 ml of 2% glutaraldehyde in 0.1 M HEPES-Na buffer at pH 7.2 for 2 h at 4^{o}C. The fixative was

changed at least two times. The material was removed by centrifugation and washed with 50 mM HEPES-Na buffer three times for 10 min. The rinsed cells were then dehydrated in ethanol/water solutions of 35% (v/v), 70% (v/v), and 90% (v/v) each for 10 min, and two times in 100% (v/v) for 10 min. Dehydrated samples were immersed for 10 min each in 50% and 100% pure hexamethyldisilazane (HMDS) (Pierce Biothechnology, Inc, obtained from Fisher Scientific) followed by 10 min of air-drying to allow liquid to evaporate from a sample (Fratesi et al. 2004). The dehydrated specimens were then kept in the desiccators until time of the EDS assay. Uranium treated and control samples were mounted on aluminum stubs with double-sided sticky carbon tape and then coated for 30 seconds with a thin layer of gold to increase conductivity. The cell surface composition of gold-coated samples (Pelco SC-7, Auto sputter coater) was analyzed using a SEM-Energy-Dispersive-Spectrometry (SEM-EDS) Noran System Six Model 200 at magnifications of 2000-5000.

AFM microscopy analysis on bacteria uranium interactions

Sample Preparation for AFM Imaging

Sample preparation procedures require that bacterial cells be firmly attached onto silicon wafer substrates such that the cells remain stable when subjected to tip forces. Bacterial samples, preliminary washed with DIW from U(VI) residuals, were immobilized onto the 3-aminopropyltrimethoxysilane coated silicon wafer substrates. A concentrated bacterial suspension of 5 µl was dropped onto a silanized silicon wafer (Dorobantu et al. 2008). Samples were dried under a low pressure nitrogen gas flow until excess moisture was evaporated completely. The substrates were fixed onto metallic discs using epoxy glue and transferred to the AFM stage for imaging.

Atomic Force Microscopy Instrumentation and Imaging

A Multimode Nanoscope IIIa system from Veeco Instruments (Santa Barbara, California) was used for all AFM imaging analysis. Phase imaging was performed by using Si_3N_4 soft tapping tips (BudgetSensors, Bulgaria) in order to ensure minimum sample damage with a force constant 7.4 N/m and resonating frequency of 150 kHz. Phase imaging is an extension of TappingMode™AFM that provides detailed information about the surface structure and its properties beyond the simple topography, which is not possible with any other scanning probe microscopy (SPM) techniques. The phase image was obtained by mapping the phase of cantilever oscillation in tapping mode scans to detect variation in composition, friction and adhesion. Frictional imaging was performed by using the contact mode tip with a force constant 0.2 N/m and resonating frequency of 15 kHz. In addition, AFM was used to acquire information on the surface topography of cells exposed to U(VI) at the three-dimensional (3D) level. 3D phase images were obtained in the tapping mode. Imaging was performed in laboratory conditions at 25ºC and 55% relative humidity. Further, roughness analysis was conducted for quantifying the change in roughness of bacterial surface under different uranium concentrations. To ensure cells viability, the complete AFM analysis was performed within two hours after the sample was prepared.

Roughness Measurements

A roughness value for bacterial cell surfaces was calculated from high resolution AFM topography image. The roughness value was calculated according to the relative heights of individual pixel in the image (Fung et al. 2010) over a selected area. The average roughness (Ra)

was calculated from the average of the absolute values of profile height deviations from the mean level, as shown below.

$$R_a = \frac{1}{n}\sum_{j=1}^{n}|Z_j| \quad (12)$$

Here, *Z* is the maximum vertical distance between highest and lowest data points and *n* is the number of scan points.

Force Spectroscopy

Force spectroscopy (FS) is a powerful tool for studying surface topography and nanometer-scale resolution changes in the surface physiochemical and mechanical properties including bacterial cells. The dynamic changes occurring on the bacterial cell membrane before and after exposure to the various concentrations of uranium were evaluated using force spectroscopy analysis. The interaction force between the tip and the sample surface was recorded during intermittent approach and retraction of the tip (tapping) from the bacterial surface by monitoring the laser reflection from the deflecting cantilever using a position sensitive diode (PSD). This experimental approach allows for the monitoring of forces on the piconewton scale.

These interaction forces detect physiochemical changes over the desired region when scanned with similar tips (size and material), since the force is unique for the tip and underlying chemical domains on the cell membrane. The force was calculated by using a force distance (FD) curve (Noy et al. 1997, Takano et al. 1999, Cappella and Dietler 1999) obtained by plotting the deflection of cantilever against the Z position of piezo. These FD curves were processed using SPIP software by ImageMetrology, Denmark (version 4.8) to determine adhesion forces. The average adhesion force reported in this study was obtained from 20 different FD curves generated randomly in about 2 µm × 2 µm area on the sample surface.

TASK 1.2 RESULTS AND DISCUSSION

Bioleaching of U(VI) from Autunite

The release of aqueous U(VI) over time during the autunite leaching experiments is presented in Figure 10. U(VI) concentrations in the abiotic control that did not contain bicarbonate ($HCO3^-$) equilibrated over a period of 13 days and reached an average of 308.73087± 131.66 ppb; this concentration has not changed since then. Autunite dissolution caused the uranium concentration to grow exponentially (R^2=0.978) in the solution as a function of increasing bicarbonate concentration. In bicarbonate amended reactors, U(VI) leaching from autunite was strongly enhanced. All bioreactors reached a steady state within 13 days, prior to G975 strain inoculation, with U(VI) concentrations measured at 475.2±265.4 ppb, 2342.2±833.7 ppb, 5908.9±1654.1 ppb, and 19338.5±1263.3 ppb for 1 mM, 3 mM, 5 mM, and 10 mM $KHCO_3$, respectively. The uranyl release from autunite in the studied bicarbonate concentrations range prior to G975 inoculation was increased by a factor of 1.5±0.6, 7.6±1.1, 19.1±9.8, and 62.6±27.0 compared to the no-bicarbonate control, respectively. There was a statistically significant difference in the mean uranium values among the different levels of bicarbonate concentration ($P < 0.001$). A previous study (Steward and Mones 1997) indicated that carbonate has a much stronger control on uranium hydroxide dissolution rates than pH in the alkaline regime (pH 8–10). Similar results of the bicarbonate effect on uranium leaching were obtained for the dissolution of synthetic Na-boltwoodite (Ilton et al. 2006).

After bacteria inoculation, U(VI) measured in the reactors increased 7.5±3.9, 6.3±3.6, 3.0±1.0, 1.9±0.5, and 1.4±0.1 fold, respectively, compare to the corresponding bicarbonate-bearing controls at a steady-state (Figure 10). Even though there is a much increased amount of U(VI) leached out into the solution driven by the presence of bacteria (P=0.011), the effect of bacteria on autunite leaching is reduced as the concentration of $[HCO_3^-]$ increases. This trend is expected since the thermodynamic stability constants for the interactions between carbonate and both the autunite and the bacteria are higher than the autunite-cell interactions. Since the steady-state U(VI) concentration is higher for larger $[HCO_3^-]$, the increase in soluble U(VI) concentration induced by bacteria is dwarfed. Therefore, as $[HCO_3^-]$ increases, a diminishing trend on the effect of bacteria on autunite leaching is observed. The increase in U(VI) concentrations after the bacteria addition was followed by a gradual decrease in U(VI) observed after a week of G975 inoculation; however, this decrease was not observed for the reactors amended with 10 mM of bicarbonate. The mechanism responsible for the decrease in U(VI) may comprise of either or both bacterial accumulation and re-precipitation of autunite or secondary minerals. These hypotheses are discussed below. The dissimilatory U(VI) reduction to U(IV) was not considered in this study since G975 is an aerobic bacteria grown in reactors exposed to atmospheric oxygen.

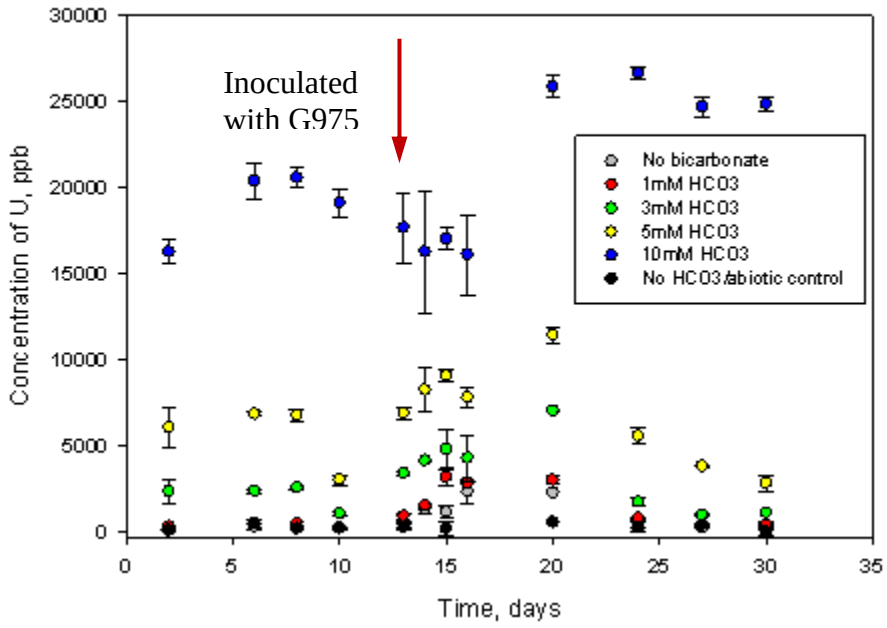

Figure 10. Changes for aqueous U(VI) as a function of time for the natural autunite dissolution experiments inoculated with *Arthrobacter* G975 strain.

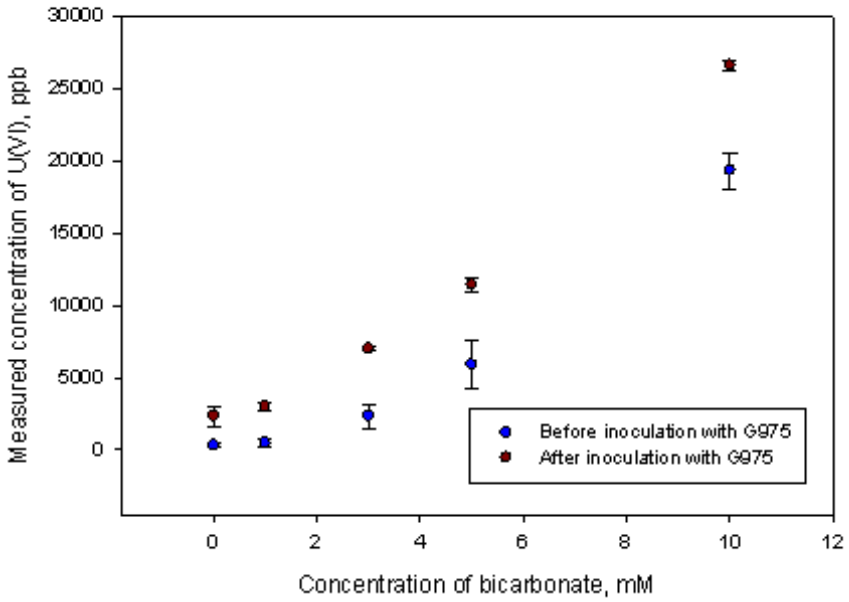

Figure 11. Measured U(VI) concentrations before and after inoculation with G975.

In parallel non-contact mode experiments using sterile cultureware with inserts (Figure 12), the U(VI) leaching was investigated with the autunite mineral separated from the bacteria. The release of aqueous U(VI) over time during the autunite leaching in non-contact experiments is presented in Figure 13. The steady-state maximum concentrations of U(VI) detected were 1.0±0.7, 1.1±0.6, 1.2±0.9, and 4.6±3.11 fold higher than the abiotic control without the bicarbonate amendment. Even though these values are lower than those found in the bacteria-mineral mixed contact experiment, the amount of leached U(VI) between treatment groups is not great enough to exclude the possibility that the difference was due to random sampling variability (P=0.161). Factors that may have attributed to this increase in variability include slower uranium diffusion between the autunite- containing wells and the bacteria-bearing inserts, and the possible presence of bacterial cells in the aliquot samples withdrawn from the inserts, which were not filtered before KPA analysis. Similarly, after bacteria inoculation, U(VI) concentrations, measured in the reactors, increased 0.5±0.3, 1.1±0.9, 3.1±1.3, 4.3±3.0, and 3.2±1.4 fold, respectively, compared to the U(VI) concentration at steady-state prior to inoculation (Figure 14). More replicates are required to draw statistically significant results.

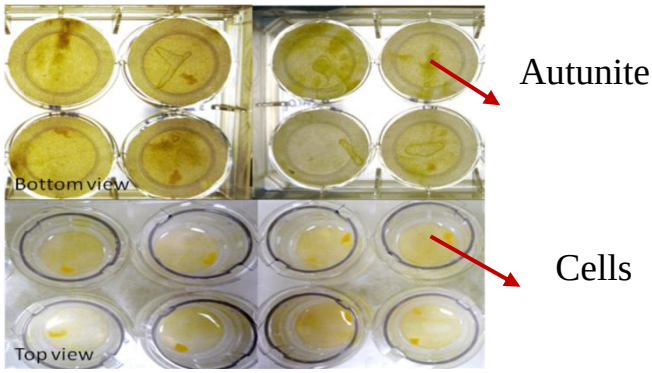

Figure 12. Top and bottom view of Cell Culture Insert with autunite mineral powder separated from bacteria.

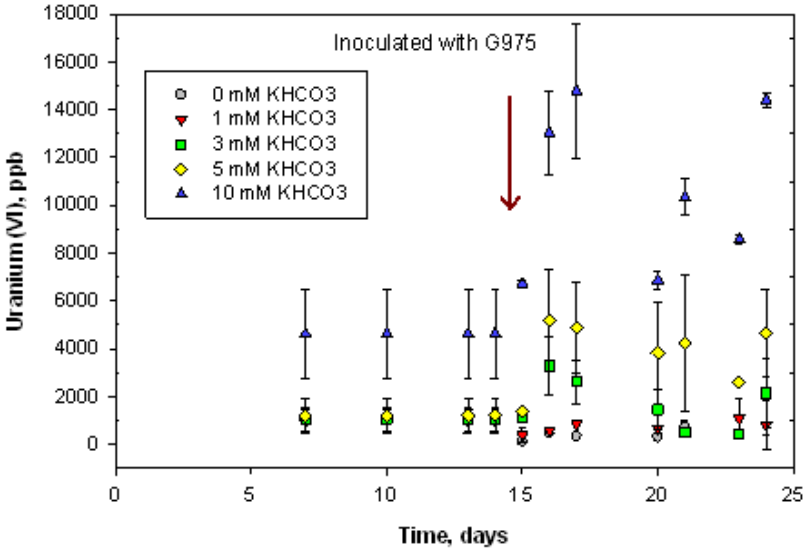

Figure 13. Changes for aqueous U(VI) as a function of time for the non-contact natural autunite dissolution insert experiments inoculated with *Arthrobacter* G975 strain separated by a 0.4um porous membrane (n=2).

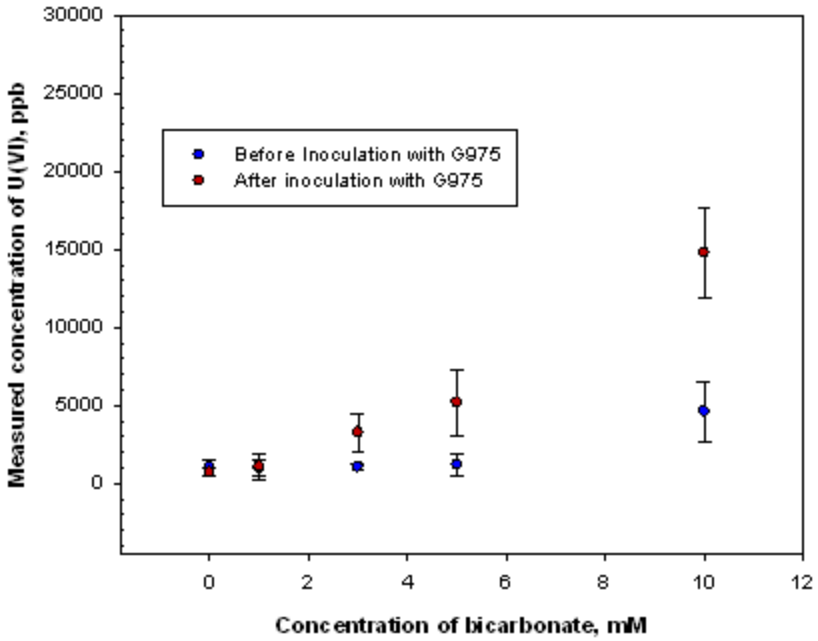

Figure 14. Measured U(VI) concentrations before and after inoculation with G975 in the insert non-contact natural autunite dissolution experiment (n=2).

The results show that bacteria could be responsible for further autunite dissolution through secretion of metabolites, and are able to influence U(VI) leaching while not in direct contact with the mineral. This process was not related to media acidification since a substantial drop in pH on the surrounding medium was not recorded. The pH of 20 mM Na-HEPES buffered media was not stable over the course of the experiment and was observed in the range of 7-8.4, slowly drifting from the initial value of 7.5. This change is mostly due to the equilibration of carbonate-containing media solution with the atmosphere.

Previous experiments (Wellman et al. 2006) have demonstrated that the mechanisms of uranium release from autunite minerals is controlled by a surface-mediated reaction with the U polyhedra and the Ca-autunite P release was less than that quantified for U. Bicarbonate can promote mineral dissolution by binding to surface U(VI) ions causing bonds to weaken, which is followed by detachment of the U(VI) species into solution (Sparks 1999). The liberation of U(VI) influences congruent reactions to release P from the mineral (Figure 15).

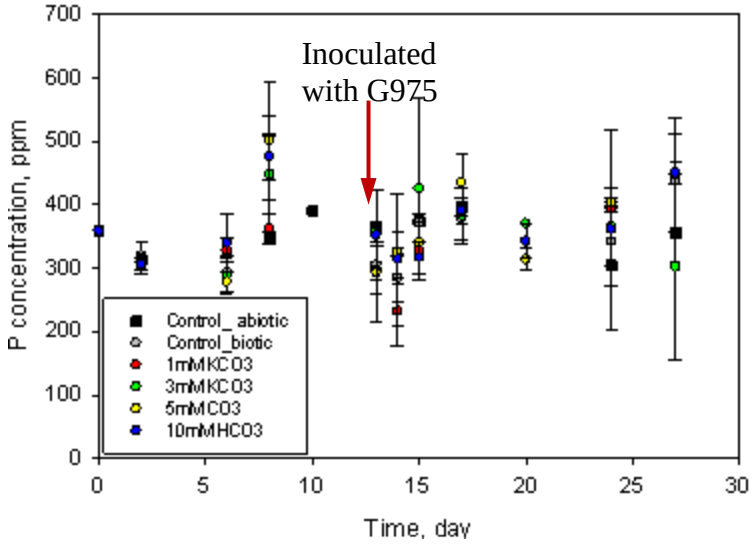

Figure 15. Aqueous P release as a function of time for the natural autunite dissolution experiments inoculated with *Arthrobacter* G975 strain.

During the autunite dissolution period without bacteria, P concentrations were increased compared to the non-carbonate abiotic control. After inoculation, P concentrations in the biotic reactors were found to decrease for all studied bicarbonate concentrations. This was correlated with the exponential growth phase of bacteria that were seeded into the reactors. P is an essential nutrient requirement for bacteria for the synthesis of DNA, ATP, polyphosphates, and cell wall phospholipids. In addition, bacteria create a very efficient phosphatase-mediated mechanism to activate excess secretion of orthophosphate, protecting cells from the toxic effects of radionuclides via passive U(VI) complexation by the negatively charged cell wall extracellular polymers (Beazley et al. 2007, Macaskie et al.1994, Renninger et al. 2004, Martinez et al. 2007). These requirements force microorganisms to access insoluble phosphate-bearing minerals via microbial dissolution. It is well known that many soil microorganisms are able to dissolve P-bearing minerals (Vazques et al. 2000, Goldstein 1986). The mechanisms to scavenge P from insoluble mineral sources are discussed by several authors. Some considered that microorganisms produce and exudates low molecular weight organic acids that play a role in the solubilization of inorganic phosphate from minerals (Vazques et al. 2000, Goldstein 1986). According to Goldstein (2000), the bioprocess of rock phosphate solubilization is more complicated than acid dissolution. He assumed that the bacteria form biofilms on the surface of the ore particles, which produce unique physiochemical conditions. These biocatalytic processes that involve simultaneous occurring biosynthetic and chemical reactions greatly enhance the rate and efficiency of phosphorus bioleaching. As a result of bioleaching, phosphorus containing compounds and earth metal ions such as Ca^{2+} and Na^{+} could move to the solution (Ivanova et al. 2006).

Grown in phosphorus-limiting 5% PTG media, bacteria were forced to liberate P by breaking the O-P bond from autunite sheets. A similar effect was noted by Smeaton et al. (2008), who examined the release of U from the meta-autunite mineral by the dissimilatory metal-reducing bacterium *Shewanella putrefaciens* 200R. Their spectroscopy measurements (XANES) indicated that the U dissolution was promoted by the uptake and immobilization of P by the bacterial cells.

Similar to U(VI), aqueous Ca release over the period of autunite dissolution without bacteria was noted to increase as a function of bicarbonate concentrations (Figure 16). For the same period, Ca concentrations in the non-carbonate abiotic control increased from the initial value of 11 mg/L, detected in bacterial growth media, to an average of 66±4 ppb and then remained stable without further changes.

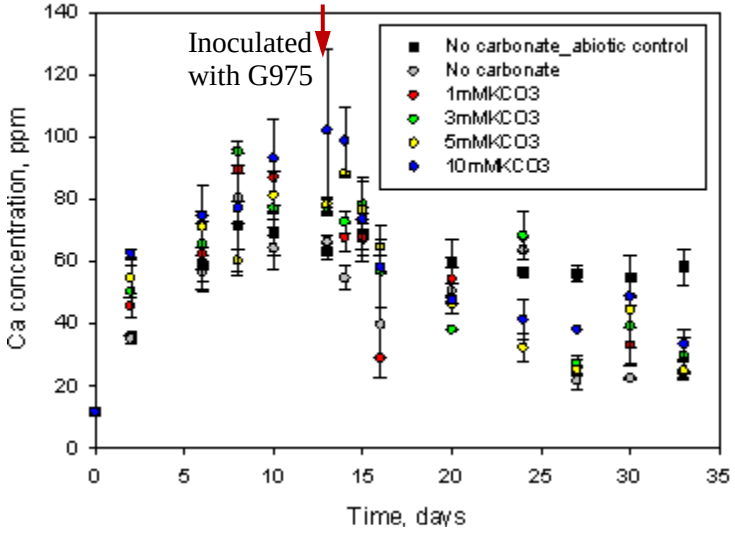

Figure 16. Aqueous Ca release as a function of time for the biotic reactors inoculated with *Arthrobacter* G975 strain and the abiotic no carbonate control (black squares).

The vulnerability of autunite to weathering is related to its basal sheet structure. The interlayer contains Ca atoms that form weak connections with several H_2O groups (Locock and Burns 2003). The dissolution of the mineral occurs through attack of the crystal from the edges by water molecules. Separation of the autunite sheets during dissolution slowly releases the interlayer cations from the structure into solution (Wellman et al. 2006). The dissolution process of autunite can alter the exposed reactive surface area due to enlarged natural fractures and basal plane cleavage, which result in a greater surface area compared to initial values. Higher surface areas provide new opportunities for bacterial attachment and are more conducive for the formation of biofilm. The bacteria can simultaneously contact the mineral and oxidize media organics to powerful organic acids which, in turn, dissolve the phosphate in the solution. Figure 17 shows biofilm formation with G975 cells attached to a mineral surface which, through growth and continuing colonization, spread across that surface. Bacteria penetrated the mineral cleavages and biofilm formation was found inside the cavities and fractures. SEM observations showed that mineral surface colonization by bacteria tended to increase concomitantly with bicarbonate concentrations (Figure 17). In reactors amended with 1mM and 5mM of bicarbonate, there was a greater density of microbial mineral colonization compared to the biotic bicarbonate-free reactors.

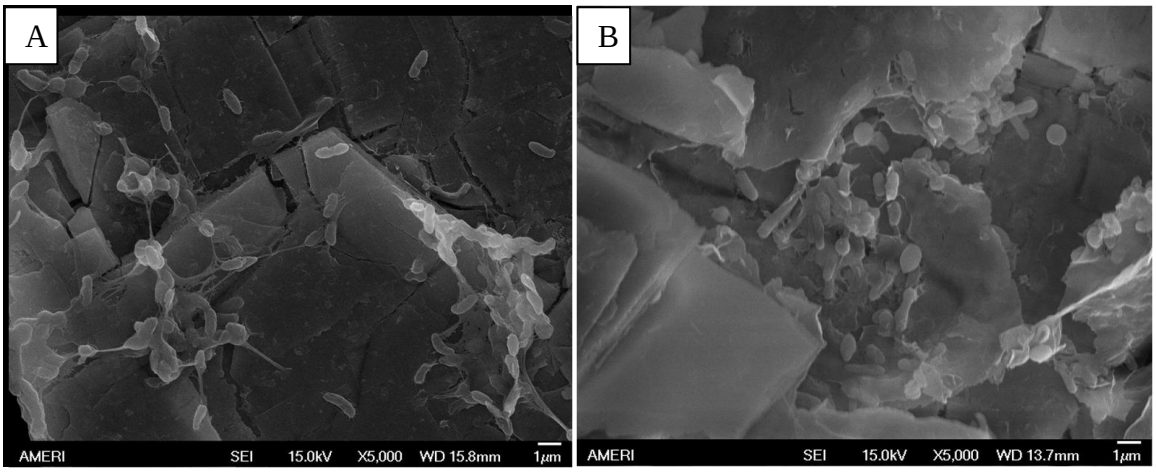

Figure 17. SEM images of biofilm created by G975 A. strain on the autunite mineral surface A) 1mM $KHCO_3$; B) 5mM $KHCO_3$.

Parallel experiments examining the toxicity of U(VI) on bacterial cell growth found that, in the presence of bicarbonate, the growth rate of cells and their density for the U(VI)- free controls and samples treated with 20 ppm of U(VI) in the presence of 5 mM of bicarbonate yielded similar values (Figure 34). The presence of bicarbonate can reduce the U(VI) toxicity by stripping uranyl from the cell surface and then forming uranyl-carbonate complexes in solution (Bencheikh-Latmani and Leckie 2003).

The bioleaching process becomes greatly enhanced in the presence of bicarbonate due to the formation of highly soluble and stable uranyl-carbonate and calcium uranyl carbonate complexes, $UO_2(CO_3)_3^{4-}$ and $CaUO_2(CO_3)_3^{2-}$. SEM analysis of post-reacted autunite samples revealed larger fractures and cleavage planes in the biotic reactors as a function of bicarbonate concentrations (Figure 18).

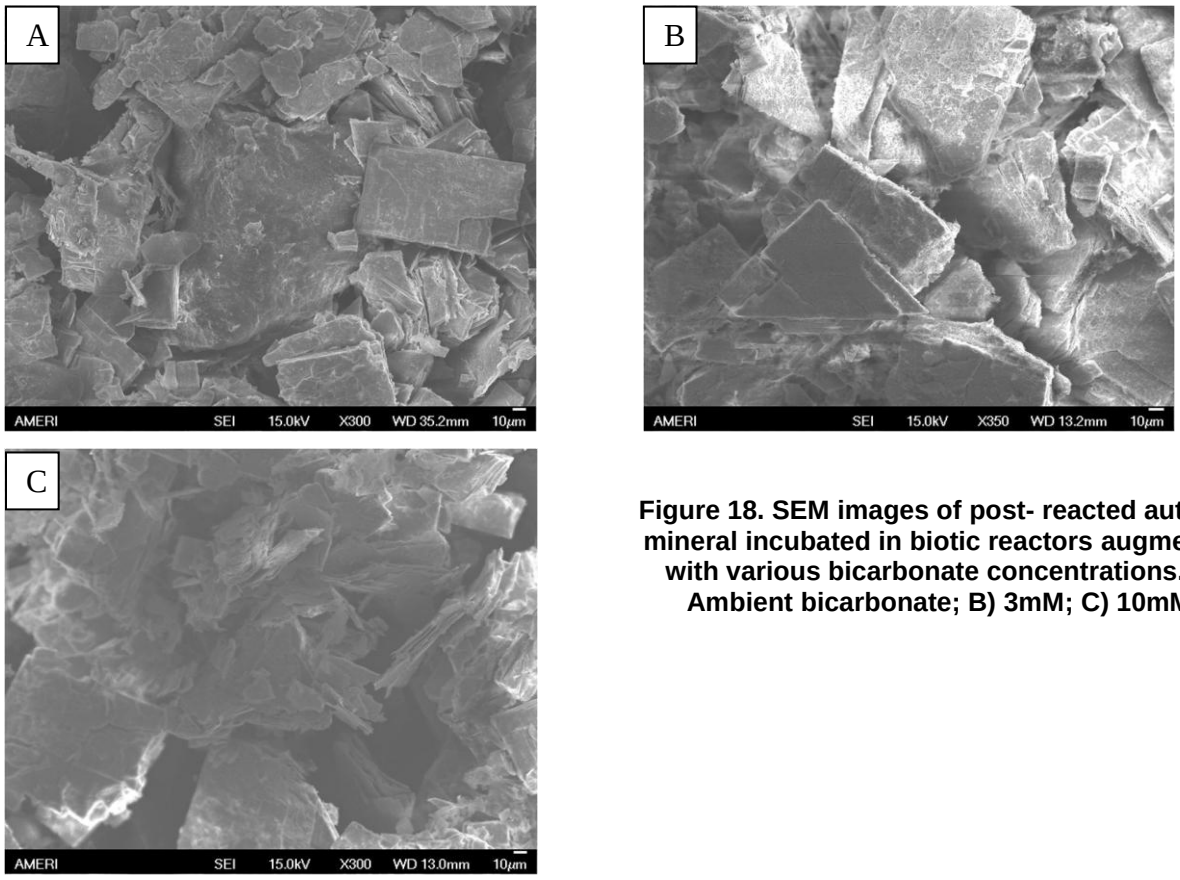

Figure 18. SEM images of post- reacted autunite mineral incubated in biotic reactors augmented with various bicarbonate concentrations. A) Ambient bicarbonate; B) 3mM; C) 10mM.

The formation of secondary minerals as observed in previous studies (Sandino and Bruno 1992, Smeaton et al. 2008) was not identified by SEM analysis on samples containing 1 and 5 mM of bicarbonate. This could be due to multilayered biofilms formed on the mineral surface and cleavage planes concealing secondary precipitates. However, at 10 mM bicarbonate, the formation of secondary minerals was seen on the autunite mineral surfaces (figure is not shown).

Speciation of the dissolved elements using the visual MINTEQ model suggested that the presence of aqueous Ca and P have a pronounced effect on the system. The results indicate that the biotic system becomes saturated with respect to various calcium phosphates across the bicarbonate range investigated and to calcite at 10 mM HCO_3^- (

Table 9). This occurrence is coupled with the decrease in Ca concentrations after the inoculation with bacteria (Figure 16). However, the system remains under- saturated with respect to all potential U(VI) secondary minerals except Na-autunite.

Table 9. Mineral Saturation Indices Based on Solution Compositions from Dissolution of Natural Autunite in 5% PTG Media in 20mM Na-HEPES Amended with Various Bicarbonate Concentrations

Minerals	Saturation indices (SI)[a]			
	no carbonate	1mMHCO3	5mM HCO3	10mM HCO3
$Ca_3(PO_4)_2$ (am1)	0.547	0.079	0.336	0.57
$Ca_3(PO_4)_2$ (am2)	3.297	2.829	3.086	3.32
$Ca_3(PO_4)_2$ (beta)	3.967	3.499	3.756	3.99
$Ca_4H(PO_4)_3 \cdot 3H_2O$	4.704	3.988	4.12	4.215
$CaHPO_4$	0.982	0.734	0.609	0.469
$CaHPO_4 \cdot 2H_2O$	0.702	0.454	0.329	0.189
Hydroxyapatite	12.719	12.033	12.67	13.279
Na-Autunite	3.474	3.69	3.933	4.051
Calcite	under saturated	under saturated	under saturated	0.073

[a] Saturation index (SI = log IAP – log K_{sp})

Table 10 summarizes the modeling results based on the highest U(VI) concentrations observed during the bioleaching of natural autunite. The aqueous species $CaUO_2(CO_3)_3^{2-}$ accounted for 49.5-56.5% of the dissolved U in all bicarbonate concentrations with the remainder occurring as $Ca_2UO_2(CO_3)_3$ (5.3-15.8%) and $UO_2(CO_3)_3^{4-}$ (9-36.8%). In comparison, in bicarbonate-free solution, the aqueous species $UO_2PO_4^-$ accounted for greater than 94% of the dissolved U. Calcium forms strong complexes with U(VI) and CO_3^{2-} that can increase the rate of mineral dissolution (Liu et al. 2007). The higher percentage of Ca-U-carbonate species in the 5 mM and 10 mM amended reactors correlated with higher U(VI) concentrations in the solutions which occurred via dissolution of the autunite structure.

Table 10. Distribution of U(VI) Species in Aqueous System from Dissolution of Natural Autunite in the Presence of a 20 mM Na-HEPES and Various Bicarbonate Concentrations

U species	Molar percent distribution,%			
	no carbonate	1mMHCO3	5mM HCO3	10mM HCO3
UO_2OH^+	0.02	ND	ND	ND
$UO_2(OH)_3^-$	0.03	0.01	ND	ND
$UO_2(OH)_2$ (aq)	0.08	0.02	ND	ND
UO_2HPO_4 (aq)	5.2	0.9	ND	ND
$UO_2PO_4^-$	94.7	20.8	0.1	0.0
$Ca_2UO_2(CO_3)_3$ (aq)	ND	15.8	9.8	6.3
$CaUO_2(CO_3)_3^{2-}$	ND	49.5	62.4	56.5
UO_2CO_3 (aq)	ND	0.2	ND	ND
$UO_2(CO_3)_2^{2-}$	ND	3.8	0.8	0.4
$UO_2(CO_3)_3^{4-}$	ND	9.0	26.9	36.8

Results of this study demonstrated bio-enhanced dissolution of the natural Ca-autunite in the presence of various concentrations of bicarbonate. The *Arthrobacter* species are ubiquitous in subsurface microbial communities and can play significant roles in the dissolution of minerals and the formation of secondary minerals. The stability of uranyl- phosphate complexes makes them a strong candidate for the remediation efforts to sequester U in the subsurface. However, in a bicarbonate-rich oligotrophic environment, which is typical for the Hanford Site oxidized subsurface, autunite showed a high liability to dissolution in the presence of bacteria. Autunite, as a P-containing mineral, can attract bacteria to liberate P to meet their needs for nutrients, which may result in U mobilization into the environment.

U(VI) biosorption

Kinetics analysis

The dry weight of bacteria was calculated indirectly from the cell count in their exponential growth phase by means of a hemocytometer based on the linear relationship shown in Figure 19. This relationship between cell numbers and dry cell weight is outlined in eq. 13 (R^2= 0.90, n=2). The weight of a single G975 *Arthrobacter* cell was estimated as 600±115 fg. The large standard deviation can be attributed to variations in size and shape of the studied strain. The ability of the A. species to undergo marked changes in form during their growth was observed during the course of this study and confirmed with the literature (Van Waasbergen et al. 2000). Cells can be rod shaped during the phase of exponential growth and cocci in their stationary phase; in addition, they can change from Gram- positive to Gram- variable.

$$\text{Dry cell weight (mg)} = \frac{6^{-10}\text{mg}}{\text{Cell}} * \text{Number of Cells} \qquad (13)$$

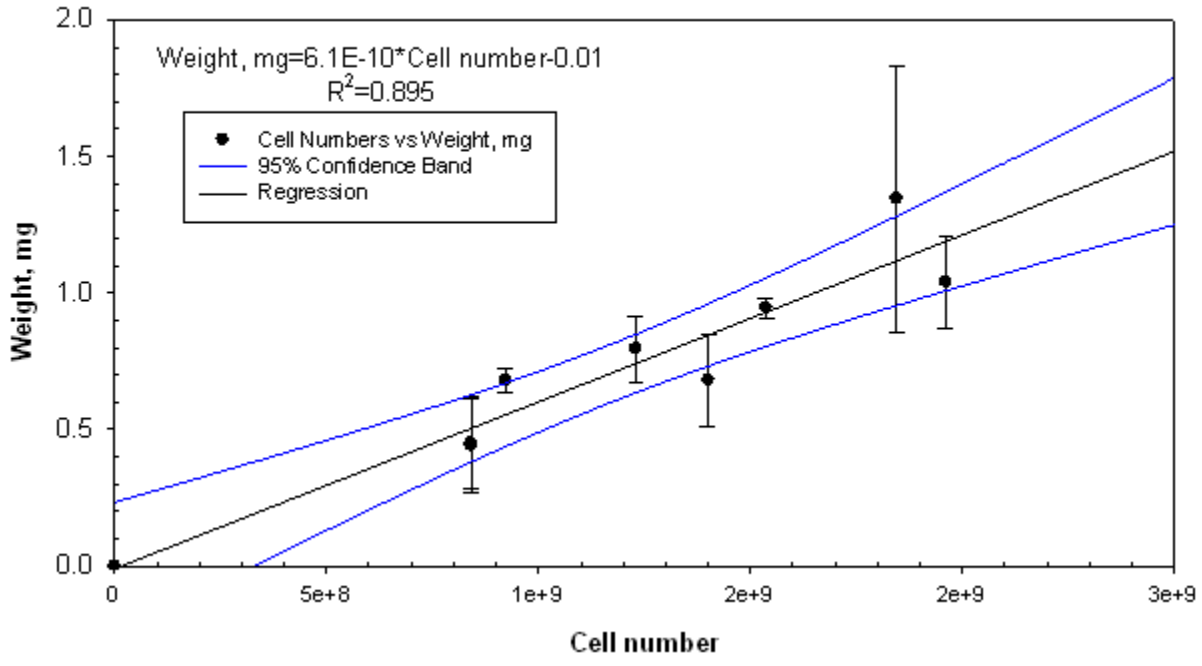

Figure 19. Correlation between weight vs. cell number for Arthrobacter G975 stain.

The uptake rate of U(VI), $\frac{mg}{g*min}$, under various environmental conditions, provides insight on the mechanisms of bioadsorption and establishes the exposure time required for soluble U(VI) to reach sorption equilibrium, characterized by the unchanging U(VI) concentration in the solution.

The preliminary results of the G975 bacteria and uranium adsorption kinetics with carbonate-free SGW are shown in Figure 20. The results show that within the first 15 minutes, 29.09 ±16.3% of the U(VI) was taken up by the cells following a linear relationship (R^2 =0.99) with the rate of $99.53\frac{\mu g}{L\ hr}$. However, the large standard deviation for each sample does not reject the possibility of second order kinetics. Within 5.25 hours, 87.57±17.48 % of the total uranium concentration was removed by the bacteria. Based on these results, we determined that the sampling process required continuing beyond 5.25 hours in order to determine if the process had reached equilibrium. Consequently, subsequent sorption kinetics samples were taken in 2 hour intervals up to 6 hours, followed by 24 and 48 hours.

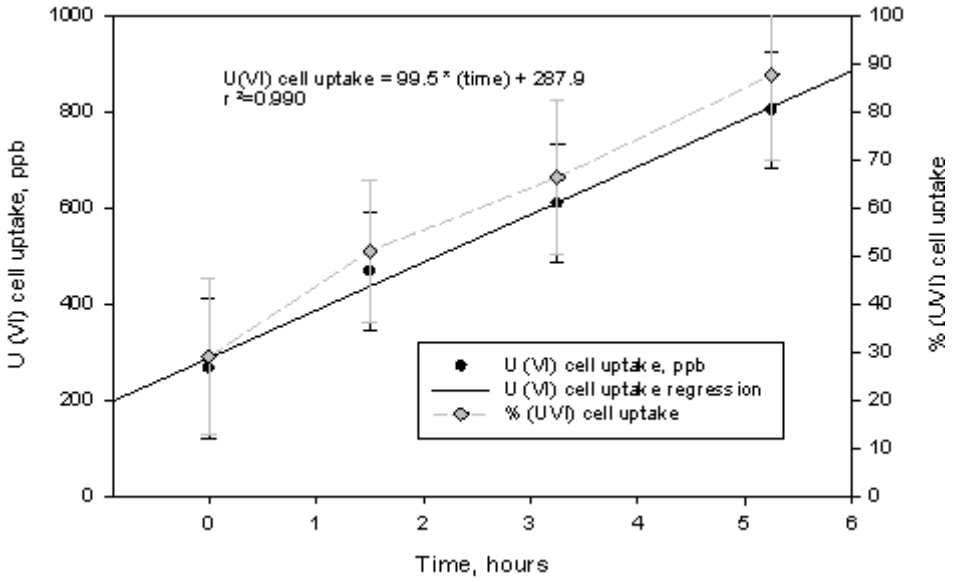

Figure 20. Preliminary results on biosorption kinetics using G975 strain with 917.2 ±120.6 ppb of initial U(VI) in CF-SGW; (n=3).

The bioadsorption experiments conducted with bicarbonate-free SGW solutions showed that *Athrobacter* sp. G975 can effectively remove soluble U(VI). In aqueous solutions at equilibrium with CO_2 atmospheric pressure, the total uranium uptake by bacteria rises to 90±19% and 83±21% for low and high initial uranium concentrations, respectively. The system reached equilibrium at 24 h (Figure 21); however, U(VI) adsorption was noted 12-32% across the studied concentration range within the initial 25 minutes of bacterial exposure to uranium.

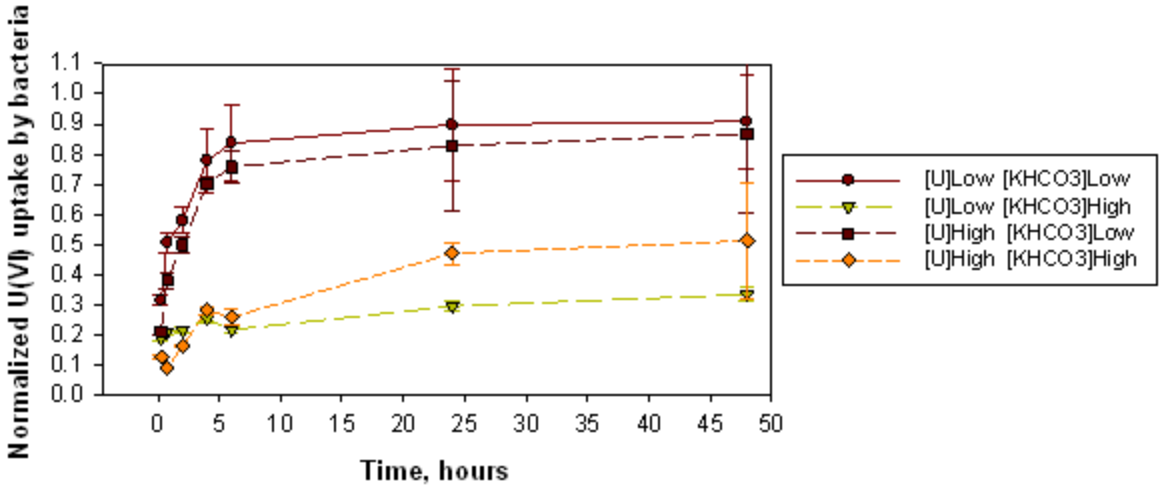

Figure 21. Percent of U(VI) uptake by *Arthrobacter* sp. G975 vs. Time, under low (0.3 ppm U(VI) and high (14.7 ppm U(VI)) concentrations of U(VI) and 0 and 2.5 mM of bicarbonate in SGW, pH 7.3, 25^{0}C.

The system amended with 2.5 mM of bicarbonate exhibited at equilibrium a significant decrease in bioadsorption to 47±4% at high initial concentration of U(VI), and with a more pronounced decrease to 30±2% in the systems with lower initial U(VI) concentrations. The low removal efficiency of U(VI) in the presence of competing ligands like carbonate is expected in these conditions considering the strong binding affinity of actinides toward carbonate ligands.

All bicarbonate-bearing experiments showed an increase of U(VI) adsorption by *Arthrobacter* sp. G975 within the first hour under all test conditions; however, after the initial fast uptake period, the process of U(VI) uptake was gradually slowed until it reached equilibrium at 24 hours (Figure 22).

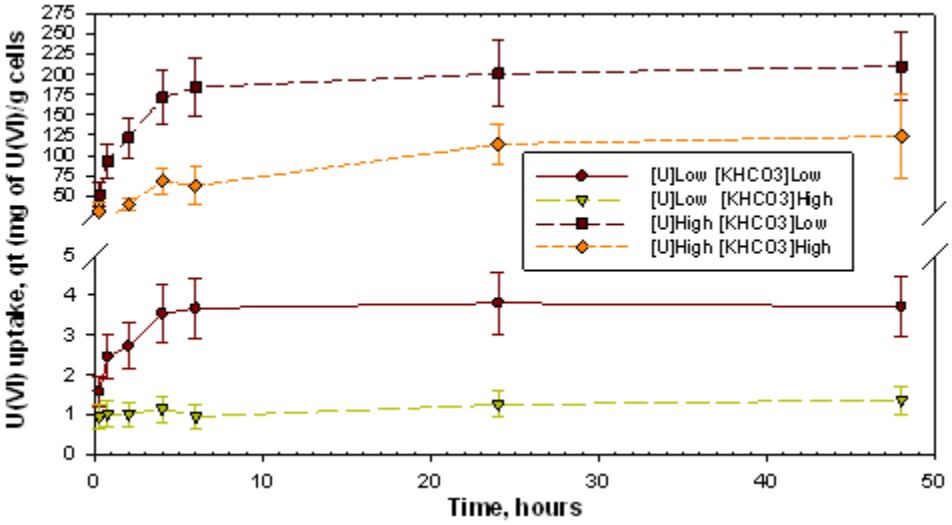

Figure 22. U(VI) uptake by *Arthrobacter* sp. G975 (mg/g) vs. Time, under low and high U(VI) concentrations and in bicarbonate amended SGW at pH 7.3, 25^{0}C. Calculated values are based on the cells dry weight.

Kinetics data analysis to interpret the experimental data and understand the controlling mechanisms of biosorption kinetics were conducted by means of the first-order, second-order, and the pseudo-second-order kinetic models (Benguella 2002; Aksu, Z. 2001). Only the pseudo-second-order model could delineate our results with very little error; its equation is expressed as:

$$dq_t/d_t = k_2(q_e - q_t)^2 \quad (14)$$

Integrating leads to

$$[1/ (q_e - q_t)] = (1/q_e) + k_2 t \quad (15)$$

or

$$(t/q_t)=(1/k_2 q_e^2)+(1/q_e)\, t \quad (16)$$

Where q_e is the equilibrium adsorption capacity, q_t represents the adsorption capacity of time t (mg g^{-1}). The plot of t/q_t (mg/g) against time, t, gave a linear relationship and the k_2 and q_e was obtained from the intercept and slope, respectively (Figure 23).

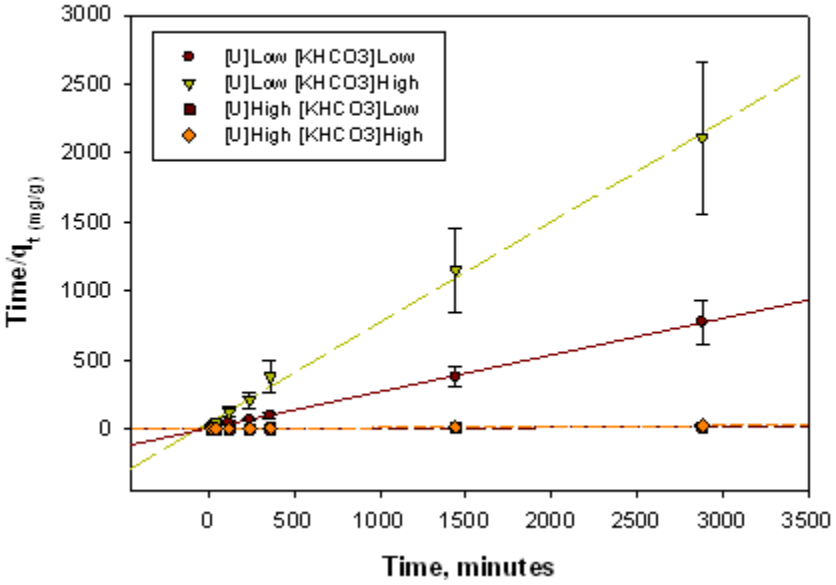

Figure 23. Pseudo second -order rate equation regressions for *Athrobacter* sp. G975, under low and high U(VI) concentrations in bicarbonate amended SGW at pH 7.3, 25^{0}C.

The model provides a good fit to the observed adsorption behavior in the bicarbonate-bearing experiments over the U(VI) concentrations tested. The correlation coefficient (R^2>0.991) adequately describes the kinetics of uranium biosorption by the bacteria and the U(VI) uptake rates determined by the model agree very well with the experimental data shown in Table 11. In addition, the theoretical q_{eq} values were in accordance with the experimental q_{eq} values. From these two facts, we can conclude that adsorption follows the pseudo second-order model with the assumption that biosorption may be the rate limiting step and the rate is proportional to the square of the number of unoccupied sites.

Table 11. Pseudo 2nd-order Model Simulation Sorption Kinetic Rates, k Rate Constant (mgU(VI)/g/min), and Equilibrium Adsorption Capacity (Qe=mgU(VI)/g) for Arthrobacter Sp. G975 in Carbonate Amended SGW at pH 7.3, 25°C.

		Factor B	
	Pseudo 2nd Order $\frac{dQ_t}{dt} = k(Q_e - Q_t)^2$ $\frac{t}{Q_t} = \frac{1}{kQ_e^2} + \frac{t}{Q_e}$	**[$KHCO_3$]** **Low** **0 mM**	**[$KHCO_3$]** **High** **2.5 mM**
Factor A	**[U(VI)] Low 299.1 ppb**	**k=0.014 ± 0.01 Q_e=3.76 (R^2=0.997)**	**k =0.012 ± 0.01 Q_e=1.37 (R^2=0.997)**
	[U(VI)] High 14,721.4 ppb	**k =7.16E-5 ± 1E-5 Q_e=213.7 (R^2=1)**	**k =3.24E-5 ± 8E-6 Q_e=132.6 (R^2=0.991)**

2^2 Factorial design uranium sorption at equilibrium

The results from the three- factors factorial design experiment indicated that the efficiency of the bioadsorption process is strongly dependent on the initial U(VI) concentrations, the concentrations of bicarbonate in the solution and time. The trend effect on the U(VI) adsorption by bacterial cells for each of the factors is shown in Figure 24.

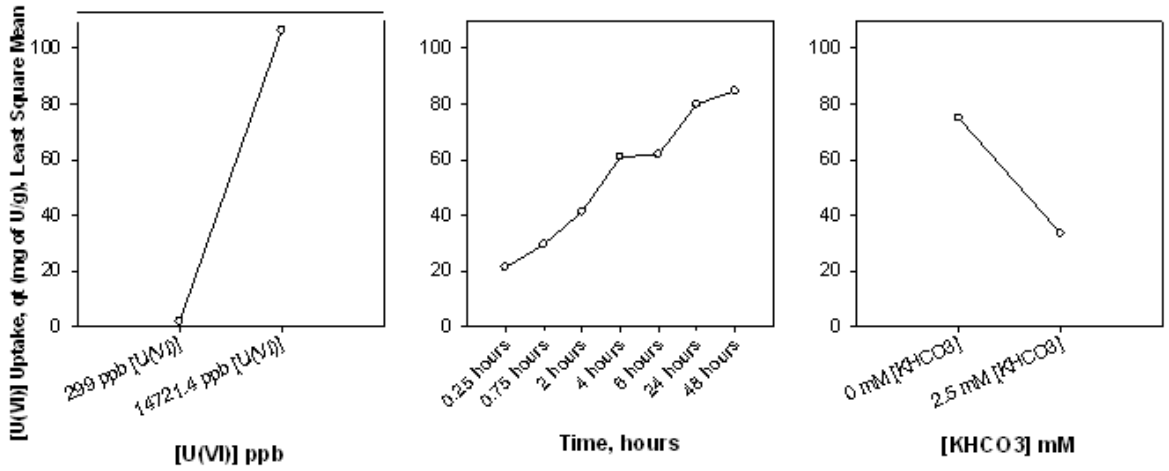

Figure 24. Profile plots derived from the factorial design experiment; least square means of U(VI) uptake (mg/g), time, and HCO_3 concentrations.

The plots present sharp changes in the metal uptake, which increases directly proportional to the initial U(VI) concentration, and inversely proportional to the bicarbonate concentration in solution. As bacterial exposure time increases, the metal uptake follows smoothly. The 2-Way ANOVA statistical analysis at equilibrium, shown in

Table 12, concludes that both the uranium initial concentration and the bicarbonate concentration are statistically significant factors that control the response variable of metal uptake ($p<0.001$, Power=1). Unfortunately, because the interaction between uranium and bicarbonate concentrations is also statistically significant, the main effects cannot be properly interpreted. However, the response variable can still be successfully modeled. The statistically obtained non-linear response surface plot[1] describing the U(VI) and bicarbonate interactions at equilibrium is in agreement with the experimentally derived data ($R^2=0.995$) (Figure 25).

Table 12. Two Way ANOVA: Effects of U(VI) and Bicarbonate Concentrations on the Uranium Uptake by Arthrobacter sp. G975 at Equilibrium (24 hours), in SGW pH 7.3, 25°C

Normality Test (Shapiro-Wilk): Passed (P = 0.081)			**Equal Variance Test:** Passed (P = 0.352)		
Source of Variation	**DF**	**SS**	**MS**	**F**	**P**
[Uranium], ppb	1	63919.902	63919.902	1049.660	<0.001
[KHCO3], mM	1	5302.704	5302.704	87.078	<0.001
[Uranium], ppb x [KHCO3], mM	1	4712.750	4712.750	77.390	<0.001
Residual	7	426.271	60.896		
Total	10	82335.378	8233.538		
Power of test with alpha = 0.05: 1.00 for [Uranium], 1.00 for [KHCO3], and 1.00 for [U(VI)]x[KHCO3].					

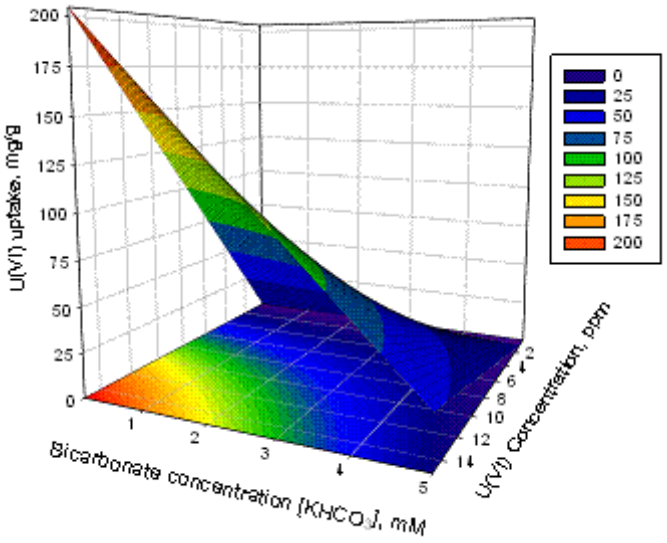

Figure 25. Response surface model, *Arthrobacter* sp. G975 uranium uptake (mg/g) vs. U(VI) and bicarbonate concentrations at equilibrium (24 hours), in SGW, pH 7.3, 25°C.

Sorption isotherm

To examine the relationships between the bacteria adsorbed (q) and equilibrium concentrations (C_e) in solution, the Langmuir, Freundlich, and linear isotherms were fitted to the experimental data of different bicarbonate concentrations. The different models are illustrated in Figure 26,

[1] A missing sample for high uranium and high bicarbonate was replaced by the mean substitution method.

Figure 27, and Figure 28. The figures strongly suggest that linearity prevails in the equilibrium relationship between adsorbed and solution concentrations for the entire range of initial U(VI) and bicarbonate concentrations studied.

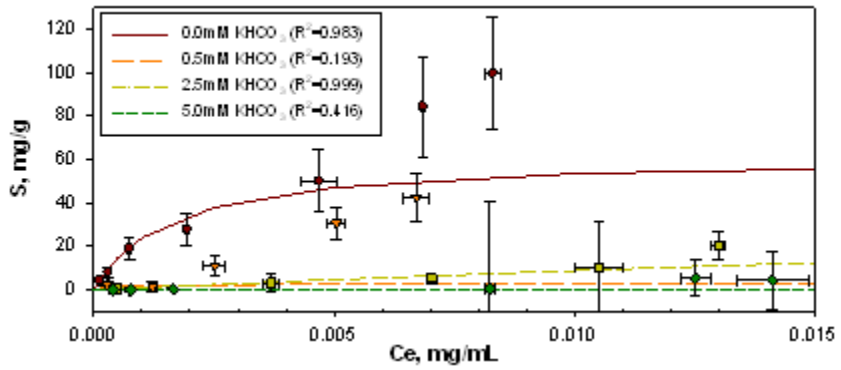

Figure 26. Calculated Langmuir U(VI) biosorption isotherms of *Arthrobacter* sp. G975 with bicarbonate concentrations varying in SGW from 0.0 to 5mM at pH 7.3, 25^{0}C, 24 hours.

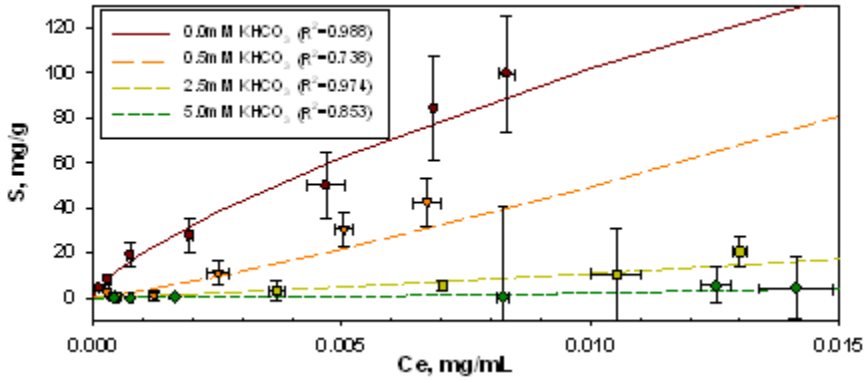

Figure 27. Calculated Freundlich U(VI) biosorption isotherms of *Arthrobacter* sp. G975 with bicarbonate concentrations varying in SGW from 0.0 to 5mM at pH 7.3, 25^{0}C, 24 hours.

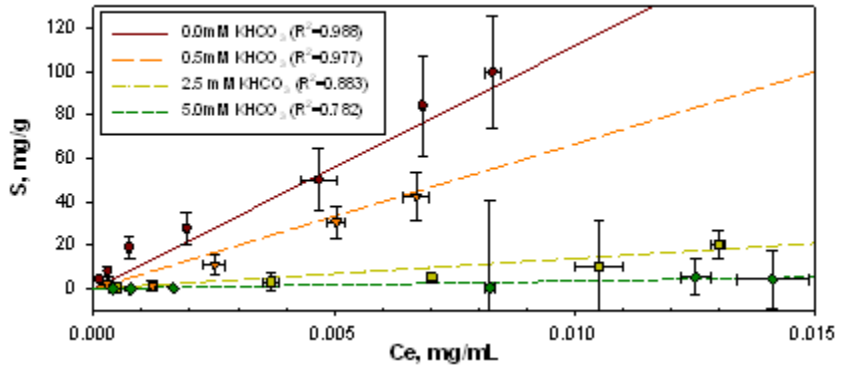

Figure 28. Calculated Linear U(VI) biosorption isotherms of *Arthrobacter* sp. G975 with bicarbonate concentrations varying in SGW from 0.0 to 5mM at pH 7.3, 25^{0}C, 24 hours.

The linear isotherm model provides the closest fit to the experimental results. This observation is supported by the Freundlich model whose mean n value of 0.93±0.3 is close to 1 and indexes of determination are as high as those calculated for the linear isotherm. Because neither the linear nor the Freundlich isotherms provide an approximate of the maximum adsorption capacity of the

bacterial surface, S_{max}, we attempted to obtain the estimate from a regression of the data with the Langmuir isotherm model. The regression results show very low indexes of determination for all bicarbonate concentrations tested, that reaffirms the Linear isotherm as the best relationship to represent the equilibrium behavior of U(VI) based on the A.G975 strain used in this study. A summary of the results fitted to the simulated models are shown in Table 13. The agreement of the data with the Linear isotherm and the low correlation for the Langmuir is conclusive.

Table 13. Simulated Results of Biosorption Isotherm with Langmuir, Freundlich, and Linear Equations Arthrobacter sp. G975 at Various Bicarbonate Concentrations in SGW, pH 7.3, 25°C, 24 Hours (n=3)

$KHCO_3$,mM	K_L, mL/mg	S_{max}	R^2	K_F, mL/g	n	R^2	K_d, mL/g	R^2
0	624.0 ± 205.6	62.1 ± 20.1	0.983	2,660.7 ± 79.2	1.4 ± 0.1	0.988	11,161.0 ± 555.3	0.988
0.5	1,783.7 ± 2,225.5	2.7 ± 1.9	0.193	11,803.2 ± 2,933.4	0.8 ± 0.3	0.738	6,654.7 ± 513.8	0.977
2.5	10.2 ± 17.9	95.2 ± 166.9	0.999	2,119.3 ± 153.6	0.9 ± 0.1	0.974	1,394.7 ± 253.3	0.883
5	110.8 ± 692.7	0.2 ± 1.2	0.416	5,623.4 ± 1,391.6	0.6 ± 0.1	0.853	352.5 ± 93.1	0.782

The U(VI) adsorption capacity of A.G975 at equilibrium with atmospheric CO_2 partial pressure and an initial U(VI) concentrations up to 14.5 mg/L were calculated as 150.2 ± 71.4 mg/g. We observed a decrease in the adsorption capacity in bicarbonate–bearing experiments similar to data derived from the factorial design experiments with the initial U(VI) concentrations ranging between 0.4-14 ppm. In fact, based on the K_d values of the linear isotherm depicted in Figure 29, the adsorption capacity exponentially decays (R^2=0.99) as the bicarbonate concentration is increased in solution. We can, therefore, assume that there exists a limit close to 5 mM of HCO_3 at which point carbonate-bearing experiments exhibit no measurable loss of U(VI) due to sorption onto the bacterial surface.

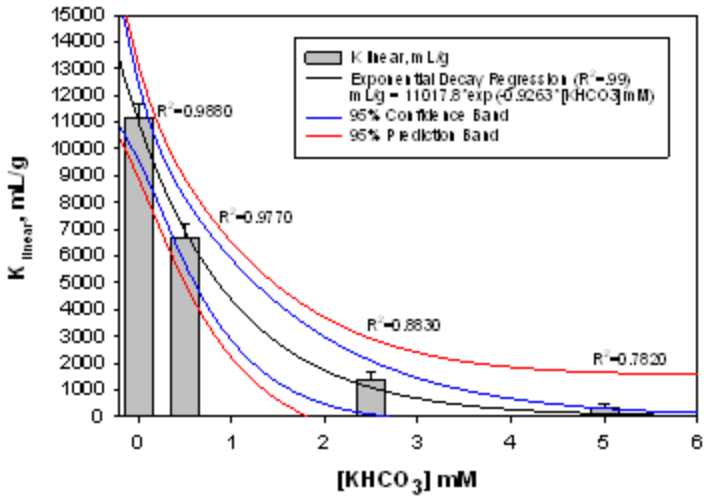

Figure 29. K_d values from the linear isotherm of *Arthrobacter* sp. G975 with bicarbonate concentrations varying in SGW from 0.0 to 5mM, pH 7.3, 25^{0}C, 24 hours.

Further evidence of diminishing uranium uptake by bacteria under increasing carbonate-bearing experiments is presented in Figure 30. The results strongly support the observation that the percent of U(VI) uptake is decreased with increasing concentrations of dissolved carbonate in the solution.

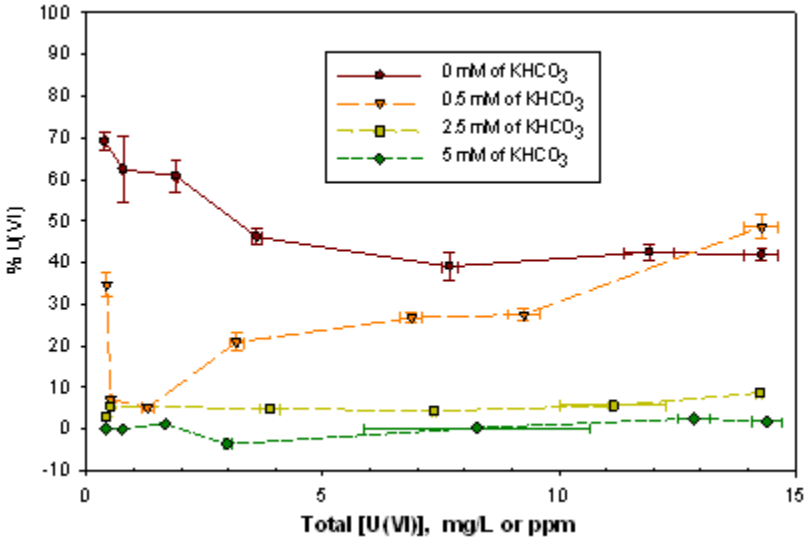

Figure 30. Percent of U(VI) uptake by *Arthrobacter* sp. G975 in SGW amended with bicarbonate concentrations varying from 0.0 to 5mM, pH 7.3, 25^{0}C, 24 hours (n=3).

In solutions without additional bicarbonate but at equilibrium with atmospheric CO_2, 70% of U(VI) were removed by bacteria. The increase in initial U(VI) concentrations tend to diminish the percentage of U uptake to 40-50%; however, this effect could be attributed to the U(VI) toxicity on bacterial cells. A pronounced decrease in percentage of U(VI) uptake by bacteria was originated from increasing bicarbonate concentrations in the SGW media. The addition of 5 mM

bicarbonate concentration yielded substantially lower values of bacterial uptake of U(VI), measured as 3%.

Desorption experiments

Desorption experiments were conducted to differentiate the amount of U(VI) externally adsorbed on the cell surface from that taken up by cells for internal accumulation. A 10 mM Na_2EDTA washing solution, a strong complex forming agent, successfully released U(VI) from the cell surface.

The theoretical value of accumulated U(VI) inside the cell was calculated via mass balance. The results shown on Figure 31 revealed the presence of U(VI) accumulation inside the cell across the experimental range of studied U(VI) concentrations (0.4-14 ppm). The percentage of U(VI) uptake inside the cell was found comparable to the external accumulation on cells wall. The addition of 2.5 mM of bicarbonate to the media solution resulted in limited biosortion and, as a consequence, accumulation inside the cell. Further studies on TEM/EDS microtome microscopy are required to identify uranium inside the bacteria.

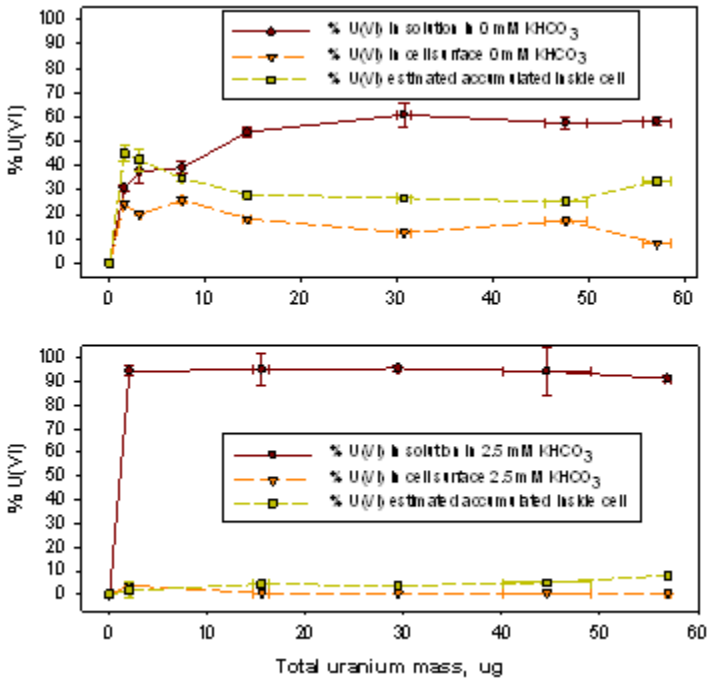

Figure 31. Calculated percentages of U(VI) distribution in SGW solution, adsorbed on bacterial cell, and accumulated inside cells at 0 and 2.5mM bicarbonate concentrations (at pH 7.3, 25^{0}C, 24 hours).

Cell Viability

We previously determined that *Arthrobacter* Sp. G975 is able to withstand the toxic effects of uranium to concentrations up to 40 ppm of U(VI**).** Cell viability was further evaluated through a 2x2 factorial design experiment with procedures previously described in this chapter. Viability assays were performed after 24 hours of cell incubation with the appropriate uranium and bicarbonate concentration treatment. Samples of each treatment were plated and incubated on 5% PTYG hard media and then counted for colony-forming units (CFU) (Figure 32). As

expected, the cells treated with a high concentration of U(VI) and low bicarbonate were less viable than those treated with a high bicarbonate concentration.

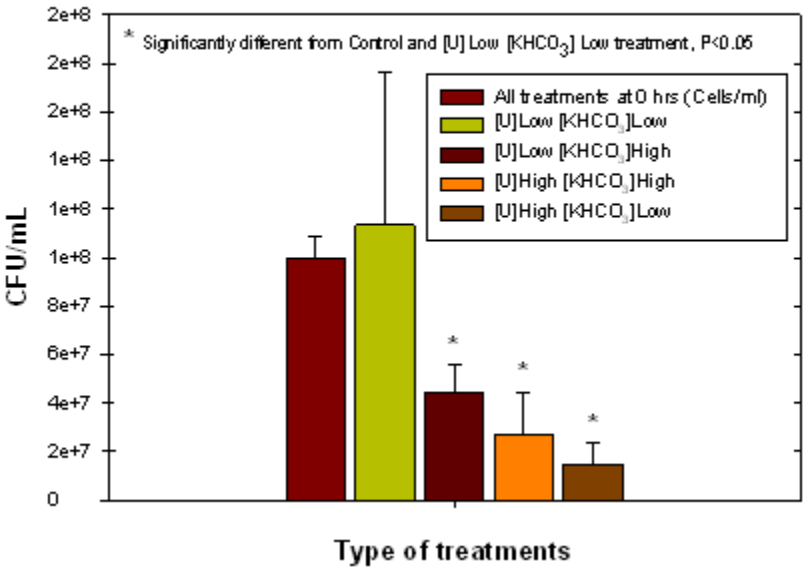

Figure 32. Colony Forming Units (CFU/mL) of all treatments after 24 hours of exposure to bacteria.

This can be explained by the uranium binding with bicarbonate forming highly soluble U(VI)-carbonate complexes that apparently lessen the U toxicity on bacterial cells. The same trend was not observed for the low concentrations of uranium tested. This could be attributed to a higher cell density in one of the samples bearing the low uranium and bicarbonate concentrations, which apparently caused higher standard deviations for this treatment. To test the hypothesis that the presence of bicarbonate reduces the toxicity of U(VI) on bacterial cells growth, the experiment was extended to evaluate the cell growth by mean of a spectrophotometer at 660 nm wavelength. The measurement of cell concentrations in bacterial suspensions by optical density yielded a linear relationship with a high correlation coefficient (R^2>0.99) (Figure 33).Working with the UV instrument in the kinetic mode and measuring the time-dependent changes in absorbance, we determined that the addition of bicarbonate did not impair cell growth. The cell growth rate in the 20 ppm U(VI)–amended solutions and U(VI)-free control treated with 0 and 5 mM of bicarbonate yielded the same 203,704 cells/min over a 24 h period. In contrast, a negative growth rate was observed in the bicarbonate-free treatment amended with 20 ppm of U(VI) over the same time period (Figure 34). The cell density in the treatments with positive growth rates yielded log 8.6 cells, after the 20 hours of incubation time, whereas the bicarbonate–free samples amended with 20 ppm of U(VI) exhibited a reduction in optical density corresponding to a log 8.4 cells. The only noticeable difference was a smaller length of the lag time period followed by a phase of rapid exponential growth.

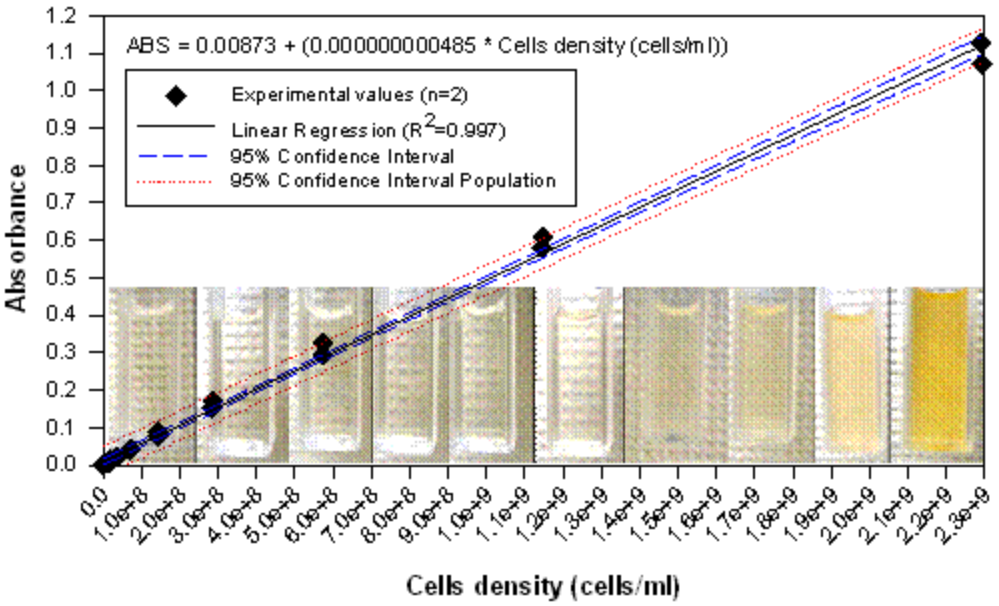

Figure 33. Spectrophotometer calibration curve for *A.* G975 in 5% PYTG medium.

Inhibition of bacteria activity appears to be associated with the binding of uranyl to the cell envelope. The passive binding of uranyl to cell surfaces reduces membrane fluidity and permeability, thus limiting media nutrient uptake. However, the presence of carbonate can strip uranyl from the cell surface by forming uranyl-carbonate complexes in solution (Bencheikh-Latmani and Leckie 2003).

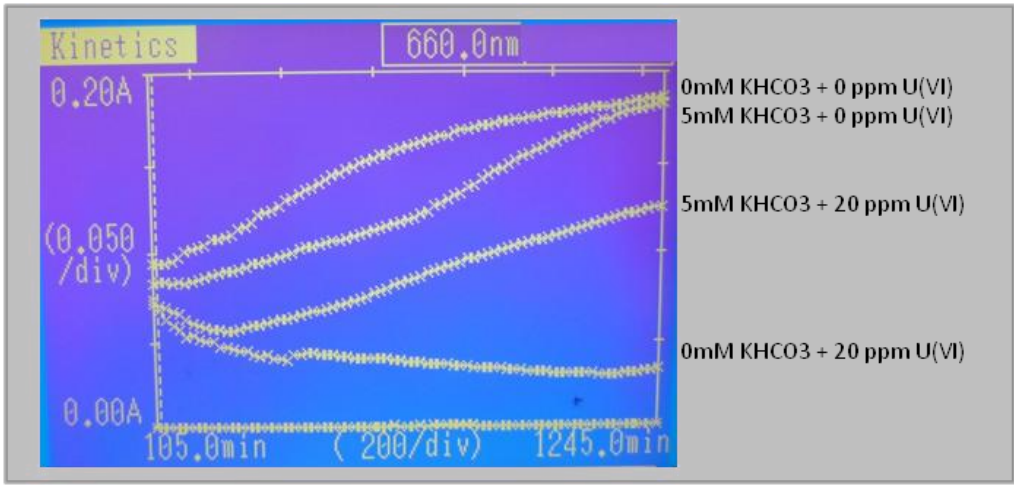

Figure 34. Time-depended changes in optical density of *Arthrobacter* sp. G975 cells in 5%PTYG media after 24 hours of exposure to low and high concentrations of uranium and bicarbonate (0 ppb U(VI) and 20 ppm/0.336 uM U(VI) against 0 and 5 mM of $KHCO_3$ respectively in SGW, pH 7.3, 25^0C.

Effect of Uranium on Microbial Surfaces Using Atomic Force Microscopy

Arthrobacter have developed very efficient molecular adaptation mechanisms that enhance the stability of nucleic acids, proteins, and lipids, allowing the bacteria to survive in stressful conditions (Mongodin et al. 2006). This phenomenon is associated with cell metabolism and, reportedly, with a very efficient phosphatase-mediated mechanism that the bacteria created to activate the secretion of phosphate groups. In fact, they can produce excess orthophosphate protecting cells from the toxic effects of radionuclides via passive U(VI) complexation by the negatively charged cell wall extracellular polymers (Beazley et al. 2007, Macaskie et al. 1992, Macaskie et al. 1994, Renninger et al. 2004, Martinez et al. 2007). Uranium bioprecipitation reactions involving ligands, liberated by phosphatase activity, result in a deposition of U(VI) on the bacterial cell wall as crystalline uranyl phosphate minerals (Macaskie et al. 2000). Despite considerable efforts to develop an understanding of how bacteria mediate biomineralization, our knowledge is far from complete and further research is needed to evaluate the interactions between uranyl ions and microbes.

Atomic force microscopy (AFM) was used to monitor changes at the nanoscale level in cell surface topography, roughness and adhesion before and after the cells exposure to various concentrations of uranium. The aim of this task was to present high-resolution AFM results on the formation of microbial uranyl-phosphate precipitates on the bacterial surface. The results demonstrated the ability of this method to qualitatively and quantitatively analyze uranium precipitation on live bacterial cell surfaces of various strains of *Arthrobacter* sp.

Uranium Precipitation on the Microbial Cell Surface

Microscopic observations specified the cell surface localized bioprecipitation of uranium. The phase images in Figure 35-Figure 40 [the image on the left represents the height data (Z range 250 nm) and the image on the right represents the phase data (phase angle 60º)] revealed extracellular precipitates deposited on the surface of uranium-loaded strains. Uranium precipitation is distinctly visualized as clearly defined crystalline deposits on the cell surface of uranium treated samples. For the uranium-free control samples, the formation of precipitates was not observed (Figure 35, Figure 37, and Figure 39).

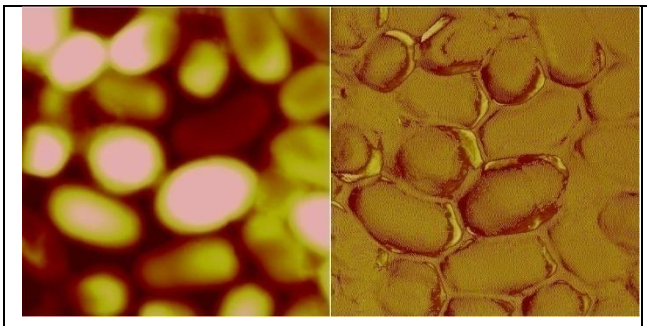

Figure 35. G968 control sample (scan size 4.89 × 4.89 μm^2). Phase image clearly shows no precipitation on the cell surface.

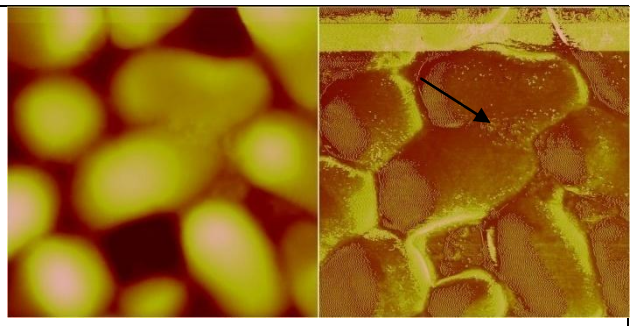

Figure 36. G968 cultured in the media amended with 0.5ppm of U(VI) (scan size 3.25 × 3.25 μm2). Phase image clearly shows crystalline deposits on the cell surface, which can also be visualized in height image.

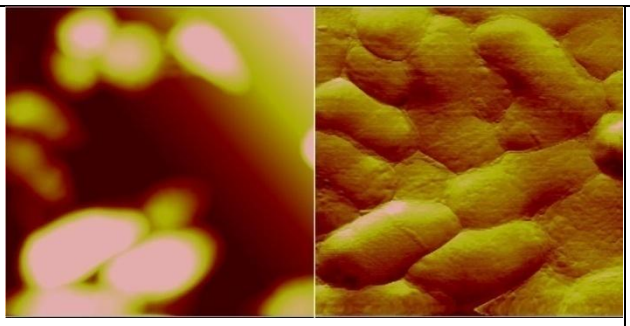

Figure 37. G954 control sample (scan size 4.77 × 4.77 µm2; Z range 200 nm and frictional image (0.3 V).

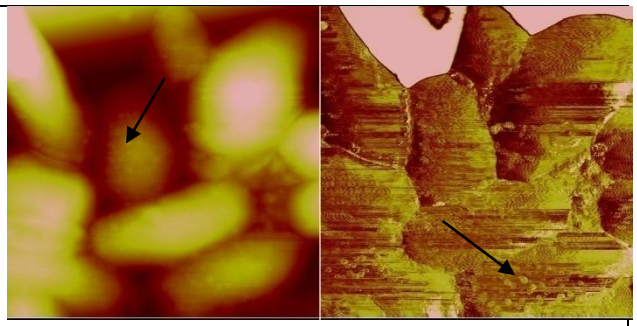

Figure 38. G954 cultured in the media containing 0.5ppm uranium (scan size 3.89 × 3.89 µm2; Z range 250nm and phase angle 60º). Height and phase images clearly show precipitation on the cell surface.

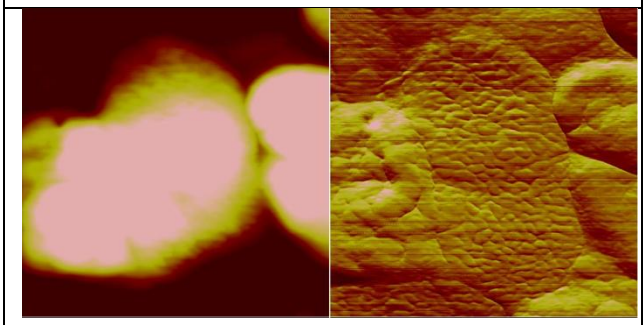

Figure 39. G975 control sample (scan size 2.94 × 2.94 µm2) showing its unusual wrinkled surface morphology. The topography image on the left (Z range 200 nm) and frictional image (0.3 V) on the right.

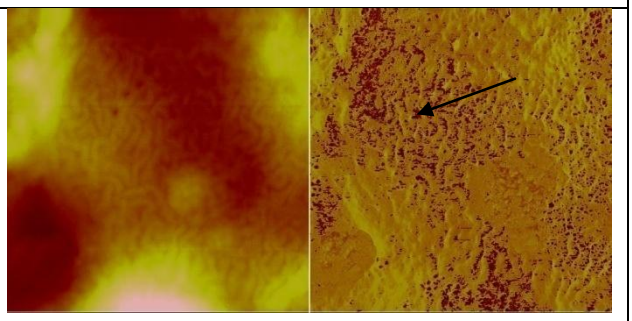

Figure 40. G975 cultured in the media amended with 10ppm of U(VI), (scan size 1.45 × 1.45 µm2; phase angle 60º). Phase image clearly shows crystalline deposition on the cell surface.

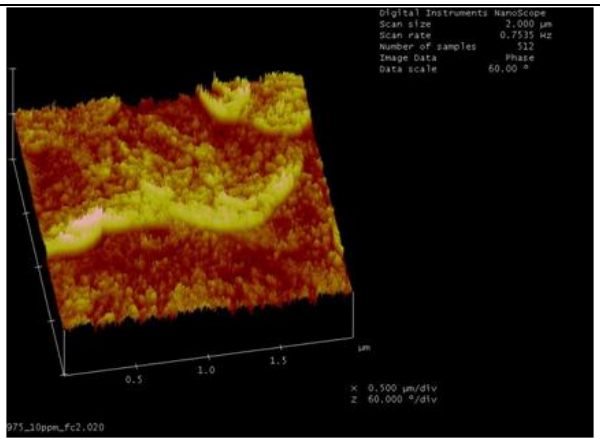

Figure 41. 3D micrograph of cell surface topology of G975 cultured in the media amended with 10ppm of U(VI). Scan size 2µm.

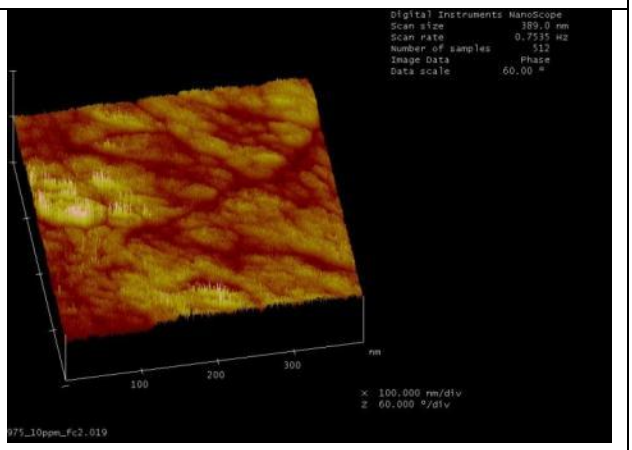

Figure 42. 3D micrograph of cell surface topologies of G975 cultured in the media amended with 10ppm of U(VI). Scan size 389nm.

3D AFM phase images show the variation in the G975 bacterial surface when treated with 10 ppm of U(VI). Brighter areas are an indication of higher adhesion regions due to higher surface elevation of uranium precipitates on the surface and darker regions correspond to lower adhesion

areas of bacterial surface (Figure 41, Figure 42). Brighter regions visualized on the cell surface can explain a significant increase in the surface roughness and changes in the adhesion forces.

The identification of the deposit composition was achieved by EDS analysis. EDS spectrums of uranium-loaded samples has confirmed the presence of uranium in the cell surface elemental composition, which was primarily composed of uranium (U), oxygen (O), phosphorus (P), sodium (Na), silica (Si) and potassium (K). The identity of cell-surface localized crystals was proven to be uranyl phosphate, $HU0_2P0_4.4H_20$, as reported in previous research (Beazley et al. 2007, Renninger et al. 2004, Macaskie et al. 2000).

The precipitation was clearly seen on the surface of all strains; however, the amount of precipitates accumulated on the surface of the G975 overshadowed that on G968 and G954. This may be due to the unique irregular surface structure of the G975 strain, which is seen in the topographic image (on the left, Z range 200 nm) and frictional image (on the right, 0.3 V) presented in Figure 40. The unusual wrinkled cell wall region may offer a larger surface area to provide higher accessibility for reaction with the soluble uranium for the formation of biogenic uranium precipitates. It was noted earlier that high surface area geometries can enhance reaction turnover rates (Castner and Ratner 2002). In addition, it was observed that higher concentrations of uranium in media solutions well correlated with an increase in uranium bioprecipitation on the cell surface. This was supported by EDS analysis of samples prepared on cells cultivated in media amended with various concentrations of U(VI). The EDS spectrum data indicates that higher U(VI) content found on the bacterial cell surface correlates with higher concentrations of uranium loaded to the culture broth (Table 14).

Table 14. Average U(VI) Bioaccumulation by Bacterial Cells

Strain	G975			G968		G954	
U(VI), ppm	9.5	19	27	0.5	5	0.5	5
U weight, %	0.52±0.25	2.51±0.7	2.82±0.8	1.23±0.13	1.46±0.45	0.16±0.3	4.88±1.3
U uptake, %	88.1±8.2	91.29±7.8	92.4±4.7	24.6±3.6	2.75±0.9	34.2±15.5	7.43±6.2

Roughness Analysis

Changes in the cells surface roughness of the three bacterial strains before and after exposure to various concentrations of uranium were monitored using AFM roughness analysis (

Table 15). Exposure was for 24 hrs and the concentrations of uranium ranged from 0.5 ppm to 19.5 ppm.

Table 15. Average Roughness (Ra) and Standard Deviation (SD) of Three Arthrobacter Strains Grown at Various Concentrations of Uranium

Uranium Concentration	G954		G968		G975	
	Mean Ra (nm)	SD	Mean Ra (nm)	SD	Mean Ra (nm)	SD
U-free controls	2.8	1.45	3.24	2.01	3.88	2.33
0.5ppm	3.74	0.63	2.92	1.51	8.48	2.64
5ppm	2.6	0.72	2.28	0.49	6.05	1.59
10ppm	-	-	2.8	0.64	7.12	1.09
19.5ppm	-	-	-	-	9.01	2.67

From

Table 15, it is clear that the difference in the mean roughness values among the strains for the control treatment is not great enough to exclude the possibility that its due to random sampling variability (P=0.803). For this reason, no trend or correlation was observed between the increase in uranium concentration and the roughness values for all strains. It was anticipated that the roughness parameter would increase with higher uranium concentration, specifically for G975, since an increase in uranium bioprecipitation on the bacterial surface was detected via EDS analysis and AFM. There is a slight trend for the G975 strain, and for some treatments (5ppm of U(VI)), the roughness mean for G975 is greater than values observed for both the G968 and G954 strains. However, the difference of the means are not statistically significant (P=0.82) for the samples tested. The relationship between roughness values and bacterial cells surface changes occurring with uranium exposure are not fully understood and require further investigation.

Force Spectroscopy Analysis

In previous studies, it has been shown that adhesion forces are very sensitive to surface modifications (Stegemann et al. 2007). Therefore, physiochemical changes occurring on bacterial cell surface membranes, when treated with various concentrations of uranium, were monitored with force spectroscopy analysis.

Table 16 demonstrates that changes in the adhesion force values of the control and uranium-treated samples is due to the increase in uranium concentration in the cultivation media, which caused chemical modifications of the bacterial cell surface. This significant change may be due to the physico-chemical reactions on the cells surface resulting in extracellular uranium deposition via secretion of extra orthophosphate protecting cells from the toxic effects of uranium (Beazley et al. 2007). The results shown in

Table 16 indicate a significant statistical difference in adhesion values between control samples and those exposed to uranium: 15.86 nN for G954, 1.649 nN for G968, both treated with 0.5 ppm of U(VI), and 10.02 nN for G975 treated with 5 ppm of U(VI). Our data suggests that each strain has a unique adhesion force parameter ($P<0.001$) that decreases exponentially as the uranium concentration is increased.

Table 16. Comparison of Adhesion Forces for Arthrobacter Strains

	G954		G968		G975	
	Adhesion(nN)	SD	Adhesion(nN)	SD	Adhesion(nN)	SD
Control	23.56	0.35	11.6	1.68	26.48	0.69
0.5ppm	7.7	0.54	9.97	0.73	N/A	N/A
5ppm	6.7	0.19	7.14	0.26	16.45	0.15
10ppm	N/A	N/A	4.58	0.26	15.86	0.7
10.5ppm	N/A	N/A	N/A	N/A	6.1	0.15

TASK 1.2 CONCLUSIONS

The effect of bicarbonate on the autunite mineral microbial leaching experiments was evaluated in mixed reactors comprised of autunite powder, media solution and bacteria and in a bacteria-autunite non-contact mode employing culture ware with inserts. The *Arthrobacter* G975 strain, which roughly accounted up to 25% of subsurface isolates, was used in the experiments. The uranyl release from autunite prior to the *Arthrobacter* G975 strain inoculation in mixed reactors was increased by a factor of 1.5±0.6 - 62.6±27.0 compared to the no-bicarbonate control. After bacteria inoculation, U(VI) measured in the reactors increased 7.5±3.9 - 1.4±0.1 fold when compared to the corresponding bicarbonate-bearing controls at a steady-state. A diminishing trend on the effect of bacteria on autunite leaching was observed as bicarbonate concentrations were increased in the solution. In a non-contact autunite biodissolution, the steady-state maximum concentrations of U(VI) detected were 1.0±0.7 - 4.6±3.11 fold higher than the abiotic control without the bicarbonate amendment. After bacteria inoculation, U(VI) concentrations increased 0.5±0.3 - 3.2±1.4 fold compared to U(VI) concentration at steady-state prior to inoculation. The data suggests that bacteria is responsible for autunite dissolution and is able to influence U(VI) leaching while are not in direct contact with the mineral. The aqueous concentrations of U(VI), P, and Ca released during the dissolution of autunite were non-stoichiometric over the range of experimental conditions. After inoculation, P concentrations in the biotic reactors were found to decrease. SEM analysis revealed biofilms on the surface of the autunite particles that apparently produce unique physiochemical conditions leading to U(VI) dissolution.

Visual MINTEQ was applied to evaluate the aqueous speciation and saturation state of the solutions with respect to key minerals and aqueous phases. The predicted saturation indices suggested that the biotic system would become saturated with respect to various calcium phosphates and to calcite at 10mM HCO_3^-. However, the system would remain under- saturated with respect to all potential U(VI) minerals except Na-autunite.

Our results confirmed that *Arthrobacter* sp. G975 can effectively remove soluble U(VI) ions from aqueous solution. The U(VI) biouptake obtained by conducting a 2^2 factorial design experiment was shown in the 83-90% range for the aqueous solutions at equilibrium with CO_2 atmospheric pressure.

Kinetics data analysis confirmed that the process follows a pseudo second-order kinetics model (R^2>0.991). The equilibrium for biosorption experiments was reached at 24 hours. It was

conclusively proven that bicarbonate ions affect the sorption behaviors of U(VI). The maximum biosorption capacity of U(VI) ions in the studied U(VI) concentration range at 25°C by *Arthrobacter* sp. G975 was observed at 154.7±60.6, 42.4±10.8, 20.6±6.5, and 5.5±8.0 mg/g for 0, 0.5, 2.5, 5 mM bicarbonate-bearing solutions, respectively. The incremental increase in aqueous bicarbonate concentrations exponentially reduced the U(VI) microbial uptake compared to values obtained in carbonate-free SGW. Experimental data indicates that increasing bicarbonate concentrations to 0, 0.5, 2.5 and 5 mM reduced the maximum U(VI) uptake by 0%, 72±13%, 87±7% and 96±5%, respectively. The linear isotherm models produced a higher correlation coefficient with the experimental data than the Freudlich and Langmuir adsorption models. Despite the large biosorption capacity, there is experimental evidence to suggest that not all uranium is adsorbed by the cell surface; it is also accumulated inside the cell. In the presence of bicarbonate, when highly soluble and mobile carbonate complexes dominate the aqueous speciation of U(VI), the viability of cells treated with high concentration of U(VI) was noted to increase.

AFM was used to investigate qualitative and quantitative changes on microbial cell surfaces when the cells interact with the uranyl ion. Our quantitative results show the ability to capture the surface phenomenon for three different strains of *Arthrobacter* sp. It was found that the level of precipitation is not uniform across the cell membrane and it also differs from strain to strain. Roughness analysis shows that an increase in the uranium concentration does not have any significant effect on cell surface roughness for all strains ($P>0.012$). The force spectroscopy results reveal an exponential decay relationship between the adhesion force and the concentration of uranium added to the growth media. Each strain has a unique adhesion force parameter ($P<0.001$) that decreases as the uranium concentration is increased. Further, force spectroscopy results indicate that the cell membrane adhesion properties change due to chemical interactions with various concentrations of uranium.

TASK 1.2 REFERENCES

Acharya, C., Joseph, D., Apte, S.K.. Uranium equestration by a marine cyanobacterium, Synechococcus elongatus strain BDU/75042. Bioresource Technology, 100 (2009). p. 2176–2181.

Aksu, Z. Equilibrium and kinetic modelling of cadmium(II) biosorption by C. vulgaris in a batch system: effect of temperature. Separation and Purification Technology. 21 (2001). P. 285–294.

Balkwill, D. L., Reeves, R. H., Drake, G. R., Reeves, J. Y., Crocker, F. H., Baldwin K, M., and D. R. Boone, 1997. Phylogenetic characterization of bacteria in the subsurface microbial culture collection," FEMS microbiology reviews, vol. 20, pp. 201-216.

Beazley, M. J., Martinez, R. J., Sobecky, P. A., Webb, S. M., and M. Taillefert, 2007. Uranium biomineralization as a result of bacterial phosphatase activity: insights from bacterial isolates from a contaminated subsurface, Environ. Sci. Technol, vol. 41, pp. 5701-5707.

Benguella, B., Benaissa, H. Cadmium removal from aqueous solutions by chitin: kinetic and equilibrium studies. Water Research, 36, (2002). P. 2463–2474.

Bencheikh-Latmani, R. and Leckie, J.O., 2003. Association of uranyl with the cell wall of Pseudomonas fluorescens inhibits metabolism. Geochimica et Cosmochimica Acta, Vol. 67, No. 21, pp. 4057–4066, 2003.

Bernhard, G., Geipel, G., Reich, T., Brendler, V., Amayri, S., Nitsche, H., 2001. Uranyl(VI) carbonate complex formation: validation of the $Ca_2UO_2(CO_3)^3$(aq.) species. Radiochim. Acta 89, 511–518.

Boylen, C.W., 1973. Survival of Arthrobacter crystallopoietes during prolonged periods of extreme desiccation. Journal of Bacteriology, vol. 113, pp. 33.

Burns, P.C., Miller, M.L. and R.C. Ewing, 1996. U^{6+} minerals and inorganic phases: a comparison and hierarchy of crystal structures, The Can. Mineralogist 34, p. 845–880

Cappella, B. and G. Dietler, 1999. Force-distance curves by atomic force microscopy. Surface Science Reports, vol. 34, pp. 1-104.

Castner, D., Ratner, B. 2002. Biomedical surface scinece: Foundations to frontiers. Surface Science 500 , 28-60.

Chang, T.W., Wang, M.K.. Assessment of sorbent/water ratio effect on adsorption using dimensional analysis and batch experiments. 2002, Chemosphere, pp. 419-426.

Crocker, F. H., Fredrickson, J. K., White, D. C., Ringelberg, D. B. and D. L. Balkwill, 2000. Phylogenetic and physiological diversity of Arthrobacter strains isolated from unconsolidated subsurface sediments, Microbiology, vol. 146, pp. 1295.

Devivo, B., Ippolito, F., Capaldi, G., Simpson, P. R. (Eds), Uranium Geochemistry, Mineralogy, Exploration and Resources. The Institution of Mining and Metallurgy, London, 1984, p. 43.

Dong, W., Brooks, S, 2006. Determination of the Formation Constants of Ternary Complexes of Uranyl and Carbonate with Alkaline Earth Metals (Mg^{2+}, Ca^{2+}, Sr^{2+}, and Ba^{2+}) Using Anion Exchange Method. Environ. Sci. Technol. 2006, 40, 4689-4695.

Dorobantu, L.S., Bhattacharjee, S., Foght, J. M., and M. R. Gray, 2008. Atomic force microscopy measurement of heterogeneity in bacterial surface hydrophobicity, Langmuir, vol. 24, pp. 4944-4951.

Finch R.J. and Murakami, T., 1999. "Systematics and paragenesis of uranium minerals. in" Uranium: Mineralogy, Geochemistry and the Environment", PC Burns & B. Finch, eds," Rev. Mineral. Geochem, vol. 38, pp. 91–179.

Fratesi, S. E., Lynch, F. L., Kirkland, B. L. and L. R. Brown, 2004. Effects of SEM Preparation Techniques on the Appearance of Bacteria and Biofilms in the Carter Sandstone. Journal of Sedimentary Research, V. 74, 6, p. 858–867.

Fredrickson, J. K., Zachara, J. M., Balkwill, D. L., Kennedy, D., Li, S. W., Kostandarithes, H. M., Daly, M. J., Romine, M. F. and Brockman, F.J. , 2004. Geomicrobiology of high-level nuclear waste-contaminated vadose sediments at the Hanford Site, Washington State, Applied and Environmental Microbiology, vol. 70, pp. 4230.

Fung, C. K. M., Seiffert-Sinha, K., Lai, K. W. C., Yang, R., Panyard, D., Zhang, J., Xi, N. and A. A. Sinha, 2010. Investigation of human keratinocyte cell adhesion using atomic force microscopy, Nanomedicine: Nanotechnology, Biology and Medicine, vol. 6, pp. 191-200.

Goldstein, A.H., 1986. Bacterial mineral phosphate. Am. J. Alt. Agric. 1(2), p.51-57.

Goldstein, A.H., 2000. Bioprocessing Of Rock Phosphate Ore: Essential Technical Considerations For The Development Of A Successful Commercial Technology.Proc. IFA Technical conference. New Orleans, pp. 1-21.

Guillaumont, R., Fanhänel, T., Fuger, J., Grenthe, I., Neck, V., Palmer D.A. and M.H. Rand, 2003. Chemical Thermodynamics, OECD Nuclear Energy Agency vol. 5, Elsevier, 919 pp.
Ho, Y.S. and C.C.Wang. Sorption equilibrium of mercury onto ground-up tree fern. 2008, Journal of Hazardous Materials, pp. 1421-1430.

Ilton, E S., Liu, C., Yantasee, W., Wang, Z., Moore, D.A., Felmy, A.R., Zachara, J. M., 2006. The dissolution of synthetic Na-boltwoodite in sodium carbonate solutions. Geochimica et Cosmochimica Acta 70, p.4836–4849

Ivanova, R., Bojinova, D., Nedialkov, K., 2006. Rock phosphate solubilization by soil bacteria. Journal of the University of Chemical Technology and Metallurgy, 41, 3, 297-302

K.Schluter. Sorption of Inorganic Mercury and Monomethyl Mercury in an Iron-Humus Podzol Soil of Southern Norway Studied by Batch Experiments. 1997, Environmental Geology, pp. 266-279.

Kalmykov, S. N.; Choppin, G. R., 2000. Mixed $Ca^{2+}/UO_2^{2+}/CO_3^{2-}$ complex formation at different ionic strengths. *Radiochim. Acta. 88*, p.603-606.

Langmuir, D., 1978. Uranium solution-mineral equilibria at low temperatures with applications to sedimentary ore deposits. Geochimica et Cosmochimica Acta, 42, pp. 547-569.

Langmuir, D., 1997. Aqueous environmental geochemistry Prentice Hall. Upper Saddle River, NJ.

Liu, C., Jeon, B., Zachara, J.M., Wang, Z., 2007. Influence of Calcium on Microbial Reduction of Solid Phase Uranium (VI). Biotechnology and Bioengineering, 97, 6, p.1415-1422.

Locock, A.J., and P.C. Burns, 2003. The crystal structure of synthetic autunite, $Ca[(UO_2)(PO_4)]_2(H_2O)_{11}$. American Mineralogist, 88, p.240–244.

Macaskie, L. E., Bonthrone, K. M., and D. A. Rouch, 1994. Phosphatase-mediated heavy metal accumulation by a Citrobacter sp. and related enterobacteria," FEMS microbiology letters, vol. 121, pp. 141-146.

Macaskie, L. E., Bonthrone, K. M., Yong, P. and Goddard, D. T., 2000. Enzymically mediated bioprecipitation of uranium by a Citrobacter sp.: a concerted role for exocellular lipopolysaccharide and associated phosphatase in biomineral formation," Microbiology, vol. 146, pp. 1855.

Macaskie, L. E., Empson, R. M., Cheetham, A. K., Grey, C. P. and A. J. Skarnulis, 1992. Uranium bioaccumulation by Citrobacter sp. as a result of enzymically mediated growth of polycrystalline HUO sub 2 PO sub 4," Science (Washington, DC);(United States), vol. 257.

Martinez, R. J., Beazley, M. J., Taillefert, M., Arakaki, A. K., Skolnick, J. and P. A. Sobecky, 2007. Aerobic uranium (VI) bioprecipitation by metal resistant bacteria isolated from radionuclide and metal contaminated subsurface soils," Environmental Microbiology, vol. 9, pp. 3122-3133.

Merroun ML, Raff J, Rossberg A, Hennig C, Reich T, Selenska-Pobell S. 2005. Complexation of Uranium by Cells and S-Layer Sheets of Bacillus sphaericus JG-A12. Applied and Environmental Microbiology 71(9): 5532–5543.

Mongodin, E. F., Shapir, N., Daugherty, S. C., Deboy R. T., Emerson, J. B., Shvartzbeyn, A., Radune, D., Vamathevan, J., Riggs, F. and V. Grinberg, 2006. Secrets of soil survival revealed by the genome sequence of Arthrobacter aurescens TC1," PLoS Genet, vol. 2, pp. e214.

Murphy W. M. and Shock E. L. (1999) Environmental Aqueous Geochemistry of Actinides. In Uranium: mineralogy, geochemistry and the environment, Vol. 38 (ed. P. C. Burns and R. Finch), pp. 221-254. Mineralogical Society of America.

Nedelkova M, Merroun ML, Rossberg A, Hennig C, Selenska-Pobell S. 2007. Microbacterium isolates from the vicinity of a radioactive waste depository and their interactions with uranium, FEMS Microbiol. Ecol. 59:694-705.

Noy, A., Vezenov, D. V., Lieber, C. M., 1997. Chemical force microscopy. Annual review of materials science 27, (1), 381-421.

Rai, D., Xia, Y., Rao, L., Hess, N.J., Felmy, A.R., Moore, D.A., and D.E. McCready, 2005. Solubility of $(UO_2)_3(PO_4)_2 \cdot 4H_2O$ in H^+-Na^+-OH^--$H_2PO^-_4$ -HPO^{2-}_4 -PO^{3-}_4 -H_2O and its comparison to the analogous PuO^{2+}_2 system. Journal of Solution Chemistry, Vol. 34, No. 4.

Renninger, N., Knopp, R., Nitsche, H., Clark, D. S. and J. D. Keasling, 2004. Uranyl precipitation by Pseudomonas aeruginosa via controlled polyphosphate metabolism, Applied and environmental microbiology, vol. 70, pp. 7404.

Sandino, A., Bruno, J, 1992. The Solubility of $(UO_2)_3(PO_4)_2 \bullet 4H_2O(s)$ and the Formation of U(VI) Phosphate Complexes: Their Influence in Uranium Speciation in Natural Waters. Geochim. Cosmochim. Acta 56, 4135-4145.

Smeaton,C.M., Weisener,C.G., Burns,P.C., Fryer,B.J. and Fowle,D.A., 2008. Bacterially enhanced dissolution of meta-autunite. American Mineralogist, 93, 1858-1864.

Sowder, A.G., Clark, S. B., Fjeld, R. A., 2001. The impact of mineralogy in the U(VI)–Ca–PO_4 system on the environmental availability of uranium. Journal of Radioanalytical and Nuclear Chemistry, 248, 3, p.517–524

Sparks, D. Kinetic and mechanisms of soil chemical reactions at the soil mineral/water interface.-, 1999. In: D.L Sparks, Editor, Soil Physical Chemistry.

Stegemann, B., Backhaus, H., and E. Santner, 2007. Spherical AFM probes for adhesionf orce measurements on metal single crystals, In Méndez-Vilas, A. & DÍAZ, J.(Eds.) Modern Research and Educational Topics in Microscopy.

Steward, S.A., Mones, E.T., 1997. Comparison and modeling of aqueous dissolution rates of various uranium oxides. Mat. Res. Soc. Symp. Proc. 465, pp. 557–564

Stumm, W. and J.Morgan. Aquatic Chemistry. Chemical equilibrium and rates in natural waters. 1996, John Wiley & Sons, Inc, p. 1022.

Suzuki Y. and Banfield, J. F., 2004. Resistance to, and accumulation of, uranium by bacteria from a uranium-contaminated site," Geomicrobiology Journal, vol. 21, pp. 113-121.

Takano, H., Kenseth, J. R., Wong, S. S., O'Brien, J. C. and M. D. Porter, 1999. Chemical and biochemical analysis using scanning force microscopy, Chem. Rev, vol. 99, pp. 2845-2890.

Van Waasbergen, L.G., Balkwill, D. L., Crocker, F. H., Bjornstad, B. N., and R. V. Miller, 2000. Genetic diversity among Arthrobacter species collected across a heterogeneous series of terrestrial deep-subsurface sediments as determined on the basis of 16S rRNA and recA gene sequences. Applied and environmental microbiology, vol. 66, pp. 3454.

Vazques, P., Holguin, G., Puente, ME., Lopez-Cortes, A., Bashan, Y, 2000. Biol. Fertil. Soil, 460-468.

Vermeul, VR., Bjornstad, BN., Fritz, B.G., Frutcher, JS., Mackley, RD., Mendoza, D.P., Newcomer, D.R., Rochhold, ML., Wellman, DM., Williams, M.D, 2009. 300 Area Uranium Stabilization Through Polyphosphate Injection: Final Report. PNNL-18529. Prepared for the U.S. Department of Energy under Contract DE-AC05-76RL01830.

Wellman, DM., Gunderson, KM, Icenhower, JP., Forrester, S.W., 2007. Dissolution kinetics of synthetic and natural meta-autunite minerals, $X_{3-n}^{(n)+}$ $[(UO_2)(PO_4)]_2 \cdot xH_2O$, under acidic conditions. Geochemistry, Geophysics, Geosystems, V. 8, 11

Wellman, DM., Icenhower, JP., Gamerdinger, A.P., Forrester, S.W., 2006. Effects of pH, temperature, and aqueous organic material on the dissolution kinetics of meta-autunite minerals, $(Na, Ca)_{2-1}[(UO_2)(PO_4)]_2 \cdot 3H_2O$. American Mineralogist, V. 91, p. 143-158.

Xie, S., Yang, J., Chen, C., Zhang, X., Wang, Q., Zhang, C.. Study on biosorption kinetics and thermodynamics of uranium b citrobacter freudii. Journal of Environmental Radioactivity, 99 (2008), p. 126-133.

Zachara, J.M., Davis, J.A., McKinley, J.P., Wellman, D.M., Liu, C., Qafoku, N., Yabusaki, S.,B., 2005. Uranium Geochemistry in Vadose Zone and Aquifer Sediments from the 300 Area Uranium Plume. PNNL-15121. Prepared for the U.S. Department of Energy under Contract DE-AC05-76RL01830.

Zachara, J.M., Smith, S.C. Groundwater Sampling and Characterization of 300-FF-5 Uranium Plume Sediments and Groundwaters. Pacific Northwest National Laboratory. May 10-11, 2004.

TASK 1.3 EFFECT OF BICARBONATE ON THE DISSOLUTION OF META-AUTUNITE

TASK 1.3 BACKGROUND

The Hanford Site 300 Area was primarily involved in the production of nuclear fuel, leading to the production of a variety of chemical and radioactive wastes. Since 1990, extensive remediation and restoration activities have been carried out to treat liquid waste disposal sites and solid waste burial grounds. Uranium is the most prominent contaminant present at the 300 Area. Its levels exceed the maximum contamination limit set by the EPA. Uranium (VI) is the most stable valence of uranium under oxidizing conditions, and due to its complicated chemical behavior, readily forms complexes with a variety of ligands (Grenthe et al. 1992). Common ligands in the environment that form stable uranyl solid phases include hydroxyl, phosphate, carbonate, silicate and organic substances (Burns et al. 1996, Lenhart et al. 2000, and J. A. Davis 2001).

The presence of phosphate in groundwater can limit the mobility of the uranyl cation (UO_2^{2+}) in the subsurface due to the formation of sparingly soluble autunite minerals $\{(X^{1-2+})_{2-}[(UO_2)(PO_4)]_2\ xH_2O\}$ that can persist under intense weathering conditions over geologic periods of time (Devivo et al. 1984). It has been shown that the long-chain soluble forms of polyphosphate delay the precipitation of phosphate in phases.

The release of uranium from autunite takes place during slow dissolution of the mineral structure. The log of the solubility product (K_{sp}) of uranyl phosphate, have been measured from 49 to 53 (Grenthe et al. 1992, Sandino and Brumo 1992), which is slightly less soluble than other autunite phases such as calcium ($\log K_{sp}=44.7$).

Information on the stability of uranyl-phosphate phases is limited to conditions involving pH, temperature, and a few aqueous organic materials (Wellman et al. 2006). Kinetic dissolution studies of autunite conducted under a wide range of pH and temperature conditions in flow-through and batch experiments illustrated a strong linear dependency of dissolution rates with respect to pH but were relatively insensitive to temperature variations (Wellman et al. 2007, Wellman et al. 2006, Zheng et al. 2006). The limited data available about autunite stability relates to complexation with ligands; however, the ability of ligands to form complexes tends to increase the solubility of minerals.

Bicarbonate anion is an important complexing agent for U(VI), that forms several soluble complexes with uranium (VI) in oxidized environments. $UO_2CO_3^0$, $UO_2(CO_3)_2^{2-}$, and $(UO_2)^2(CO_3)_3^{4-}$ are predominant at a pH > 4 (Langmuir 1978). The stability constants for these reactions are presented in Table 8 (Langmuir 1997).

Sowder et al. (2001) examined the extent of uranium dissolution from meta-autunite under conditions relevant to environmental contamination and spent nuclear fuel disposal. The results from 100 mM sodium bicarbonate dissolution tests suggest rapid uranium recovery occurs within 8 hours.

The use of carbonate/bicarbonate leach solutions is traditionally used to extract uranium from contaminated soils, especially in mining. Mason et al. (1997) examined carbonate leaching of uranium from contaminated soil at the Fernald site in southwest Ohio. The leach solution of

$K_2CO_3/KHCO_3$ at a 1:1 ratio with 0.5 M total concentration of carbonate effectively removed 80% of uranium from soil within 48 h and an additional 5% over the next 288 h. Increases in the reaction temperature often enhance the solution reaction rate. However, no appreciable changes were noted in the removal rate at temperatures of 25, 45, and 65°C using 0.5 M HCO_3^- as a leaching solution (Mason et al. 1997).

TASK 1.3 OBJECTIVE

The objective of the experimental work was to quantify the effect of bicarbonate on the stability of synthetic meta-autunite created as a result of uranium stabilization through polyphosphate injection. The polyphosphate technology with the formation of autunite is identified as the most feasible remediation strategy to sequester uranium in contaminated groundwater and soil in situ. The experimental work will help to quantify the dissolution kinetics of meta-autunite minerals in the presence of bicarbonate and investigate the influence of factors such as temperature and pH on the dissolution kinetics.

A series of dissolution experiments were conducted in a single pass flow through (SPFT) reactor using a mixture of carbonate and TRIS buffer solution subjected to various temperatures. The parameters that were tested are carbonate concentrations in the range of 0.5 - 3.0 mmol/L, pH (6 - 11), and temperature (5 - 60 °C).

TASK 1.3 MATERIALS AND METHODS

Synthetic Sodium Meta-autunite

Sodium meta-autunite, Na $[UO_2\ PO_4]\ 3H_2O$, was synthesized at Florida International University (FIU) by the direct precipitation method using uranyl nitrate, $UO_2(NO_3)_2 \cdot 6H_2O$, obtained from International Bio-analytical Industries, Inc. A literature review revealed two main approaches to synthesizing uranium phosphate minerals: direct and indirect precipitation. Wellman et al. (2005) described the direct precipitation method modified from Vochten and Deliens (1980).

The indirect precipitation of sodium meta-autunite can be accomplished by modification of the method described in Pekarek et al. (1965). This includes mixing 110 mM uranyl nitrate and 1.1 M phosphoric acid in a volumetric ratio of 1:1 at room temperature while stirring. A rapid reaction will occur yielding a lemon-yellow crystalline product (Wellman et al. 2005). The product should be cured at room temperature for 24 hours without stirring. The precipitate should be filtered using a 0.45 µm filter. To obtain sodium autunite salt, the crystals should be immersed in 200 ml aliquots of 2 M NaCl solution for 2 days, and the resulting crystals should be filtered using a 0.45 µm filter followed by washing with DI water and isopropyl alcohol. Crystals should be dried until a constant weight is achieved.

$$UO_2\ (NO_3)_2\ 6H_2O + H_3PO_4 \longrightarrow H[(UO_2)\ (PO_4)]\ nH_2O + 2HNO_3 \quad (17)$$

$$H[(UO_2)\ (PO_4)]\ nH_2O + NaCl \longrightarrow Na[(UO_2)(PO_4)]\ nH_2O + HCl \quad (18)$$

The precipitation of Na-autunite via the direct precipitation method was accomplished by mixing uranyl nitrate solution and sodium phosphate dibasic, $Na_2HPO_4 \cdot 7H_2O$ in a volumetric ratio of 1:7.5 while stirring at 70°C. The overall reaction is as follows:

$$Na_2HPO_4\ 7H_2O + UO_2(NO_3)_2\ 6H_2O \longrightarrow Na[UO_2PO_4]\ nH_2O + NaNO_3 + HNO_3 \quad (19)$$

Heating was terminated after a yellowish green precipitate formed rapidly while stirring was continued until the solution returned to room temperature. The solids were cured for 24 hours without stirring followed by recovery from solution using a disposable 0.45 µm filter. The crystals were washed with DI water heated to 70° C, then rinsed with isopropyl alcohol. The crystals were allowed to dry at room temperature until a constant weight was achieved.

Autunite Characterization Studies

The synthesized and partially reacted autunite solids were characterized by JSM-5900-LV low vacuum scanning electron microscope (SEM) at 15kV. Also, the composition of the particles was analyzed using a Noran System Six Model 200SEM Energy Dispersive X-Ray Spectroscopy (EDS). Pre-experimental analysis also included surface area analysis using BET and compositional analysis using Bruker 5000D XRD instruments.

Carbonate pH Buffer Solutions

Dissolution rate experiments with sodium autunite were conducted using 0.5 - 3.0 mmol/L carbonate buffer solutions to determine the dissolution rate of synthetic autunite. Carbonate pH buffer solutions were prepared by dissolving potassium bicarbonate powder, $KHCO_3$ (Fisher Scientific), in de-ionized water to attain concentrations of 0.5, 1.0, 2.0, and 3.0 mmol/L. The pH of buffer solutions was adjusted by using 0.1 mol/L hydrochloric acid, HCl (Fisher Chemicals), to obtain the target pH range of 6-11. 0.05 M Tris-hydroxymethyl aminomethane, $(HOCH_2)_3CNH_2$ (Fisher Argos Chemical), was added to buffer solutions to stabilize the pH of the solutions.

Single-Pass Flow-Through (SPFT) Experiments

The SPFT system (Figure 43) for dissolution kinetics of sodium autunite consists of a programmable Kloehn V6 syringe pump (55022), Kloehn Inc., that transfers carbonate-buffered fresh pH solutions from an influent reservoir via Teflon lines into two-port (1/4") 60-mL capacity perfluoroalkoxide (PFA) Teflon reactor vessels obtained from Savillex (Minnetonka, MN). The reactors were kept in an oven or refrigerator under the temperature controlled conditions during continuous system operation to maintain the specific operating temperature between 5° - 60° C and the solution flow rate was maintained from 1 - 2.5 L/day. The effluent solution was continuously collected and aliquots were retained for pH measurements and for elemental analysis (mainly U, P, alkalinity and inorganic carbon). Experimental conditions for the SPFT test utilized the following variables: pH range of 6-11 controlled by carbonate buffer solutions and constant temperature in the 5° - 60° C range controlled by the oven or refrigerator.

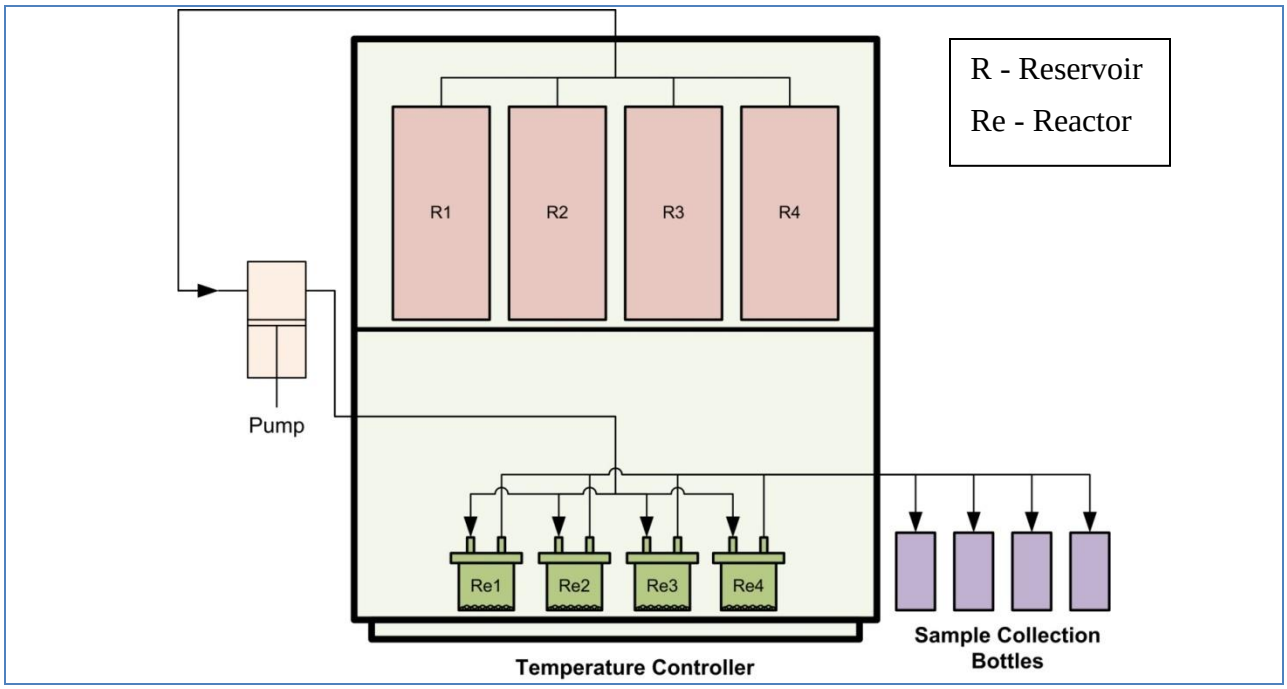

Figure 43. Single-pass flow through experimental setup.

Dissolution rate calculations

Dissolution rates obtained from the SPFT test are based on steady-state concentrations of the elements released from the solid phase to the effluent solution. The rates are normalized with respect to the element mass fraction, shown in Table 17, by the following formula:

$$r_{i,j} = \frac{(C_{i,j} - C_{i,b})\, q_j}{f_i\, S_j} \qquad (20)$$

where $r_{i,j}$= normalized release rate based on element i at the j^{th} sampling, g/m^2·d; $C_{i,j}$ = concentration of the element of interest, i, in the effluent at the j^{th} sampling, g/L; $C_{i,b}$ = average background concentration of the element i in the influent, g/L; q_j = flow rate at the j^{th} sampling, L/d; f_i = mass fraction of the element in the sample, dimensionless; S_j = surface area of the powdered specimen at the jth sampling, m^2.

Table 17. Element Mass Fractions for Sodium Meta-Autunite

Element	Formula Weight	Fraction Weight	Mass Fraction	Sample Mass
Na	22.98	22.98	0.0520	0.01
O	15.999	143.991	0.3258	0.08
U	238.029	238.029	0.5385	0.13
P	30.974	30.974	0.0701	0.02
H	1.008	6.048	0.0137	0.00
Total	-	442.022	1.0000	0.25

Sample Analysis

Sample analysis was carried out using the Kinetic Phosphorescence Analyzer (KPA) for uranium and Inductively Coupled Plasma Optical Emission Spectroscopy (ICP-OES) for sodium and phosphate.

Sample Preparation

Leach solutions contain organic matter; hence, pretreatment of samples is required before they can be processed using KPA and ICP-OES. Wet and dry ashing techniques modified from Brina et al. (1992) were used to remove organic content from the samples as follows:

Wet ashing

1 mL of sample, 0.5 mL of concentrated nitric acid (HNO_3) and 0.5 ml of hydrogen peroxide (H_2O_2) were added to a 20 mL scintillation vial. The mixture was placed on a hot plate and was dried slowly till a white precipitate was obtained. Occasionally, some samples turned yellow during this process due to the incomplete digestion, so 0.5 mL of hydrogen peroxide was added to those samples and were processed until a white precipitate was obtained.

Dry ashing

After the sample was wet ashed, it was placed in a muffle furnace preheated to 450 ^{o}C, for 15 - 20 minutes to dry ash the sample. Sample was allowed to cool after the ashing and 1 mL of 2 M nitric acid was added to bring the sample to the original volume.

TASK 1.3 RESULTS AND DISCUSSIONS

Dissolution Kinetics

Sample analysis is being carried out for concentrations of uranium, phosphate and sodium using KPA and ICP-OES. So far, twelve sets of samples were analyzed and the data for uranium rate of release at 23^{o}C and different pH values and at bicarbonate concentration of 0.0005 M and 0.001 M is presented in Table 18. Upon completing the sample analysis and data processing, results obtained will be presented as concentration of bicarbonate (M) vs. uranium rate of release (mol m^{-2} L^{-1}) and will be compared with the results obtained from natural autunite leaching experiments and conclusions will be made.

Table 18. Variation of Rate of Release of Uranium at 23 ^{o}C and at Different pH

pH	Rate of release of uranium (mol m^{-2} L^{-1})	
	0.0005M Bicarbonate	**0.001M Bicarbonate**
6	4.35E-14	2.32E-14
7	4.73E-14	8.39E-14
8	1.77E-13	2.33E-13
9	1.97E-13	2.28E-13
10	2.4E-13	1.03E-13
11	2.54E-13	1.77E-13

TASK 1.3 CONCLUSIONS

Experiments were completed successfully with different leach solutions (0.0005M - 0.003M Bicarbonate) at different temperatures (5 - 60 ^{o}C) and at different pH values (6 - 11). Samples are being processed and data for the concentration of uranium, sodium and phosphate is being collected. Preliminary data shows that the rate of release of uranium in (mol m^{-2} L^{-1}) increases with pH and concentration of bicarbonate. There is a significant change in the rate of release as the pH of the leaching solution increases from neutral range to basic range.

TASK 1.3 REFERENCES

Burns, P. C., Miller, M.L., Ewing, R.C. U^{6+} minerals and inorganic phases: a comparison and hierarchy of crystals structures. *The Can Mineral*, 1996, 34, 845-880.

Sutton, M., Warwick, P., Halla, A., Jones, C. Carbonate induced dissolution of uranium containing precipitates under cement leachate conditions. *J. Environ. Monit*., 1999, 1, 177-182

Langmuir, D. Uranium solution-mineral equilibria at low temperatures with application to sedimentary ore deposits. *Geochim Cosmochim Ac*, 1978, 42, 547-569

Langmuir, D. 1997.Aqueous Environmental Geochemistry. Prentice Hall, Inc, pp 602.

Locock, A. J., Burns, P.C. The crystal structure of synthetic autunite, $Ca[(UO_2)(PO_4)]_2(H_2O)_{11}$. *American Mineralogist*, 2003,88, 240-244.

Grenthe I., Fuger J., Konings R. J. M., Lemire R. J., Muller A. J., Nguyen-Trung C., and Wanner H, 1992. Chemical Thermodynamics of Uranium. Elsevier, Amsterdam.

Lenhart J. J., Cabaniss S. E., MacCarthy P., Honeyman B. D. Uranium(VI) complexation with citric, humic and fulvic acids. *Radiochim Acta*, 2000, 88, 345-353.

Davis, J. A., 2001. Surface Complexation Modeling of Uranium (VI) Adsorption on Natural Mineral Assemblages. Report NUREG/CR- 6708. U. S. Nuclear Regulatory Commission, Rockville, MD.

Casas, I, De Pablo, J, Gimenez, J, Torrero, M. E., Bruno, J., Cera, E., Finch, R.J. Ewing, R. C. The role of pe, pH, and carbonate on the solubility of UO_2 and uraninite under nominally reducing conditions. GeochimCosmochim Ac, 1998, 62, p. 2223-2231.

Devivo, B., Ippolito, F., Capaldi, G., Simpson, P. R. (Eds), Uranium Geochemistry, Mineralogy, Exploration and Resources. The Institution of Mining and Metallurgy, London, 1984, p. 43.

Mason, C. F., Turney, W. R., Homson, B. M., Lu, N., L, P. A., Chisholm-Brause, C. J. *Environ Sci Technol*, 1997, 31, 2707.

Sowder, A.G., Clark, S. B., Fjeld, R. A.. The impact of mineralogy in the U(VI)–Ca–PO_4 system on the environmental availability of uranium. *J Radioanal Nucl Ch*, 2001, 248, 517-524

Torrero, M. E., Baraj, E., De Pablo, J., Giménez, J., Casas, I.. Kinetics of corrosion and dissolution of uranium dioxide as a function of pH. *International Journal of Chemical Kinetics*, 1996, 29, 261-267.

Zheng, Z.P., Tokunaga, T.K., Wan, J.M. Influence of calcium carbonate on U(VI) sorption to soils. *Environ Sci Technol*, 2003 37, 5603-5608.

Ilton, E. S., Liu, C., Yantasee, W., Wang, Z., Moore, D. A., Felmy, A. R., Zachara, J. M. The dissolution of synthetic Na-boltwoodite in sodium carbonate solutions. *GeochimCosmochim* Ac, 2006, 70, 4836-4849.

De Pablo, J., Casas, I., Gimenez, J., Molera, M., Rovira, M., DURO, L.,J. Bruno, J. The oxidative dissolution mechanism of uranium dioxide. I. The effect of temperature in hydrogen carbonate medium. *Geochim Cosmochim Ac*, 1999, 63, 3097-3103.

Perez, I., Casas, I., Martin, M. Bruno, J. The thermodynamics and kinetics of uranophane dissolution in bicarbonate test solutions. *Geochim Cosmochim Ac*,2000, 64, p. 603-608.

Burns, P.C., Miller, M.L. Ewing, R.C. U^{6+} minerals and inorganic phases: a comparison and hierarchy of crystal structures, *Can Mineral*, 1996, 34, 845-880

Van Haverbeke, L., Vochten, R., Van Springel, K. Solubility and spectrochemical characteristics of synthetic chernikovite and meta-ankoleite. *Mineralogical Magazine*, 1996, 60, 759-766.

Wellman, D.M, Gatalano, J.G., Icenhower, J., P, Gamerdinger, A., P. Synthesis and characterization of sodium meta-autunite, Na $[UO_2PO_4]$ $3H_2O$. *Radiochim Acta* 2005, 93, 393-399.

Vochten, R., Deliens, M. Transformation of curite into meta-autunite: Paragenesis and electro-kinetic properties. *Phys Chem Miner*, 1980, 6, 129-43.

Pekarek, V. Vesely, V. A study on uranyl phosphates-II. Sorption properties of some 1- to 4-valent cations on uranyl hydrogen phosphate heated to various temperatures. *Journal of Inorganic and Nuclear Chemistry*, 1965, 27, 1151-1158.

Brunauer, S., Emmett, P.H., Teller, E. *J. Am. Chem. Soc.*, 1938, 60, 309.

Rossella, B., Miller, A.G. Direct detection of trace levels of Uranium by laser-induced kinetic phosphorimetry. *Analytical Chemistry*, 1992, 64, 1413-1418.

TASK 2: URANIUM (VI) STABILIZATION IN THE HANFORD SITE VADOSE ZONE (200 AREA) SEDIMENT UTILIZING IN SITU CALCITE MINERAL

TASK 2 INTRODUCTION

Uranium is a naturally occurring radioactive substance and is globally mined in large quantities. While mining may have been the major cause of uranium contamination elsewhere, some of the unintended releases of uranium during utilization and storage have caused extensive contamination of soil, groundwater and surface water systems at some of the nuclear facilities in the United States (Eisenbud and Gesell 1997). Due to the potential threat on human health, the U.S. Environmental Protection Agency (U.S. EPA) has set a maximum contaminant level of 30 µg/L for uranium concentration in drinking water (USEPA 2001).

Among several other uranium contaminated areas in the United States, DOE's Hanford Site in Washington State was included on the National Priorities List (NPL) in 1989. The Hanford Site covers approximately 586 square miles and was established to produce nuclear material for national defense (PNNL 2007). This site was further divided into 4 NPL sites, including the 100 Area, 200 Area, 300 Area, and 1100 Area. The 200 Area at Hanford, also referred to as the Central Plateau, lies in the middle of the Hanford Site and encompasses approximately 75 square miles. It is divided into two sections known as the 200 East Area and 200 West Area.

During its operation beginning in 1944, uranium fuel rods from the reactors were transported to the 200 Area facilities for the removal and refinement of plutonium (PNNL 2008). This process produced millions of gallons of radioactive and hazardous waste. The cribs, trenches, and ponds that initially contained the radioactive waste, leaked into the soil and water environment, causing extensive contamination. Further, to accommodate the waste, 149 single-shell underground storage tanks were built between 1943 and 1964 at the 200 Area. Another 28 tanks, referred to as double-shell tanks (so called due to the presence of an additional protective shell), were added between 1968 and 1986. The underground storage tanks (n=177) are organized into 18 groups of tank farms spread throughout the 200 Area and contain over 53 million gallons (200 million liters) of high level radioactive waste. While the double-shell tanks have remained intact, many of the single-shell tanks (around 67) have been found to be leaking radioactive waste into the vadose zone. It has been estimated that the leakage could be anywhere between 1 to 2 million gallons (3.79-7.58 million liters) of radioactive waste. The vadose zone of the 200 Area ranges in depth from approximately 164 feet (50 meters) in the West Area to 341 feet (104 meters) in the southern area. The groundwater beneath the 200 Area has been reported to contain some of the hazardous and radioactive contaminants that are similar to the chemicals stored in the tank farm, thus indicating contaminant migration from the vadose zone (Zachara et al. 2008).

Vadose zone soil/sediment in the 200 Area is reported to contain natural calcite minerals (calcium carbonate) in abundance (Zachara et al. 2007). Several studies have reported the affinity of uranium to form complexes with calcite or its constituents-carbonate/calcium (Kitano and Oomori 1971, Russel et al. 1994, Sturchio et al. 1998, Kelly et al. 2003, and Joseph et al. 2011). Three of the complexes have been reported for uranium and carbonate (uranyl carbonate): rutherfordine, UO_2CO_3 (Smith 1984); blatonite, $UO_2CO_3.H_2O$ (Vochten and Deliens 1998); and joliotite, $UO_2CO_3.nH_2O$, n~2 (Gaines et al. 1997). There are other complexes that

include both carbonate and calcite, such as wyartite, $Ca(CO_3)U^{5+}(UO_2)_2O_4(OH)(H_2O)_7$ (Burns and Flinch 1999); zellerite, $Ca(UO_2)(CO_3)_2(H_2O)_5$ (Gaines et al. 1997); liebigite, $Ca_2(UO_2)(CO_3)_3(H_2O)_{11}$ (Vochten et al. 1994); and sharpite, $Ca(UO_2)_6(CO_3)_5(OH)_4(H_2O)_6$ (Cejka et al. 1984), to mention a few. There are many uranyl-carbonate complexes that also integrate elements other than calcium (e.g. Cu, Na, Pb, Zn, Mg etc.), but are not discussed here. It has been found that the co-precipitation mechanism plays a significant role in the formation of uranyl-carbonate complexes as discussed above. Leu et al. (2004) reported the co-precipitation of U (VI) with calcite in the Hanford vadose zone sediment. According to these authors, calcite maintains an equilibrium with the sediment pore water and facilitates the complexation of uranium (VI) with calcium and carbonate, thus forming a majority of $Ca_2UO_2(CO_3)_3^0(aq)$ species in the vadose zone pore water. This species is regarded as the major aqueous U(VI) species in the vadose zone porewater at the site. In a separate study based on laboratory investigation, Reeder et al. (2000) reported co-precipitation of uranyl species with carbonate at pH 8.1 to 8.2, forming predominantly the triscarbonato complex, $UO_2(CO_3)_3^{4-}$. These authors reported this complex to be stable and water soluble.

Given the affinity of U (VI) to form complexes with carbonate and calcium, the natural presence of in situ calcite may influence the mobility of uranium in the soil environment. Conversely, this kind of affinity of uranium for the calcite constituents may be better utilized in a cost-effective way to stabilize uranium in the vadose zone by means of co-precipitation (which involves pH manipulation to facilitate calcite dissolution and co-precipitation). This work involved studying adsorption of uranium in the Hanford sediment and a study on calcite dissolution and its influence on the adsorption process. The information provided in this report will be helpful in understanding uranium mobility in the Hanford sediments in the presence and absence of calcite minerals. Further, the results of this task may help in the development of a remediation plan utilizing calcite-based technology.

TASK 2 MATERIALS AND METHODS

High purity chemicals were obtained from Fisher Scientific, including a uranium standard (UO_3 in 3% HNO_3, U= 1,000 ppm), calcite crystals ($CaCO_3$), pH reference standards, and pH buffers (explained below), to be used in the studies. Various other laboratory supplies and equipment, such as digital pipettes and regular glassware, deionized water, PTFE 0.45 µm filters, and disposable 10 mL plastic syringes, were also utilized.

The study utilized **t**hree different types of pH buffers**:** a glycine/NaOH system for pH 9.0, a trisminomethane/HCl system for pH 7.5, and citric acid for pH 5.5. In order to prepare the glycine/NaOH system, the stock solutions of 0.1 M glycine and 0.1 M NaOH were used in titration until the desired pH was obtained. Continuous monitoring/measurements were made during the titration using MetrohmTitrando titration systems. The tris-amino methane/HCl system was prepared using 0.1 M tris aminomethane solution, which was titrated with dilute HCl until pH 7.5 was reached.

Experimental sediment

Adsorption experiments utilized Hanford sediment that was collected at the Hanford Site 300 Area. The bulk sediment from this area has been reported to contain quartz as its dominant mineral with feldspar and hornblend in small proportions (Wellman et al. 2008). The sediment was air dried under the laboratory hood by spreading it on a paper towel and then homogenized

with a scoop. In order to ensure uniform particle size distribution, homogenized sediment was randomly sampled (n=3), while still spread on the paper towel, and separately sieved through a 2-mm pore size sieving tray. The sieving results indicated a 44.92 ± 1.74% (± std. error) fraction of the sediment (by weight) contained particle sizes > 2 mm and a 55.08 ± 1.74% sediment fraction that was </= 2 mm. The same sediment contained a 47.48 ± 1.98% fraction with particle size </= 1 mm. It was noted that the sediment with particle size > 2 mm contained gravel of various sizes and thus interfered with the homogenization process (standard error above). Removal of the gravel (>2 mm) from the sediment samples provided a relatively lower error, 0.99% (mean = 86.15%), for the sediment size fraction < 1 mm. This sediment was deemed sufficiently homogenized due to the small fraction of error. The experiments utilized the sediments with particle size < 1 mm, after proper sterilization (autoclaving) to get rid of the sediment microorganisms. Autoclaving was done twice at 121 °C/103 kPa for 30 minutes in a 24-hour interval.

Uranium adsorption experiments

The batch equilibrium adsorption experiments were conducted for a period of 48 hours. The sterilized sediment samples that had been sieved (<1 mm) and homogenized were used along with the buffer solution (pH 7.5) that was prepared using tris-amino methane and HCl. The experiments were conducted for the uranium concentrations of 50, 100, 150, 200 and 250 µg/L. Adsorption experiments were performed in triplicate by placing 2 g of the sediment in each 42-mL glass vial (for total of 18, including 3 controls). The vials were then filled with 10 mL buffer solutions and allowed to saturate overnight (~24 h). After the saturation period, the required volume of uranium solution (based on the desired concentration of uranium) was added to the vial and the final volume of the aqueous phase was brought to 20 mL. In order to facilitate proper mixing and achieve equilibrium, the vials were held horizontally in a box and then placed on a shaker table at 100 rpm for 48 hours at 23^{o}C. After the 48-hour equilibration period, the liquid in the vials were subjected to sedimentation and the supernatant liquid was decanted and then filtered through PTFE syringe filters (0.45 µm followed by 0.2 µm). The filtrate was further processed in order to get rid of any organics that would interfere with the analysis for uranium. Briefly, the samples for uranium analysis were prepared using a dry-ashing procedure, where a known amount of sample is treated with concentrated nitric acid and hydrogen peroxide (30%), heated on a hot plate until it dries, and then placed in a furnace at 450^{o}C for 15 minutes. Some of the samples were treated repeatedly until they showed a clear/white color for the precipitate. At the end, 0.5 mL of 2 M HNO_3 was added to the vial to dissolve the uranium salt, followed by the addition of DI water to provide the desired dilution. The samples were analyzed in the Kinetic Phosphorescence Analyzer (KPA) instrument (Chemchek Instrument Inc.) to determine the uranium concentration in aqueous samples.

Two separate sets of adsorption studies were also conducted in order to understand the role of calcite on uranium sorption. This study was aimed at providing preliminary information on adsorption behavior of uranium in the presence of calcite (calcium carbonate). Thus, the experimental duration was set to 24 hours (Wang et al. 2011) and only two of the uranium concentrations were tested. Equilibrium studies with several other concentrations (as outlined in the preceding section for the batch adsorption equilibrium experiments) were planned to be completed in FY11. The first set of adsorption experiments were conducted using calcite crystals. The sediment and the aqueous phase (buffer solution) remained the same as that of the equilibrium adsorption experiments explained previously. The vadose zone sediments at the

Hanford Site have been found to contain a varing percentage of calcite, often reported in the range of 1 to 5% with an average 1.79 % (Serne et al. 2004). For this experimental study, 10 mg calcite crystals (<1 mm in size) had been homogenized with the sediment (2 g), giving a value of 0.5 % for the calcite that had been added, with an assumption that the sediment already contained some amount of natural calcite. More detailed experiments with other percentages of calcite were planned for FY11. The homogenized sediment containing calcite was placed in the 42-mL vials (n=3) before adding 10 mL of aqueous solution and allowed to saturate (~24 h). The vials were then injected with uranium (explained below) and the final volume was adjusted to 20 mL by adding the same aqueous solution. Two different concentrations of uranium (50 and 250 µg/L) were tested at pH 9.0 and 7.5. The other set of experiments was done in a similar manner in the absence of calcite in order to compare the results. The samples were processed and analyzed following the same method described previously.

Calcite dissolution kinetics

Time series experiments were conducted to understand the rate of calcite dissolution at different pH conditions (pH 5.5, 7.5, and 9.0). The independent experiments were set up for six different time durations, including four short durations (0.05 h, 0.50 h, 0.75 h, and 1.00 h) and two long durations (24 h and 48 h). These experiments were intended to provide information on the rate of change in calcite mass rather than the equilibrium. Also, this study was conducted under laboratory conditions in order to help in designing further experiments (for FY11) that would closely simulate the field conditions. Deionized water was used to prepare the aqueous media for the desired pH with the help of the appropriate buffer. As explained previously, a glycine/NaOH system for pH 9.0, a trisminomethane/HCl system for pH 7.5, and citric acid for pH 5.5 had been used in the study. All of the solutions to be used in the experiments were purged with nitrogen gas to remove CO_2, including the vials that were to be used in the experiments. The transfer of the aqueous media into the respective vials was accomplished within an anaerobic glove box filled with nitrogen gas. Each experiment utilized 42-mL glass vials containing 10 mg of calcite immersed in 20 mL of solution, all prepared in triplicate. The experimental vials were placed on a magnetic shaker and agitated at 100 rpm for the given duration of the experiment at room temperature. At the end of the experiments, the samples were drawn out of the vials and filtered through a 0.2 µm filter for calcium analysis.

Analytical

Samples for uranium analysis were prepared using a dry-ashing procedure where a known amount of sample is treated with concentrated nitric acid and hydrogen peroxide (30%), heated on a hot plate until it dries, and then placed in a furnace at 450^{o}C for 15 minutes. Some of the samples were treated repeatedly until they showed a clear/white color for the precipitate. At the end, 0.5 mL of 2 M HNO_3 was added to the vial to dissolve the uranium salt, followed by the addition of DI water to provide the desired dilution. The samples were analyzed in the Kinetic Phosphorescence Analyzer (KPA) instrument (Chemchek Instrument Inc.) for uranium concentrations in aqueous samples. Additionally, calcium in aqueous samples was analyzed using an ICP-OES instrument (PerkinElmer).

TASK 2 RESULTS AND DISCUSSIONS

Adsorption of uranium

With increasing concentrations of uranium in water, the sorption of uranium increased in the sediments. The Pearson correlation for the initial and final concentrations of uranium in water was 0.99, which was highly significant ($p<0.001$). A Freundlich plot of log [C_{aq}] vs. log [C_{ad}] gave r^2 = 0.89, and K_F = 0.024 mL/g with 1/n = 0.45 (Figure 44). A Langmuir plot of $1/C_{aq}$ vs. $1/C_{ad}$ gave a correlation coefficient r^2=0.72, and thus it was not utilized for further calculations (Figure 45). Also, it was found that the Freundlich adsorption isotherm gave a better estimate for the experimental results as shown in Figure 46.

The Freundlich adsorption coefficient in this study was relatively low (0.024 mL/g) compared to the literature values that are commonly reported for the soil matrix. However, it should be noted that the Hanford sediment that was utilized in this study had very poor organic content (~2 %) with sandy texture. The uranium adsorption coefficient obtained in this study compares well with the values reported by Um et al. (2007) for some of the aquifer sediments (with and without gravels) at the Hanford Site.

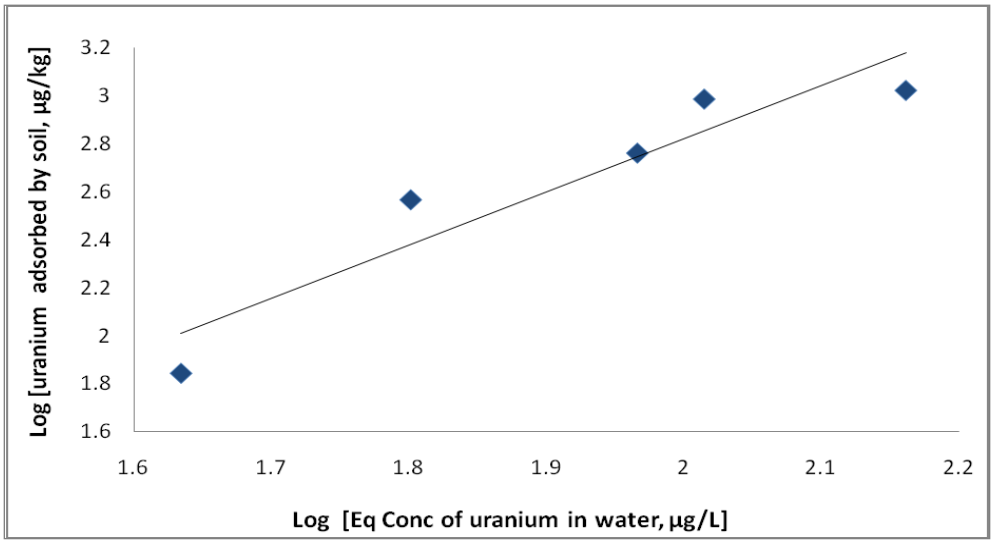

Figure 44. A plot for log Cad (adsorbed uranium) versus log Caq (aqueous uranium) in order to determine Freundlich parameters.

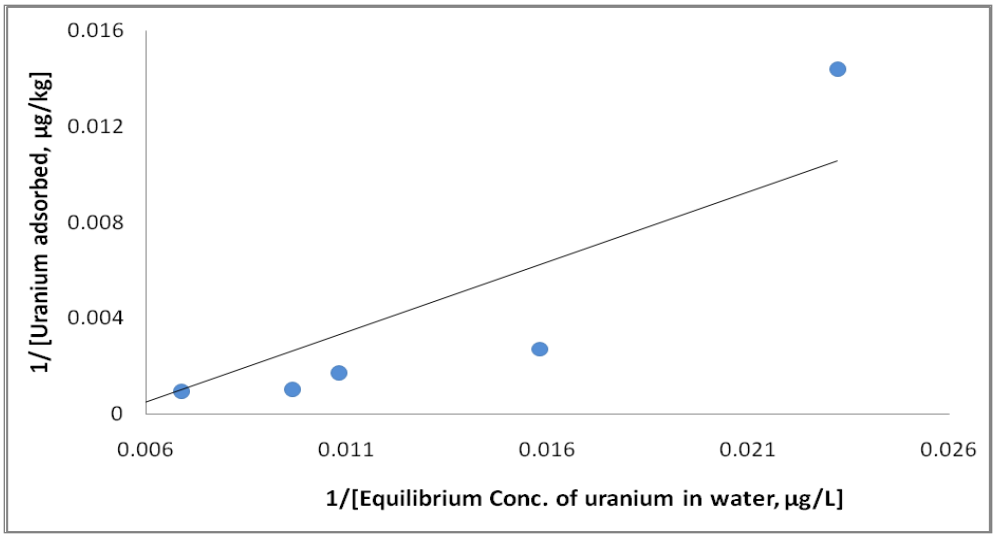

Figure 45. A plot for 1/Cad versus 1/Caq in order to determine Langmuir parameters.

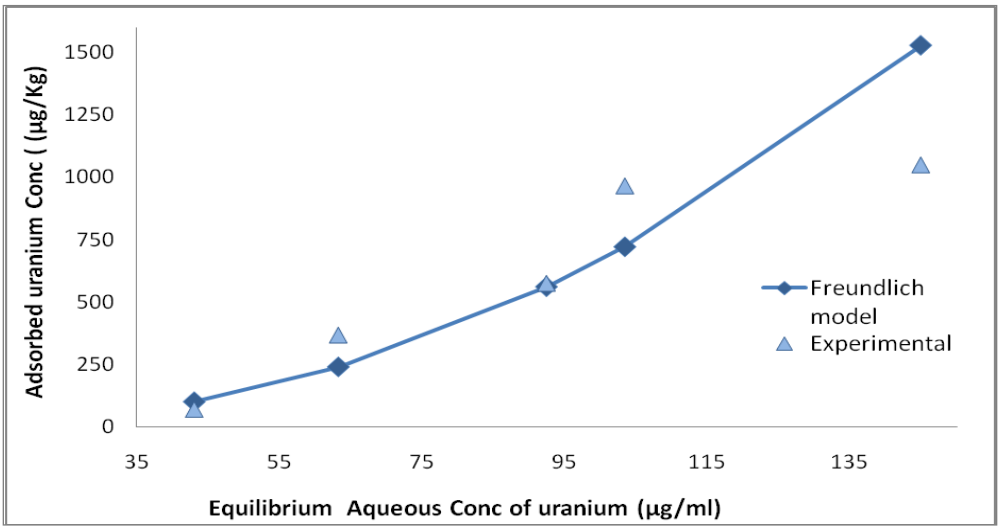

Figure 46. Comparison of two different isotherms, experimental and Freundlich.

Calcite dissolution

With respect to calcite dissolution, there was an increase in aqueous calcium concentrations at lower pH levels. For pH 5.5, the aqueous calcium ion concentrations due to calcite dissolution increased to over 206 and 338 mg/L for 24-hour and 48-hour experiments, respectively (Figure 47). The dissolution of calcite was reduced significantly at pH 7.5 and 9.0. For pH 7.5, the calcium concentrations in water was found to be just over 47 and 55 mg/L for 24- and 48-hour durations, respectively. Similarly, at pH 9.0, the calcium concentrations were reduced to just 4.8 and 4.9 mg/L for 24- and 48-hour experiments, respectively. The reduction in calcite dissolution was 77.11% (24 h) and 83.74% (48 h) for pH 7.5 and 97.69% (24 h) and 98.56% (48 h) for pH 9.0, both compared to the dissolution concentrations recorded at pH 5.5. Alkattan et al. (1998), in their studies with calcite dissolution over the pH range of -1 to 3, have reported an increase in the

dissolution rates of calcite with decreasing pH and increasing temperature. As the temperature in the present study was maintained at room-temperature for all of the experiments, the increase in dissolution at pH 7.5 and pH 5.5 can be solely attributed to the H^+ ion concentrations and not the temperature or other chemical factors (deionized water was used for the studies).

It was also revealed that the dissolution process was a function of time within the given experimental duration. The dissolution at the end of 1 hour reaction time was almost 12 times higher at pH 7.5 and 43 times higher at pH 5.5 compared to the dissolution at pH 9. As shown in Table 19 and Figure 47, there was an increase in calcium ion concentrations with increasing duration for the experiments, with few exceptions. The data in the table reveals that there was no increase in the concentrations of Ca^{+2} from 0.50 h to 0.75 h at pH 5.5, and 0.50 h to 1.00 h at pH 7.5. This kind of behavior, which is in fact a deviation from the expected outcomes and the rest of the results including that of pH 9.0, is mainly due to the experimental procedure that utilized separate vials for different experimental durations in order to generate independent data sets rather than sampling from the same solutions for each duration. Similar to the experiments conducted for 24 h and 48 h, calcite showed significant dissolution at a pH close to neutral and also in the acidic range.

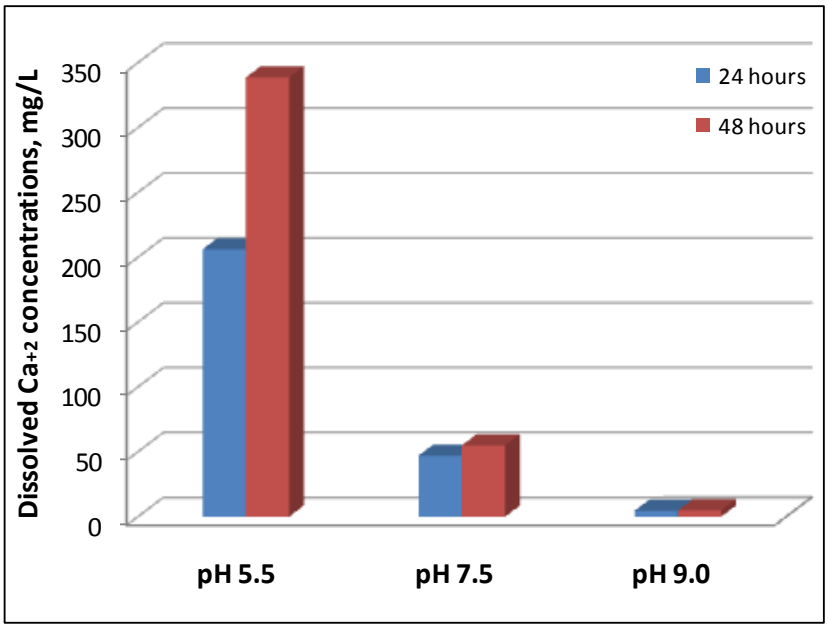

Figure 47. Calcite dissolution at three different pH conditions for 24 and 48 hour durations.

Table 19. Time Series Data Depicting the Change in Aqueous Phase Calcium Concentrations

Experimental durations (h)	Aqueous concentrations of Ca^{+2} mg/L		
	pH 5.5	pH 7.5	pH 9
0.05	34.69	10.32	0.90
0.50	74.46	25.28	1.20
0.75	74.44	18.11	1.69
1.00	86.00	24.51	2.17

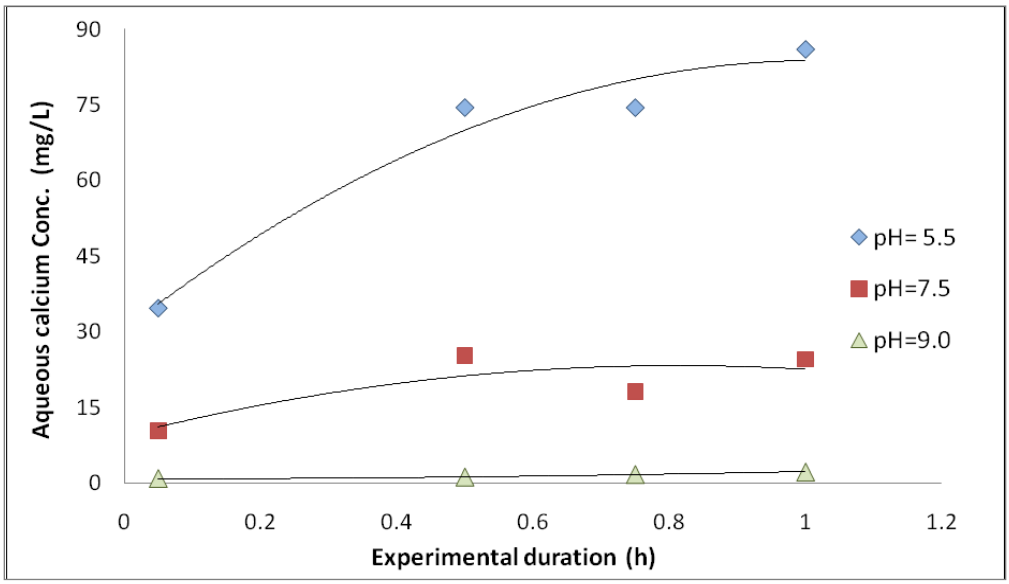

Figure 48. Calcite dissolution at three different pH conditions observed for different experimental durations within an hour period.

Influence of calcite on uranium sorption

Two separate sets of adsorption studies were conducted to understand the role of calcite on uranium sorption. One set of experiments utilized calcite crystals in addition to the sediment and water injected with the known amount of uranium; the other set of experiments was similar except for the absence of calcite. The results indicated reduced adsorption of uranium for the experiments supplemented with calcite compared to the ones without calcite for the pH levels studied (pH 9.0 and 7.5). As shown in Figure 49 and Figure 50, uranium sorption was over 55% (calculated from the initial concentrations of uranium) in the absence of calcite compared to 38% observed in the case of calcite-containing media for the initial uranium concentrations of 50 µg/L at pH 7.5. For the same initial concentrations of uranium, adsorption increased to over 70% at pH 9.0 without the calcite supplement. However, there was no increase in the adsorption of uranium when calcite was present. Similar was the outcome for the experiments that utilized a higher initial concentration of uranium (250µg/L). This kind of behavior was also observed in the initial studies carried out at pH 5.5 (not reported). The reduction in adsorption of uranium when calcite was present in the solution (prior to the injection of uranium) may indicate that more uranium remained in the aqueous phase due to its interaction with dissolved calcite, probably forming complexes with carbonate and calcium, thus making uranium less available for adsorption. Similar findings were reported by Dong et al. (2004) based on their adsorption studies related to uranium and the Hanford sediment, revealing that the carbonate-free silt/clay fraction had a higher sorption affinity for U(VI) compared to those containing calcite-saturated media. Based on their findings, the authors have suggested that calcite or other removed phases may cover or block access to higher affinity sorption sites for U(VI). Supporting evidence has been provided in earlier studies by Reeder et al. (2001) who reported complexation of uranyl species with carbonate at pH 8.1 to 8.2, forming predominantly the triscarbonato complex, $UO_2(CO_3)_3^{4-}$, which was reported as water soluble. Similar complexes were also reported by Leu et al. (2004) for the Hanford vadose zone sediment where they found calcite maintaining

equilibrium with the sediment pore water and facilitating the complexation of uranium (VI) with calcium and carbonate, thus forming a majority of $Ca_2UO_2(CO_3)_3^0$(aq) species in the vadose zone pore water.

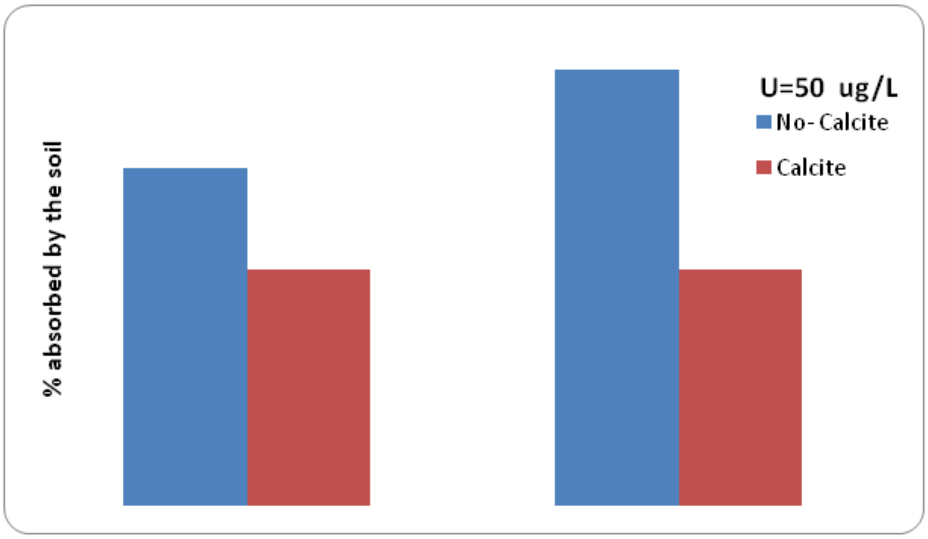

Figure 49. Percentage adsorption of uranium in the sediments compared between calcite free and calcite supplemented media at pH 7.5 and 9.0 for the initial uranium concentration of 50 µg/L.

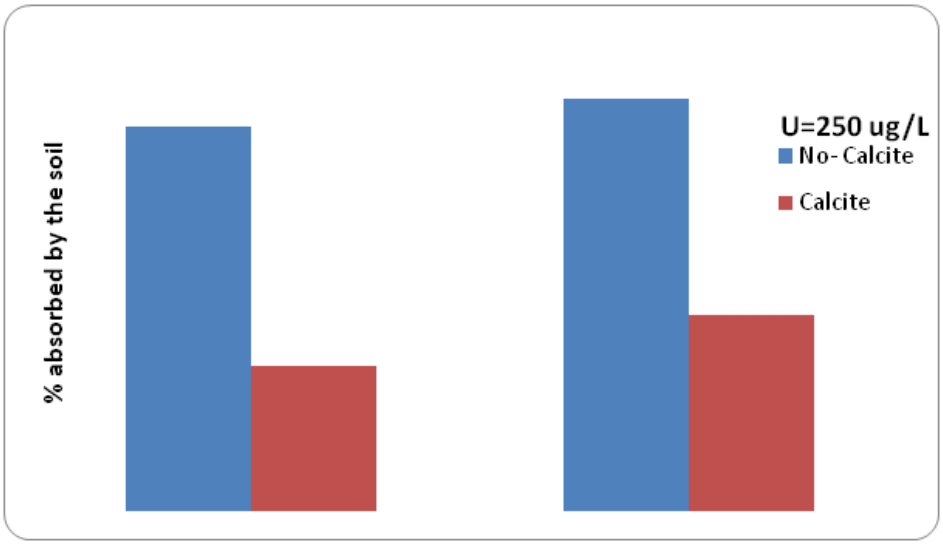

Figure 50. Percentage adsorption of uranium in the sediments compared between calcite free and calcite supplemented media at pH 7.5 and 9.0 for the initial uranium concentration of 250 µg/L.

TASK 2 CONCLUSIONS

The two studies, the adsorption of uranium in the Hanford sediment and the dissolution of calcite that influences the adsorption process, were the main focus. The adsorption coefficient for uranium in the Hanford sediment (with very low organic content) was in the order of 24 x 10^{-3} mL/g at pH 9.0, which is not high. The study also showed reduced sorption when supplemented

with calcite crystals at all pH levels tested in this study (5.5, 7.5, and 9.0). Based on these observations, it may be concluded that the uranium migration can be rapid in the sediment rich in soluble calcite. Also, the low adsorption coefficient for uranium in the sediments may imply that the soil has a lesser degree of ability to retain uranium. In this context, calcite-based technology for uranium stabilization needs a cautious approach so as to prevent uranium transport and maximize its stability in the vadose zone sediment. Further study with respect to pH manipulation leading to co-precipitation of uranium with calcite is recommended.

TASK 2 REFERENCES

Alkattan, M., Oelkers, E., Dandurand, J., Schott, J. (1998). An experimental study of calcite and limestone dissolution rates as a function of pH from -1 to 3 and temperature from 25 to 80^{o}C 151:199-214.

Burns, P.C. and Flinch, R.J. (1999). Wyartite, crystallographic evidence for the first pentavalent uranium mineral. Am Mineral 84

Cejka, J., Mrazek, Z., Urbane, Z. (1984). New data on sharpite, a calcium uranyl carbonate. N Jb Miner Mh, H3: 109-117

Dong, W., Ball, W.P., Stone, A.T., Bai, J., Liu, C., and Wang, Z. (2004). Influence of calcite solids and dissolved calcium on U(VI) sorption and desorption in Hanford subsurface sediments. Symposia papers presented before the Division of Environmental Chemistry, American Chemical Society, Anaheim, CA March 28 – April 1, 2004.

Eisenbud, M. and Gesell, T.F. (1997). Environmental radioactivity from natural, industrial and military sources, fourth ed., Academic Press, San Diego.

Gaines R.V., Skinner H.C.W., Foord E.E., Mason B., Rosenzweigh A., King V.T., Dowty E., (1997). Dana's New Mineralogy. 8th Edition. Wiley and Sons, New York, 1819 p.

Joseph, C., Schmeide, K.,Sachs, S., Brendler, V., Geipel, G., Bernhard, G. (2011). Sorption of uranium(VI) onto Opalinus Clay in the absence and presence of humic acid in Opalinus Clay pore water, Chemical Geology 284:240–250

Kelly, S.D., Newville, M.G., Cheng, L., Kemner, K.M., Sutton, S.R., Fenter, P., Sturchio, N.C., Spotl, C. (2003). Uranyl Incorporation in Natural Calcite, Environ. Sci. Technol. 2003, 37, 1284-1287

Kitano Y. and Oomori T. (1971) The coprecipitation of uranium with calcium carbonate. J. Oceanogr. Soc. Jpn. 27, 34–42.

Liu, C., Zachara, J.M., Qafoku, O, McKinley, J.P., Heald, S.M., Wang, Z. (2004). Dissolution of uranyl microprecipitates from subsurface sediments at Hanford site, USA. Geochim. Cosmochim. Acta 68: 4519-4537.

Mason C. F. V., Turney W. R. J. R., Thomson B. M., Lu N., Longmire P. A., and Chisholm-Brause C. J. (1997). Carbonate leaching of uranium from contaminated soils. Env. Sci. Tech. 31, 2707–2711.

Pacific Northwest National Laboratory (2007). Interim Report: Uranium stabilization through polyphosphate injection, Doc no. PNNL-16683, prepared for the U.S. Department of Energy

under Contract DE-AC05-76RL01830, Pacific Northwest National Laboratory, Richland, Washington.

Pacific Northwest National Laboratory (2008). 300 Area treatability test: Laboratory development of polyphosphate remediation technology for in situ treatment of uranium contamination in the vadose zone and capillary fringe, PNNL-17818.

Reeder, R.J., Nugent, M., Tait, C.D., Morris, D.E., Heald, S.M., Beck, K.M., Hess, W.P., Lanzirotti, A. (2001). Coprecipitation of Uranium(VI) with Calcite: XAFS, micro-XAS,and luminescence characterization. Geochimica et Cosmochimica Acta 65(20): 3491–3503.

Reeder R. J., Nugent M., Lamble G. M., Tait C. D., and Morris D. E. (2000). Uranyl incorporation into calcite and aragonite: XAFS and luminescence studies. Env. Sci. Tech. 34, 638–644.

Russell, A. D.; Emerson, S.; Nelson, B. K.; Erez, J.; Lea, D. W. (1994). Uranium in foraminiferal calcite as a recorder of seawater uranium concentrations. Geochim. Cosmochim. Acta, 58: 671-681.

Russell, A. D.; Emerson, S.; Mix, A. C.; Peterson, L. C. (1996). The use of foraminiferal uranium/calcium ratios as an indicator of changes in seawater uranium content. Paleoceanography, 11: 649-663

Serne, R.J., Bjornstad, B.N., Horton, D.G., Lanigan, D.C., Lindenmeier, C.W., Lindberg, M.J., Clayton, R.E. , LeGore, V.L., Orr, R.D., Kutnyakov, I.V., Baum, S.R., Geiszler, K.N., Valenta, M.M., Vickerman, T.S. (2004). Characterization of vadose zone sediments below the TX tank farm: Boreholes C3830, C3831, C3832, and RCRA borehole 299-W10-27. PNNL-14594. Pacific Northwest National Laboratory, Richland, WA.

Smith D.K. Jr (1984). Uranium mineralogy. In Uranium Geochemistry, Mineralogy, Geology, Exploration and Resources. DeVivo B, Ippolito F, Capaldi G, Simpson P.R. (Eds), Institute of Mining and Metallurgy, London, p 43-88

Sturchio, N.C. (1998). Tetravalent Uranium in Calcite. Science 281: 971-973

United States Environmental Protection Agency (2001). Use of uranium drinking water standards under 40 CFR 141 and 40 CFR 192 as remediation goals for groundwater at CERCLA sites, US-EPA directive no. 9283.

Um, W., Serne, R.J., Brown, C.F., Last, G.V. (2007). U(VI) adsorption on aquifer sediments at the Hanford Site. Journal of Contaminant Hydrology 93:255–269.

Vochten R. and Deliens M. (1998). Blatonite, $UO_2CO_3.H_2O$, a new uranyl carbonate monohydrate from San Juan County Utah. Can Mineral 36:1077-1081

Vochten R., van Haverbeke L., van Springel K., Blaton N., Peeters O.M. (1994). The structure and physicochemical characteristics of a synthetic phase compositionally intermediate between liebigite and andersonite. Can Mineral 32: 553-561

Wellman, D.M. et al. (2008). 300 Area treatability test: Laboratory development of polyphosphate remediation technology for in situ treatment of uranium contamination in the vadose zone and capillary fringe. Document number: PNNL-178181.

Zachara J.M., Freshley M.D., Mann, F.M. (2008). Science Road Map for Phase 2 of the Tank-Farm Vadose Zone Program, PNNL-17684 RPP-PLAN-38191, Rev. 0.

Zachara, J.M., Serne, J., Freshley, M., Mann, F., Anderson, F., Wood, M., Jones, T., Myers, D. (2007). Geochemical Processes Controlling Migration of Tank Wastes in Hanford's Vadose Zone. Vadose Zone J. 6:985–1003.

ACKNOWLEDGMENTS

Funding for this research was provided by US DOE Grant Number: DE-EM0000598. We would like to thank Dr. David Balkwill for providing us with *Arthrobacter* sp. strains and acknowledge Dr. Yanqing Liu from the FIU Mechanical Engineering Department for his assistance with the SEM/EDS of bacterial surface and composition analysis.

APPENDIX

Topical Report - Environmental Characterization of the Hanford Site Central Plateau (200 Area) Vadose Zone

For task entitled,

"Sequestering Uranium at the Hanford 200 Area by In-Situ Subsurface pH Manipulation Using Ammonia (NH_3) Gas Injection"

Submitted to:

U.S. Department of Energy
Office of Groundwater and Soil Remediation, EM-32

David Roelant, Ph.D.
Principal Investigator

Leonel Lagos, Ph.D.
Project Manager

Yelena Katsenovich, Ph.D.
Maite Barroso, DOE Fellow
Yulyan Arias, DOE Fellow

Applied Research Center,
Florida International University
10555 West Flagler St., EC 2100, Miami, FL 33174
http://www.arc.fiu.edu

Introduction

The Applied Research Center (ARC) at Florida International University (FIU) is assisting the U.S. Department of Energy's (DOE) Hanford Site in developing solutions to uranium contamination in the deep vadose zone, including the incorporation of emerging technologies for the efficient management of the uranium-contaminated subsurface. The investigation entitled "Sequestering Uranium at the Hanford 200 Area by In-Situ Subsurface pH Manipulation Using Ammonia (NH_3) Gas Injection" targets uranium (U) contamination in the vadose zone (VZ) of the central plateau (200 Area) that may affect groundwater migrating to the Columbia River. The Hanford Site 200 Area is subdivided into two regions, the 200 West Area and the 200 East Area (Figure 51). These two areas contain four designated plumes: (1) 200-ZP-1, (2) 200-UP-1, (3) 200-BP-5 and (4) 200-PO-1, consisting mainly of uranium, technetium, and chromium. This study focuses on the plumes contaminated with uranium, which include 200-UP-1 and 200-BP-5.

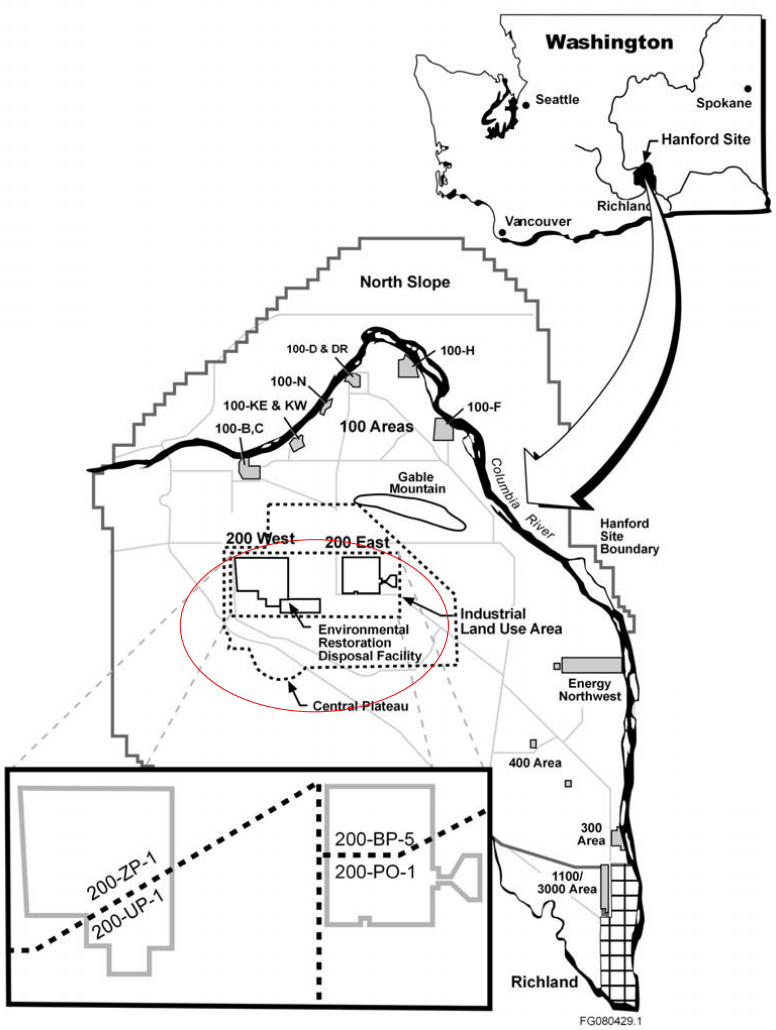

Figure 51 Hanford Site 200 Area (West and East).

This report is a preliminary review, which summarizes relevant information taken from existing reports and published literature to characterize the environmental conditions of the study area of interest (Hanford Site 200 West and 200 East Areas). The information gathered on 200 Area

porewater constituents will help to experimentally simulate the formation of uranium precipitates after the NH_3 gaseous mixture (95% air and 5% NH_3) injection, and study its effect on the mobility of uranyl cations in uranium-contaminated soil.

Background/Site History

The Hanford Site is a nuclear testing facility located on the Columbia River in the state of Washington, built in 1943 as part of the Manhattan Project for the production of plutonium for the first atomic weapons. The 200 Area, located at the Central Plateau, is the highest area in terms of its elevation. The 200 Area features "canyons" where the plutonium was chemically separated, burial grounds or "tank farms", hundreds of solid waste sites where some of the most hazardous waste was stored, an Environmental Restoration Disposal Facility, a Waste Treatment Plant, office buildings and other facilities related to the infrastructure of the site. Some of these facilities remain in use while others have long since been abandoned and are scheduled to be demolished in the future.

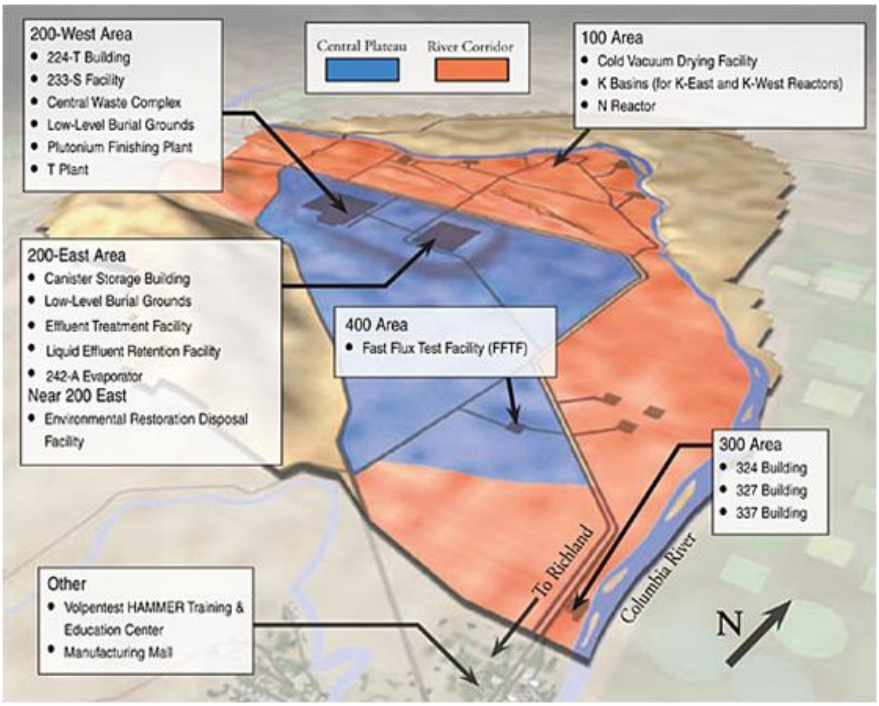

Figure 52 Hanford Site facilities (http://bnltech.com/performance-bnl-tech.html).

The main function of the facilities in the 200 Area of the Hanford Site was to remove the plutonium from the uranium fuel rods after they had been subjected to the nuclear chain reaction in the 100 Area reactors. The technology used at that time generated large amounts of radioactive waste containing uranium and other constituents. Different techniques were used to reduce this waste and to "safely" store it. One method included storage of some of the most hazardous chemical and nuclear wastes in 177 underground storage tanks spread out among eighteen tank farms, ranging in capacity from 50,000 gallons to more than 1,000,000 gallons.

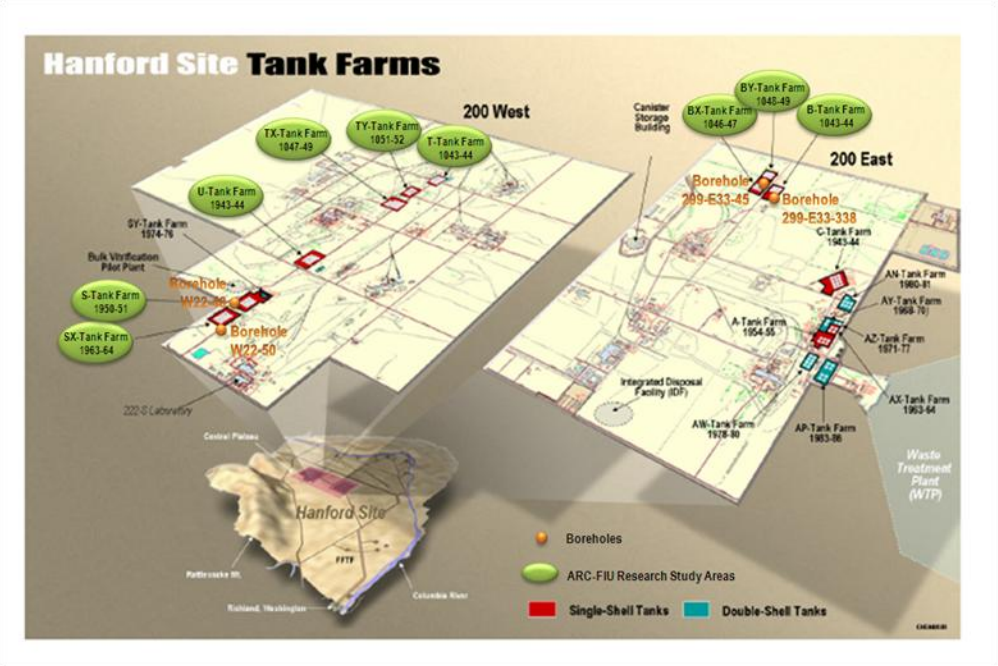

Figure 53 Hanford Site tank farms highlighting ARC-FIU research study areas.

As early as 1956, waste leakage from the tanks and underground pipes was suspected, which was confirmed in 1961. The radioactive leaks, consisting of aqueous solutions [acidic and basic with organic complexants (citrate and ethylenediaminetetraacetic acid)] and inorganic ligands (CO_3, PO_4), have been detected in 67 of the 149 single shell tanks. This is not surprising since these tanks have exceeded their design lifetime by more than 30 years. The liquid waste leakages, including 202,703 kg of uranium (Simpson et al. 2006), have soaked into the ground at the site and have created multiple plumes of contamination, which are being monitored and treated to remove contaminants. Currently at Hanford, some 53,000,000 gallons of chemical and nuclear waste remain stored in these tanks. Beginning in the 1990s, the site's main activities have revolved around restoring the site to comply with state and federally regulated contaminant levels.

Climatic Conditions

Due to its location within the semiarid shrub-steppe Pasco Basin of the Columbia Plateau in South Central Washington State, the region's climate is greatly influenced by the Pacific Ocean, the Cascade Mountain Range to the west, and other mountain ranges located to the north and east. The Pacific Ocean moderates temperatures throughout the Pacific Northwest, and the Cascade Range generates a rain shadow that limits rain and snowfall in the eastern half of Washington State. The Cascade Range also serves as a source of cold air drainage, which has a considerable effect on the wind regime at the Hanford Site. Mountain ranges to the north and east of the region shield the area from the severe winter storms and frigid air masses that move southward across Canada.

The Hanford Site is characterized as having a mild climate with 15 to 17 centimeters (6 to7 inches) of annual precipitation, and occasional high winds of up to 129 kilometers (80 miles) per hour occur throughout the year. Winds periodically exceed 48 km/h (30 mph) when Chinook wind conditions exist. There are 300 days of sunshine every year. Ranges of daily maximum

temperatures vary from 2°C (36°F) in early January to 35°C (95°F) in late July. On average, there are 52 days during the summer months with maximum temperatures exceeding 32°C (90°F) and 12 days with the maximum temperatures being greater than or equal to 38°C (100°F). The average annual temperature recorded at the Hanford Meteorology Station (HMS) located on the Hanford Site near Richland is 53.3°F. The warmest month is July, which averages 76.4°F, while the coolest month is January, which averages 30.5°F. The hottest temperature ever recorded at Hanford was 115°F in July 2006; the coldest was -23°F on February 1 and 3, 1950. The region receives occasional snow most years. Tornadoes are extremely rare; no destructive tornadoes have occurred in the region surrounding the Hanford Site.

The Hanford Site area presents unique climatic characteristics with precipitation from November to March (defined here as winter precipitation) ranging from less than 60 mm (2.4 in.) to more than 200 mm (8 in.), averaging slightly more than 100 mm (4 in.) per year. Average annual precipitation at the HMS is 17 cm (6.8 in.). Most of the precipitation occurs during the winter, with nearly half of the annual amount occurring in the months of November through February (Hoitink et al. 2005). During 1995, the wettest year on record, 31.3 cm (12.3 in.) of precipitation was measured; during 1976, the driest year, only 7.6 cm (3 in.) was measured. The wettest season on record was the winter of 1996-1997 with 14.1 cm (5.4 in.) of precipitation; the driest season was the summer of 1973 when only 0.1 cm (0.03 in.) of precipitation was measured. Days with greater than 1.3 cm (0.50 in.) precipitations occur on average less than once per year, which is less than 1% of the year. Rainfall intensities of 0.5 in/h persisting for 1 h are expected once every 10 years. Rainfall intensities of 1 in/h for 1 h are expected only once every 500 years.

Average snowfall ranges from 0.25 cm (0.1 in.) during October to a maximum of 13.2 cm (5.2 in.) during December and decreases to 1.3 cm (0.5 in.) during March. The record monthly snowfall of 59.4 cm (23.4 in.) occurred during January 1950. The seasonal record snowfall of 142.5 cm (56.1 in.) occurred during the winter of 1992-1993. Snowfall accounts for about 38% of all precipitation from December through February (Bunn et al. 2002).

Table 20 Climate Conditions at the Hanford Site

	Average	Maxima	Month/ Year	Minimum	Month/ Year
Temperature (°F)	53.3	76.4	July	30.5	January
Precipitation (in)	6.3	12.3	1995	3	1976

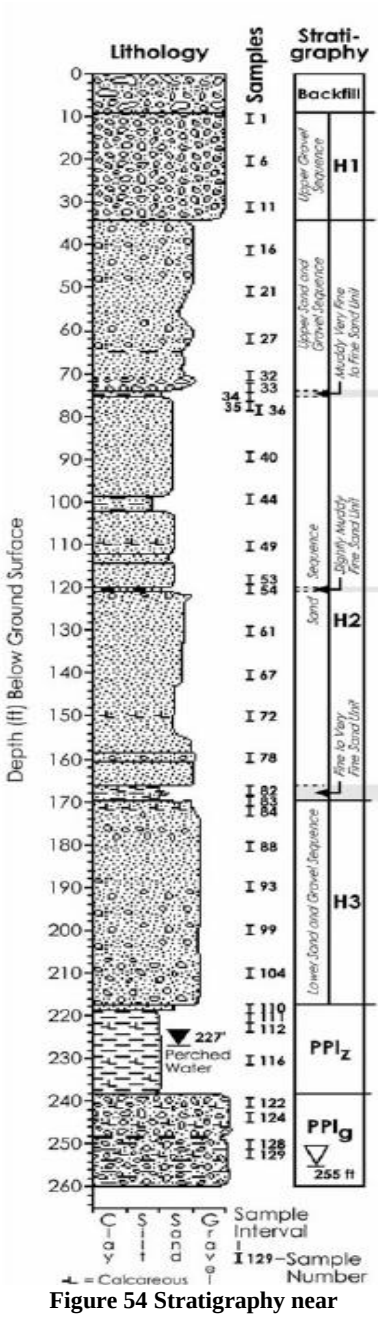

Figure 54 Stratigraphy near Tank 241 –BX- 102 in 200 East Area (Serne et al., 2002).

Geology

Stratigraphy

Three main stratigraphic units make up the vadose zone in the 200 Area of the Hanford Site: (1) Ice Age flood deposits of the Pleistocene-Age Hanford formation, (2) alluvial, eolian, and pedogenic deposits of the Pliocene/Pleistocene-Age Cold Creek unit, and (3) the fluvial, overbank, and lacustrine deposits of the Miocene/Pliocene-Age Ringold Formation (Last et al., 2006). The Hanford formation is the uppermost stratigraphic unit and makes up most of the 200 Area vadose zone. It is composed of sediments deposited during several episodes of cataclysmic flooding and consists of poorly sorted sand-containing lithic fragments from pebble to boulder size, fine- to coarse-grained sand, and silt (DOE 1988, 2002). The Hanford formation is subdivided into three subunits: H1, H2, and H3, based on composition (Figure 54). The Cold Creek Unit (CCU) follows beneath the Hanford formation and is present only in the 200 West Area (Figure 55). The CCU represents deposits that accumulated within the central Pasco Basin about 2 to 3 million years ago, which brackets two significant geologic events. The older event is a regional base-level drop and subsequent incision of the Ringold Formation (DOE 1988). The younger event is the initiation of Ice Age cataclysmic flooding, which began at the beginning of the Pleistocene, about 1.5 to 2.5 million years ago (Bjornstad et al. 2001). The older event makes up the lower subunit of the CCU and represents a calcium carbonate cemented layer (caliche-rich zone). The newer event makes up the upper subunit and is a well sorted and relatively un-weathered, brown-colored silt-rich deposit. The upper and lower portions of the Cold Creek unit strongly impede the vertical movement of pore fluids in the vadose zone. Beneath the CCU lies the Ringgold formation. Ringold Formation Unit E is fluvial-deposited pebble-to-cobble gravel with a sandy matrix.

It is characterized by complex interstratified beds and lenses of sand and gravel with low to moderate degrees of cementation (Last et al. 2006).

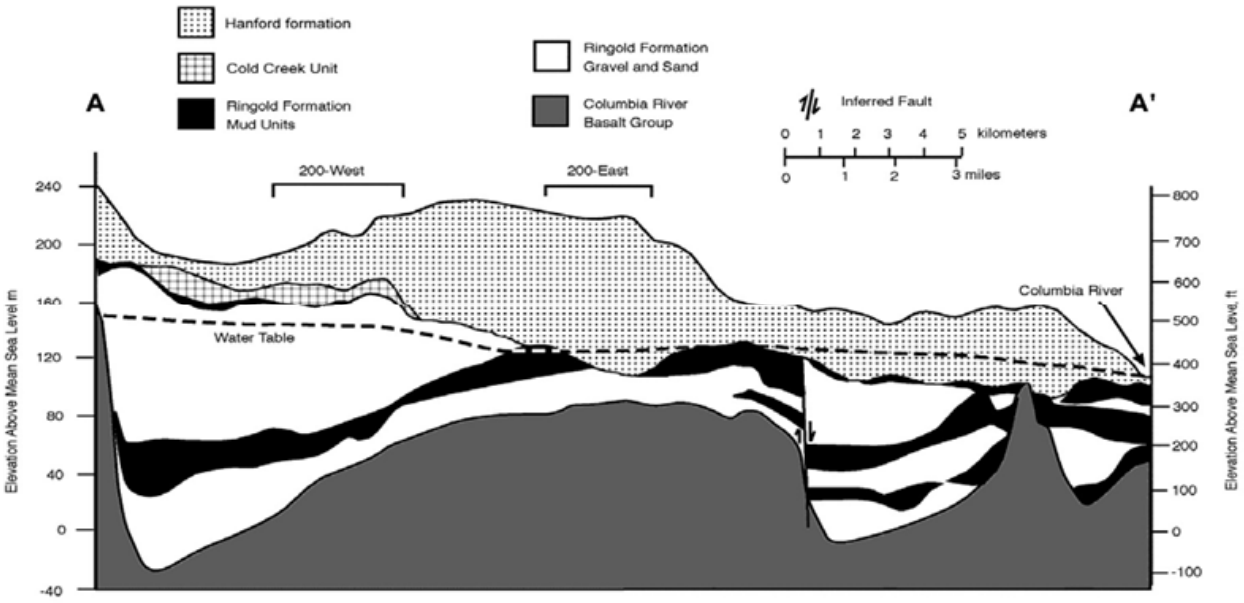

Figure 55 Generalized West-to-East Geologic Cross Section through the Hanford Site (Last et al. 2006)

Mineralogy

Generally, mineralogy data collected for both the 200 East and 200 West areas shows dominance by quartz (SiO_2) (~45% to 95%), plagioclase feldspar (~10% to 20%), and alkali feldspar (~20% to 40%) (Serne, 2008), followed by minor amounts of mica, chlorite, and amphibole (Xie, et al. 2003).

The mineralogy of the Hanford formation sediment in the 200 Area is highly variable. Gravel-dominated sediment tends to have a high abundance of lithic fragments (mostly basaltic, with some plutonic, metamorphic, and detrital caliche fragments) (30% to 50% of the total) (DOE 2002), approximately equal amounts of quartz and plagioclase feldspar (15% to 30%), and then biotite (2% to 6%) and pyroxene (0.5% to 2.5%) (Bjornstad 1990). Finer grained facies have proportionally less lithic fragments and more quartz, feldspar, and mica grains. Microprobe analysis of this fraction indicates dominance by quartz (18 to 67.1% by weight), plagioclase feldspar (5.1 to 41.5%) and microcline (1.8 to 30.1%) (Tallman, et al. 1979, Xie et al. 2003), with minor amounts of potassium feldspar (<10%). Other common minerals in this class include amphiboles up to 36.6%, pyroxenes up to 27.5%, mica (biotite/illite) up to 13.1%, and calcite up to 6.5% by weight. The clay fraction is dominated by smectite clays (10 to 30 wt%), which represent a percent of the bulk sand fraction [3.3 to 5% (Serne et al. 1993)], followed by illite (~ 40 wt% to15 wt%), chlorite (~15 to 20 wt%), and kaolinite (<10 wt%), with minor amounts of quartz and feldspair (up to ~5 to 10 wt%), and amphibole (Serne, 2008). Overall, approximately 45 wt% of the clay fraction consists of silicon, followed by lesser amounts of aluminum (~15 wt%) and iron (~12 wt%) (Serne 2008).

Analysis by transmission electron microscopy from borehole 299-W22-48 (39, 91.5, and 163.5 feet bgs) and 299-W22-50 (15.8 and 35.3 meters or 50 and 116 feet bgs) yielded the following structural formulas for smectites, illites, chlorite, and kaolinite, respectively:

$$[(Ca_{0.05}Mg_{0.10})]_{+0.30}[(Al_{0.54}Mg_{0.56}Fe_{1.07}Ti_{0.01})_{-0.01}(Si_{3.72}Al_{0.28})_{-0.28}]_{-0.29}O_{10}(OH)_4$$

$$[K_{0.74}Ca_{0.02}Na_{0.02}]_{+0.80}[(Al_{1.62}Mg_{0.29}Fe_{0.16}Ti_{0.02})_{+0.0}(Si_{3.19}Al_{0.81})_{-0.81}]_{-0.81}O_{10}(OH)_2$$

$$[(Ca_{0.03}]_{+0.06}[(Al_{1.54}Mg_{2.44}Fe_{1.51}Ti_{0.02})_{+0.60}(Si_{3.31}Al_{0.69})_{-0.69}]O_{10}(OH)_8$$

$$(Al_{3.99}Fe_{0.02})(Si_{3.96}Al_{0.04})O_{10}(OH)_8$$

Hanford formation sediment is typified as having low organic carbon content, generally <0.1% by weight, and low-to-moderate cation exchange capacity (2.6 to 7.8 milliequivalents per 100 g) (Serne et al. 1993). Small amounts of detrital calcium carbonate (less than ~3.25 wt. %) are common and can act as a weak buffer (Serne 2008). The sediment has a slightly basic pH when wet, ranging from 7.66 to 8.17 (Serne et al. 1993).

Much less mineralogy data is available for the Cold Creek unit. Tallman et al. (1979) reported that the sediments they referred to as early 'Palouse' soil are fairly similar in mineralogy to those of the Hanford formation (25.3 to 29.4% quartz, 15.1 to 18.2% plagioclase, 15 to 17.8% microcline, 7.9 to 10% amphiboles and 1.3 to 12.5% micas), but generally contain more calcite ($CaCO_3$)(8 to 8.8%), and lack pyroxenes. Bjornstad (1990) reported similar results for these fine-grained sediments, but observed that drill cuttings of the carbonate-rich facies in the 200 West Area (thin beds of caliche, previously referred to as the Plio-Pleistocene unit) consisted predominantly of calcium carbonate and/or sedimentary rock fragments, with lesser amounts of quartz and feldspars. Organic carbon in the Cold Creek unit is higher than in the Hanford formation (up to ~0.17). The inorganic content is significantly higher in the Cold Creek unit too, due to the cemented nature of this unit (up to ~38.7 wt% as CaCO3) (Serne, 2008).

The Ringold formation has similar mineralogy to the Hanford formation because of common geologic provenance. Some of the differences that have been reported are a higher quartz and lower plagioclase and pyroxene content. Unlike the Hanford formation, the Ringold formation also differs in that it contains calcic/ferric oxide cements (Bjornstad, 1990). The organic and inorganic carbon content is similar to the Hanford formation (Serne 2008).

The 200 East and 200 West areas have similar mineralogy as measured by electron microprobes (Xie et al. 2003). For the Ringold formation, however, there are significant differences between the two areas. Specifically, quartz is higher and plagioclase is lower in the 200 East Area. In addition, pyroxene, albite, epidote, and apatite do not seem to be present in the 200 East Area.

Bulk Chemical Composition

As commonly found in most environments, silicate content is much higher than the other chemicals in the 200 Area, followed closely by aluminate (Table 21). In the 200 Area, this is due to the high amount of quartz and feldspars forming rocks in the vadose zone. Other chemicals found with high abundance are calcium and iron, two elements present in the minerals plagioclase and pyroxene composing the basalt in Hanford formation. Bulk sediment samples were characterized for major and trace elements using a lithium metaborate/tetraborate fusion

procedure, and then analyzed by inductively coupled plasma-optical emission spectroscopy (ICP-OES) and ICP-MS methods. Overall, results showed very little difference in the primary elemental oxide concentrations for any of the sediment samples as a function of depth or lithology. The primary elemental oxides in decreasing concentration include: SiO_2 (58.77 to 70.33 wt%), Al_2O_3 (12.7 to 15.73 wt%), Fe_2O_3 (3.74 to 7.92 wt%), CaO (3.02 to 4.80 wt%), Na_2O (2.05 to 3.23 wt%), K_2O (1.70 to 2.65 wt%), MgO (1.64 to 2.73 wt%), TiO_2 (0.51 to 1.39 wt%), P_2O_5 (0.13 to 0.30 wt%), and MnO (0.07 to 0.12 wt%) (Lindenmeier 2003).

Calcium carbonate is also found abundantly. Content ranges between 1 and 5 wt% for the Hanford formation (Last et al. 1989) and is as high as 40 wt% in the Cold Creek unit due to pedogenic alteration and secondary cementation with calcium carbonate (caliche). Content has similar values to the Hanford formation in the Ringold formation (Serne 2008).

Table 21 Bulk Chemical Composition of Sediment Samples from Borehole 299-W22-48 (wt% as oxides) (Serne 2008b)

Depth (ft bgs)	**39.5**	**47**	**91.5**	**101.5**	**136**	**146**	**148.5**	**163.5**
Na_2O	2.25	2.68	2.26	2.25	1.62	0.63	1.06	2.01
MgO	3.32	4.23	3	3.35	4.14	7.24	4.16	2.97
CO_2	0.84	0.6	0.88	1.56	1.4	18.39	18.24	0.36
Al_2O_3	14.19	14.55	13.13	13.36	13.21	6.24	8.03	13.11
SiO_2	70.17	62.15	72.2	72.31	67.39	36.43	43.47	73.91
P_2O_5	<0.21	<0.25	<0.20	<0.21	<0.20	<0.32	<0.32	<0.19
SO_3	0.08	0.12	0.06	0.09	0.06	0.39	0.32	0.06
Cl	0.04	<0.02	0.04	0.03	<0.02	<0.02	<0.02	0.04
K_2O	2.52	1.49	2.61	2.52	2.31	0.97	1.52	2.9
CaO	3.16	7.72	3.16	3.24	3.37	24.08	20.9	2.08
TiO_2	0.61	1.53	1.53	0.59	0.64	0.55	0.39	0.54
V_2O_5	0.01	0.05	0.05	0.01	0.01	0.02	0.01	0.01
Cr_2O_3	0	0.01	0.01	0.01	0.01	0	0.01	0
MnO	0.07	0.14	0.06	0.06	0.06	0.25	0.05	0.05
Fe_2O_3	4	9.64	3.46	3.89	4.13	3.41	3.06	3.36
SrO	0.04	0.04	0.04	0.04	0.03	0.04	0.04	0.03
BaO	0.09	0.07	0.09	0.09	0.07	0.04	0.05	0.08
Total	101.61	105.28	101.75	98.67	99.01	99.01	101.65	101.7

Moisture

Data collected from the three formations from the 200 Area indicates that moisture content in the 200 Area is similar to the overall Hanford site moisture (2.5 to 26 wt%). Data collected from the Hanford formation was generally less than 10 wt% with some zones having up to 15 to 20 wt% moisture (Serne et al. 2002a). For the Cold Creek unit, moisture averaged between 5 wt% and 15 wt%, with the lower caliche-cemented subunit accounting for most of the low moisture (Brown 2007). The data collected indicates that the upper Cold Creek subunit had the greatest moisture retention capacity, and this may be causing this subunit to have a high affinity for vadose zone groundwater contamination (Brown 2007). Moisture in the Ringold formation is similar but can sometimes be as high as 20 wt% (Brown 2007). Areas of elevated moisture include the H2 subunit, probably associated with thin lenses of fine sand and/or silt that often occur at the tops of graded sand beds within the Hanford formation, the upper Cold Creek subunit, and clastics dykes in the Cold Creek and Ringold units. All data collected was consistent in that finer grained sequences reported higher moisture contents than coarse grained sequences.

Data collected shows that areas where contamination has been identified contain the highest moisture content. For instance, the uncontaminated soils in the 200 West Area near 241-S tank farm and beneath the 241-U Single-Shell Tank Farm generally average less than 10 wt% and 1 wt%, respectively, while two contaminated soils in the 200 West Area, one near the 241-S tank farm and the other near the tank SX-115, had moisture contents between approximately 2 and 25 wt% (Serne 2008) and between 2.11 to 23.33 wt%, respectively (Lindenmeier et al. 2003).

Porewater Characterization

Vadose zone sediment recovered from Borehole 299-E33-45, northeast of tank BX-102, was used to perform two types of experiments in order to characterize the porewater. The fourteen porewater samples that were extracted from the sediment using an ultracentrifuge were compared with equivalent dilution-corrected 1:1 water extracts from the same depths.

Water extracts of vadose zone sediment from Borehole 299-E33-45 were analyzed for porewater concentrations of aluminum, iron, and silicon. Some of the results revealed that the H2 middle sequence sand unit (75 to 121 ft bgs) showed higher concentrations of water-extractable aluminum and iron. The silicon concentrations calculated from the dilution-corrected 1:1 sediment to water extracts did not show any obvious pattern.

The silicon concentrations of actual porewater obtained by ultracentrifugation were lower than the calculated values obtained by the 1:1 dilution method, suggesting that water extraction is probably dissolving silicon-bearing solids. The same is true for the water-soluble iron data. It is likely that the Hanford H2 middle sand sequence contains water leachable compounds of aluminum, silicon, and iron that may be indicative of secondary (probably amorphous) precipitates from reaction of the sediments with tank fluids (Serne et al. 2002).

Table 22 Average Calculated Cation Porewater Content for Borehole 299-E33-338

Average concentrations, (mg/L)	Depth, ft		
	16-107.8	**115.9-198.6**	**200.6-240.3**
Al	1.38±1.2	2.07±1.7	0.52±0.8
B	0.63±0.3	0.78±0.4	0.49±0.4
Ca	157.44±60.2	162.18±57.4	111.75±62.3
Fe	0.63±0.4	2.39±2.1	0.64±1.2
K	55.61±13	84.6±34.9	41.5±1.2
Mg	35.98±18.3	41.93±14.5	24.93±18.7
Na	215.35±171.6	210.07±93.5	149.91±106.7
Si	139.09±32.9	199.08±79.5	118.17±112.9
Sr	0.73±0.3	0.91±0.3	0.610±0.4

Using information from Borehole 299-E33-338, it can be concluded that the highest average concentrations of aluminum (2.07 mg/L), as well as other the elements analyzed such as barium, calcium, iron, potassium, magnesium, and strontium, are found at depths between 115.9 to 198.6 ft. However, the highest average concentration of silicon (510.7 mg/L) was found at a lower depth between 200.6 and 240.3 ft.

Porewater collected from the 200 Area was also analyzed for the presence of nitrate and bicarbonate. The characterization of shallow sediments taken from Borehole 299-E33-45 showed the presence of nitrate contamination starting at the contact between the Hanford H1 and H2 units at 34 ft bgs, and extending down into the sediment of the fine-grained PPLz (Plio-Pleistocene Silty Unit) all the way to the water table at 255 feet bgs. Bicarbonate is one of the major anions calculated (from sediment-to-water extracts). Its concentration in the porewater is also elevated in the H2 middle sand sequence between 75 and 167 ft bgs; the porewater bicarbonate concentration varies between 0.1 and 0.21 M between 110 to 130 ft bgs around the paleosol layer, having a peak concentration of 0.21 M at 120 ft bgs. Figure 56 presents the distribution of bicarbonate throughout the borehole comparing calculated and actual concentrations.

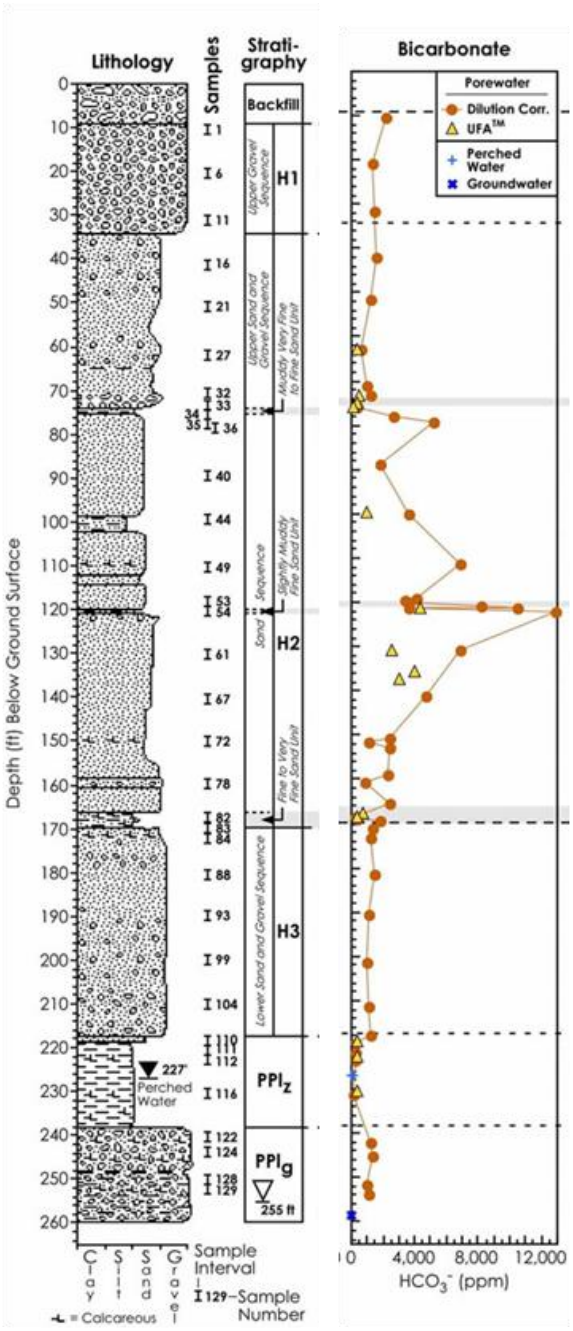

Figure 56 Bicarbonate calculated (from sediment-to-water extracts) and actual porewater from Borehole 299-E33-45 (near tank 241-BX-102). (Serne et al. 2002)

The concentration of sulfate in porewater samples appear to be slightly elevated and found in the range of 9.6 to 897 mg/L (1:1 extracts) over the soil vertical profile, but the highest concentrations were found in a narrow zone within the middle sand sequence of the H2 unit between 140 and 166 ft bgs with a maximum concentration of 897 mg/L (1:1 extracts). The porewater chloride concentrations appear slightly elevated between 70 and 255 ft bgs (i.e., the water table) with concentrations between 0.7 to 196 mg/L, compared to an average concentration of 1.7 mg/L.

The fluoride porewater distribution differs from all the other anions because it shows significant concentrations in the shallow Hanford H2 upper sand sequence. Similar to the nitrate and sulfate, the greatest concentrations of fluoride are found in the H2 middle sand sequence between 120 and 167 ft bgs. The phosphate porewater distribution in the vadose zone sediment at Borehole 299-E33-45 shows elevated concentrations between ~80 and 130 ft (24.4 to 39.6 m bgs) within the H2 middle sand sequence, in the paleosol at 120 ft bgs, and just below the paleosol to 130 ft bgs (Serne et al. 2002) .

Uranium Contamination

The contaminant of interest throughout the report is uranium, which is also a naturally occurring element that is present as a trace constituent in the earth's crust. The fabrication of natural and slightly enriched uranium into fuel elements for nuclear reactors in the Hanford 300 Area, and the reprocessing of irradiated fuel in the Hanford 200 Area to obtain plutonium and other useful radioisotopes, has led to significant uranium contamination in the vadose zone and groundwater at the Hanford Site. As a result of these activities, uranium is considered to be one of the primary risk drivers associated with long-term stewardship of the site (Zachara et al. 2007).

The large inventory of U released to the vadose zone, combined with its mobility under the oxidizing, circumneutral-to-mildly-basic geochemical conditions found at Hanford has led to the creation of three identified groundwater plumes (Hartman et al. 2007). These plumes have a combined area of 1.6 square kilometers with dissolved U concentrations that are above the U.S. Environmental Protection Agency's established maximum-contaminant level (MCL) of 30 ppb (1.2×10^{-7} mol/L).

Table 23 contains the concentration of uranium as measured in uncontaminated or background sediment samples. The data has been gathered either via recent field-sampling and characterization campaigns or is based on historical analyses of site-wide samples (near-surface soils/sediments/rocks and groundwater) from the early 1990s.

Table 23 Background Uranium-Sediment Concentrations

Location	Average Uranium Concentration (mg/kg)	Standard Deviation	Reference
WMA-B/BX/BY	1.47	0.55	Lindenmeier et al. (2003)
WMA-C	0.39	0.06	Brown et al. (2006)
WMA-S-SX	0.9	0.84	Serne et al. (2002a)
WMA-T	2.59	0.95	Serne et al. (2004b)
WMA-TX/TY	2.31	0.57	Serne et al. (2004a)
Hanford Site	2.27	0.64	DOE/RL-96-12 (1996b)

Based on the information contained in Table 23, the background uranium concentration in sediment collected throughout the Hanford Site (except the 300 Area) ranges from a low of 0.39 mg/kg to a high of 2.59 mg/kg. The range of background uranium concentrations in the 200 Area Hanford sediment is 1.47 to 2.59 mg/kg, since the two lowest concentrations reported in Table

23 were generated via strong acid digestion of the sediment, which does not solubilize all the crystalline uranium in the sample. Thus, including only the data from those analyses that quantitatively measure the entire uranium content of the sample is more accurate.

There are many wells in the 200 Area monitoring pore water contamination. Background data collected from Borehole C3393 summarizes the amount of uranium found in the pore water. This borehole is located near the U Tank Farm located in the 200 West Area. In this well, uranium was not found at elevated concentrations which varied in the range of 0.15µg/L to 9µg/L (Brown, et al. 2007).

Table 24 Average Calculated Pore Water Mobile Metal Concentrations of Uranium in C3393 Borehole Samples

Average Depth (ft)	Stratigraphic Unit	Average Uranium 238 Concentration (µg/L)	Standard Deviation
14.17	H1	23.6	18.2
89.31	H2	7.4	1.7
126	H2	15.8	5.8
139	CCU	8.1	1.1

Three different measurement methods of the total uranium content were compared using Borehole 299-E33-45 sediment samples. The three methods were: 1) measuring uranium-238 by the gamma emission from its short-lived thorium-234 daughter and converting activity to mass, 2) directly measuring total uranium mass by x-ray fluorescence (XRF), and 3) performing a strong soil sample nitric acid extraction and measuring the uranium-238 mass by an inductively coupled plasma mass spectrometer (ICP-MS) (Serne et al., 2002). Data from this contaminated borehole suggests that the significantly elevated uranium-238 activity first appears at 73.4 ft bgs in the Hanford H2 unit sediment just above the first thin lens (1 ft thick at 74.5 ft bgs). From about 90 ft to ~111 ft bgs, there is little indication that significantly elevated concentrations of uranium are present. Between 119 and 120 ft bgs, the maximum uranium content reached about 660 mg/L. Below 120 ft bgs down to 145 ft bgs, the uranium content in the sediment is quite high (reaching values between 200 and 500 mg/L). Between 145 and 167.2 ft bgs, in the lower portion of the H2 middle sequence, there are elevated uranium concentrations (between 50 and 200 mg/L). Within the fine grained lens between 167.2 and 169.8 ft bgs, the uranium concentration increases again to values between 200 and 400 mg/L. Below, in the H3 lower sand sequence and the plio-pleistocene sediments, there is no significant indication of elevated uranium, but small concentrations are still present in the sediments.

Microbiology

The population densities of aerobic heterotrophic bacteria in the contaminated vadose sediments are relatively low and are impacted by several factors, including contamination, radiation, moisture, and total organic content (TOC). It was determined that the populations of aerobic heterotrophic bacteria in contaminated sediments (taken near the SX-108 tank) including the most radioactive ones (e.g., >10 µCi of ^{137}Cs/g), range from below detection to greater than 10^4 CFU g^{-1} and both desiccation and ionization affect population sizes at this location. In the study, desiccation decreased the population sizes of aerobic heterotrophic bacteria in two samples

having populations of 2.4 log CFU g^{-1} and 5.5 log CFU g^{-1} by 2.5- and 10-fold, respectively. Ionizing radiation had an even greater effect, eliminating growth from the first sample at both doses and decreasing the population size in the second one by 3 and 4 orders of magnitude for acute exposures of 5 and 10 kGy, respectively (Feredickson et al. 2004).

Experiments performed using sediment from the deep vadose zone at the U-17 borehole by Brockman et al. (1992) suggest another trend in the microbiology at Hanford. There exists a richer and more responsive microbial community in the highly developed TOC-rich zones, which in his study was indicated by the higher number of culturable heterotrophs, greater glucose mineralization potential, higher microbial diversity based on colony morphology, and higher ATP concentration, compared to weakly developed zones within the unsaturated zone of the Hanford Site. Brockman's research also agreed with Fredrickson et al. (2004) in that higher moisture increases life in the vadose zone. Brockman also added that moisture recharge increases the number of gram-negative microorganisms (which dominates in more moist areas, making up 71% of the microbial population), but decreases the number of culturable heterotrophs, while dryer sediments are dominated by gram-positive microorganisms, which are more resistant to desiccation. The highest viable counts were obtained in laboratory experiments carried out at a temperature of 23°F, the same temperature normally found in the ground. In areas where there is contamination, the temperature is generally higher, which may influence smaller populations.

Gram-positive bacteria high in G+C content have been highly represented in contaminated vadose zone sediments from the Hanford Site. *Arthrobacter* sp. seem to be the most common among the gram-positive genera and is also among the most prevalent genera of bacteria isolated from beneath leaking radionuclide storage tanks (Fredrickson et al. 2004). Other gram-positive genera commonly represented in Hanford Site soil include Staphylococcus and Nocardia, and relatives of several unclassified bacteria high in G+C content **(**Fredrickson et al. 2004**).** Gram-negative genera are less common as they are less tolerant to drought. Representatives include *Pseudomonas* and *Sphingomonas* as well as close relatives to a number of unclassified α-, β-, and γ-proteobacteria (Fredrickson et al. 2004). Two gram-negative bacteria that have been the focus of research are *Deinococcus radiodurans* and *Shewanella oneidensis*, because of their unusual resistance to ionizing radiation and ability to reduce uranium. It has been found that *Deinococcus radiodurans* is able to withstand ionizing radiation up to 10-15 kGy without lethality (Fredrickson 2004). Wild-type *Deinococcus* has been shown to reduce uranium in the presence of humic acids under strict anaerobic conditions (Fredrickson et al. 2001). *Shewanella oneidensis* bacteria not only chemically modifiy free uranium, but also aggregates the oxide uraninite (UO_2) into nanospheres that effectively neutralize this heavy metal.

References

Bjornstad BN, KR Fecht, and CJ Pluhar. 2001. "Long history of pre-Wisconsin, ice-age, cataclysmic floods: Evidence from southeastern Washington State." Journal of Geology 109:695-713.

Bjornstad, B.N., 1990. Geohydrology of the 218-W-5 burial ground, 200-west area, Hanford site. PNNL-7336, Pacific Northwest National Laboratory, Richland, WA.

Brockman, F. J., T. L. Kieft, J. K. Fredrickson, B. N. Bjornstad, S. W. Li, W. Spangenburg, and P. E. Long. 1992. Microbiology of vadose zone paleosols in south-central Washington state. Microbial Ecology.

Brown, C. F., Geiszler, K. N., Valenta, M. M., Clayton, E. T., Serne R. J., Kutnyakov, I. V. Bjornstad, B. N., Baum, S. R., Lanigan, D. C., Lindberg, M. J., Iovin, C., Orr, R. D., Clayton. R. E., 2007. Characterization of Direct Push Vadose Zone Sediments from the 241-U Single-Shell Tank Far. Report written for CH2M HILL Hanford Group, Inc. PNNL-17163. Prepared for the U.S. Department of Energy.

Brown, C.F, et al., 2007. Characterization of Direct Push Vadose Zone Sediments from the 241-U Single-Shell Tank Farm. PNNL-17163. Prepared for the U.S. Department of Energy.

Bunn, A. L, et al., 2002. Hanford Site National Environmental Policy Act (NEPA) Characterization. PNNL-6415 Rev. 14 Prepared for the U.S. Department of Energy.

DOE 1988. Site Characterization Plan, Reference Repository Location, Hanford Site, Washington. Vol.1, Consultation Draft. U.S. Department of Energy. Richland, Washington. 1988.

Francisca Reyes-Ramirez, Paul Dobbin, Gary Sawers, and David J. Richardso. 2003. Characterization of Transcriptional Regulation of Shewanella frigidimarina Fe(III)-Induced Flavocytochrome c Reveals a Novel Iron-Responsive Gene Regulation Syste. Vol 181 p. 4564–457.1 Journal of Bacteriology. American Society for MicroBiology.

Fredrickson JK, Zachara JM, Balkwill DL, Kennedy D, Li SM, et al. (2004) Geomicrobiology of high-level nuclear waste-contaminated vadose sediments at the Hanford site, Washington state. Appl Environ Microbiol 70: 4230–4241.

Fredrickson, J. K., H. M. Kostandarithes, S. W. Li, A. E. Plymale, and M. J. Daly. 2000. Reduction of Fe(III), Cr(VI), U(VI) and Tc(VII) by Deinococcus radiodurans R1. Appl. Environ. Microbiol. 66:2006-2011

Fredrickson, K., John M. Zachara, David L. Balkwill, David Kennedy, and Shu-mei W. Li, Heather M. Kostandarithes, Michael J. Daly, Margaret F. Romine, and Fred J. Brockman . 2004. Geomicrobiology of High-Level Nuclear Waste-Contaminated Vadose. APPLIED AND ENVIRONMENTAL MICROBIOLOGY. Vol 70. p. 4230–4241.

G. V. Last, G. W. Gee, E. J. Freeman, W. E. Nichols, K. J. Cantrell, B. N. Bjornstad, M. J. Fayer D. G. Horton. 2006. Vadose Zone Hydrogeology Data Package for Hanford Assessments. PNNL-14702, Rev. 1. Prepared for the U.S. Department of Energy.

Hoitink, D.J, et al.,2005. Climatologically Summary 2004 with historical Data. PNNL-15160. Prepared for the U.S. Department of Energy.

Last, G. V. N. Bjornstad, M. P. Bergeron, D. W. Wallace, D. R. Mewcomer, J. A. Schramke, M. A. Chamnes, C. S. Cline, S. P. Airhart, and J. S.Wilbur. 1898. Hydrology of the 200 Areas Low Level Burrial Grounds – An Interim Report. PNNL- 6820 Vol. 1, Pacific Northwest Laboratory, Richland, Washington.

Last, G. V., Gee, G. W., Freeman, E. J., Nichols, W. E. , Cantrell, K. J., Bjornstad, B. N., Fayer, M. J., Horton. D. G., 2006. Vadose Zone Hydrogeology Data Package for Hanford Assessments. PNNL-14702, Rev. 1. Prepared for the U.S. Department of Energy.

Lindenmeier, C.W. , Lindberg, M.J., Geiszler, K.N., Serne, R.J., Clayton, R.E., Brown, C.F., Bjornstad, B.N., LeGore, V.L., Valenta, M.M., Gee, G.W., Kutnyakov, I.V., Vickerman, T.S., Schaef, H.T., Baum, S.R., Royack, L.J., Lanigan. D.C. 2003. Characterization of Vadose Zone

Sediment: RCRA Borehole 299-E33-338 Located Near the B-BX-BY Waste Management Area. PNNL-14121. Prepared for the U.S. Department of Energy.

Neitzel, D.A, 2003. Hanford Site National Environmental Policy Act (NEPA). PNNL-6415 Rev. 15. Prepared for the U.S. Department of Energy.

Serne RJ, Lindberg MJ, Baum SR, Last GV, Clayton RE, Geiszler KN, Gee GW, LeGore VL, Brown CF, Schaef HT, Orr RD, Valenta MM, Lanigan DC, Kutnyakov IV, Vickerman TS, Lindenmeier CW, 2008. Characterization of Vadose Zone Sediment: Borehole 299-E33-45 Near BX-102 in the B-BX-BY Waste Management Area. PNNL 14083 Rev.1. Prepared for the U.S. Department of Energy.

Serne RJ, Mitroshkov AV, Serne JN, Bjornstad BN, LeGore VL, Last GV, Schaef HT, O'Hara, MJ, Smith SC, Williams BA, Brown CF, Lindenmeier CW, Lanigan, DC, Parker, KE, Zachara, JM, Horton DG, Kutnyakov IV, Burke DS, Clayton, RE, 2008b. Characterization of Vadose Zone Sediment: Uncontaminated RCRA Borehole Core Samples and composite samples. PNNL-13757-1, rev. 1. Prepared for the U.S. Department of Energy.

Simpson, B. C., Corbin, R. A., Anderson, M. J., Kincaid. C. T., 2006. Hanford Soil Inventory Model (SIM) Rev. 1 Software Documentation – Requirements, Design, and Limitations. PNNL-16098. Prepared for the U.S. Department of Energy.

Tallman, A. M., K. R. Fecht, M. C. Marratt, and G. V. Last, 1979, Geology of the Separations Areas, Hanford Site, South-Central Washington, RHO-ST-23, Rockwell Hanford Operations, Richland, Washington.

U.S., DOE. "Hanford - Areas 100, 200, 300, 1100." Web. 25 Oct 2010. <http://response.restoration.noaa.gov/book_shelf/406_Hanford.pdf>

US DOE, Standardized stratigraphic nomenclature for Post-Ringold Formation Sediments within the Central Pasco Basin. Department of Energy, Richland Operations, Richland, Wa., DOE/RL-2002-39, 2002

US, DOE. "200 Area." Department of Energy HANFORD SITE." Web. 27 Oct 2010. <http://www.hanford.gov/page.cfm/200Area>.

US, DOE. Environmental Assessment for the Transfer of 1100 Area, Southern Rail Connection and Rolling Stock, Handford Site, Richarland, Washington, 1998. DOE/EA-1260 report

Xie Y., Last, G.V., Murray, C.J., Mackley. R. 2003. Mineralogical and Bulk-Rock Geochemical Signatures of Ringold and Hanford Formation Sediments. PNNL-14202. Prepared for the U.S. Department of Energy.

Zachara, J, et al., 2007. A Site-Wide Perspective on Uranium Geochemistry at the Hanford Site. PNNL-17031. Prepared for the U.S. Department of Energy.